

For Reference

NOT TO BE TAKEN FROM THIS ROOM

Ex LIBRIS
UNIVERSITATIS
ALBERTAEÆSIS



THE UNIVERSITY OF ALBERTA

MAGNETICALLY INDUCED INSTABILITY
IN AN ARGON PLASMA

by



ROBERT HENRY STEPHEN HARDY

A THESIS

SUBMITTED TO THE FACULTY OF GRADUATE STUDIES
IN PARTIAL FULFILLMENT OF THE REQUIREMENTS FOR THE DEGREE
OF DOCTOR OF PHILOSOPHY

DEPARTMENT OF ELECTRICAL ENGINEERING

EDMONTON, ALBERTA

FALL, 1971

Thesis
17 F
28 D

UNIVERSITY OF ALBERTA
FACULTY OF GRADUATE STUDIES

The undersigned certify that they have read, and recommend to the Faculty of Graduate Studies for acceptance, a thesis entitled "Magnetically Induced Instability in an Argon Plasma" submitted by Robert Henry Stephen Hardy in partial fulfillment of the requirements for the degree of Doctor of Philosophy.

ABSTRACT

Observations of a highly structured discharge and current instability in unseeded, shock heated argon flowing through a region of large transverse magnetic field are presented and analyzed. The experimental results are related to an extension of the theory of ionization (electrothermal) instability in partially ionized gases in which the presence of multiply charged ions is taken into account. A critical magnetic field for instability onset is predicted. The growth rate and the angular dependence of the growth rate are calculated and compared with experimental observations. An enhanced interaction between the current discharge and the plasma flow is observed. The magnitude of the interaction is compared with the magnitude of the Hall parameter in the plasma. A rotation of the current filaments to form a helical structure is observed. The formation of this structure is predicted by the use of a simple minimum energy consideration.

ACKNOWLEDGEMENTS

This work was carried out at the Department of Electrical Engineering of the University of Alberta under the supervision of Professor P.R. Smy.

In addition to the above, the author would like to thank Dr. G.B. Walker for his interest and advice during the course of the author's studies and Dr. N.H. Burnett for many useful discussions during the course of this work.

The author would like to thank Dr. H.A. Simonson (Ph.D., Rocky Mountain Institute) for many helpful comments and useful advice and the alumni of the Rocky Mountain Institute for their helpful guidance.

Much of the apparatus, including the shock tube components, was constructed under the supervision of Mr. E. Buck who also offered many suggestions concerning the design of the various components. The author would like to thank him and the other members of the shop staff for their excellent and prompt service.

The author is grateful for the receipt of an Alberta Government Telephones Centennial Fellowship and a National Research Council Studentship during the course of these studies.

Finally, the author wishes to thank his wife, Peggy, for her patience and encouragement during the course of this work.

TABLE OF CONTENTS

Chapter 1	Introduction	1
1.1	A Brief Review of the Literature	1
1.2	The Nature of the Present Work	8
Chapter 2	Description of the Experimental Apparatus and Diagnostic Techniques	11
2.1	Method of Production and Properties of the Shock Heated Gas	11
2.2	Description of the Magnetic Interaction Region	13
2.3	Diagnostic Methods	15
Chapter 3	Onset of the Ionization Instability	19
3.1	Outline of Theory	19
3.1.1	Calculation of the Electron Temperature	21
3.1.2	Equilibrium of Electrons	25
3.1.3	Effect of Radiation Losses on the Electron Energy Balance and the Electron Temperature	27
3.1.4	Calculation of the Electron Density	30
3.1.5	System of Equations for Ionization Instability	33

3.1.6	Growth Rate of the Ionization Instability	37
3.1.7	Physical Mechanism of the Ionization Instability	44
3.2	Application of the Theory to Experiment	50
3.2.1	Calculation of the Plasma Parameters for Partially Ionized, Shock Heated Argon	50
3.2.2	Variation of Hall Parameter with Applied Magnetic Field	52
3.2.3	Variation of Growth Rate with Applied Magnetic Field and Hall Parameter	56
3.2.4	Variation of the Critical Magnetic Field and Critical Hall Parameter with Shock Mach Number	63
3.2.5	Angular Dependence of the Streamer Formation	66
3.2.6	Development of Turbulence with Increasing Values of Hall Parameter	74
Chapter 4	Behavior of the Current Streamers after Formation	79
4.1	Sequence of Events after Formation	79

4.2 Force Balance on the Current Streamer and the Interaction of the Streamer with the Gas Flow	81
4.3 Helical Instability of the Current Streamers	96
Chapter 5 Applications and Suggestions for Further Research	
5.1 Applications	107
5.2 Further Research	113
List of References	119
Appendix 1 Equilibrium Properties of Shock Heated Argon	
Appendix 2 Raizer's Method for Calculation of an Approximate Ionic Charge in the Region of Multiple Ionization	141
Appendix 3 Detailed Calculation of the Growth Rate Expression for Ionization Instability	145
	151

LIST OF ILLUSTRATIONS

Figure

1.1(a)	Photograph of discharge without transverse magnetic field	4
1.1(b)	Photograph of discharge with transverse magnetic field	5
2.1	Experimental arrangement of magnetic interaction region	14
2.2	"Lockout multivibrator" circuit of Tektronix 555 oscilloscope showing modifications for delayed trigger operation	18
3.1	Ohm's Law applied to experimental arrangement	22
3.2	Physical mechanism of instability	45
3.3	Variation of E_y with applied magnetic field	53
3.3(a)	Electron temperature vs. magnetic field	55
3.4	Variation of Hall parameter with magnetic field strength	57
3.5	Growth rate vs. magnetic field	59
3.6	Growth rate vs. Hall parameter	60
3.7	e-folding time vs. Hall parameter	61

3.8	e-folding time vs. magnetic field	62
3.9	Critical Hall parameter for instability growth	64
3.10	Critical magnetic field for instability growth	65
3.11(a)	Photographs of discharge structure	69
3.11(b)	Photographs of discharge structure	70
3.12	Drawing of Frame #1 of Fig. 3.11(b)	71
3.13	Angle between perturbation current and original current	72
3.14	Angle between perturbation current and original current	73
3.15(a)	Variation of discharge structure with Hall parameter	76
3.15(b)	as above	77
3.15(c)	as above	78
4.1	Photographs taken through center of magnetic field coils	82
4.2	Photographs of shocked gas	83
4.3	Drag coefficient vs. Reynolds number	86
4.4	Helical structure of current streamers	97
A.1.1	Density ratio and flow velocity	142
A.1.2	Temperature of shocked gas	143
A.1.3	Degree of ionization	144
A.3.1, A.3.2	Orientation of current vectors	155

LIST OF TABLES

Table 3.1 Plasma parameters for shock heated argon	54
Table 4.1 Effective drag coefficient	88
Table 4.2 Correlation between effective drag coefficient and Hall parameter and Reynolds number	95
Table A.2.1 Ionization potentials and partition functions for argon	150

CHAPTER 1 INTRODUCTION

The subject of this work is the investigation of a magnetically induced instability in a partially ionized plasma. The instability manifests itself as a highly non-uniform current distribution composed of a number of current pinches or streamers when the plasma is subjected to crossed electric and magnetic fields (see Figure 1.1).

The behavior of the instability is explained by an extension of the theory of the ionization or electro-thermal instability in which the presence of multiply charged ions is accounted for.

1.1 A Brief Review of the Literature

The discovery of the ionization instability mechanism grew out of the work^{46,47,51,91} directed toward utilizing extrathermal or nonequilibrium ionization, produced by electric fields or other means,

to enhance the conductivity of the working fluid of an MHD generator. The instability mechanism was first proposed by Velikhov and Dykhne¹¹³ and Kerrebrock⁴⁹. Both authors showed that the system of equations consisting of a generalized Ohm's Law, an electron energy balance equation for $T_e > T_i$, and an ionization equilibrium relation (Saha's equation), is unstable to small perturbations in electron density and temperature. Velikhov and Dykhne derived a relation for a critical Hall parameter above which instability occurs and showed that the plasma effective conductivity will be appreciably lowered when the instability is present. Kerrebrock, restricting his analysis to the case of slight ionization and constant electron collision frequency, derived the growth rate, frequency, and wavelength of the oscillations and showed that the growth rate exhibits a directional dependence.

The first experimental investigations into the nature of the instability were performed by Nedospasov and Shipuk⁷¹ and Klepeis and Rosa⁵³. Nedospasov and Shipuk used a pulsed discharge in a mixture of argon and mercury vapor placed between the poles of an electromagnet. They found that the Hall field exhibited a saturation and ceased to depend on magnetic field,

and that the time averaged conductivity decreased inversely with Hall parameter. Klepeis and Rosa, using a disc geometry MHD generator duct with argon seeded with cesium, also observed a decreased Hall voltage as well as the formation of highly luminous radial spokes at large values of magnetic field.

This investigation was continued and extended by a number of workers^{7,45,101,114}, for example. It was shown that striations or streamers form in the plasma when the critical Hall parameter is exceeded. The streamers are inclined at a characteristic angle to the main current.

The theory of the instability was considered further by Solbes¹⁰³, Zampaglione¹¹⁹, Dykhne²¹, Velikhov et al¹¹⁵, Nelson^{74,75,76}, Hiramoto³⁴, and Gilpin²⁸. All the authors considered perturbation solutions to the above mentioned equations. Velikhov et al¹¹⁵ and Nelson⁷⁶ used numerical methods to investigate the effect of the boundary conditions due to the generator duct walls and electrodes on the behavior of the instability. Gilpin²⁸ related the instability onset conditions to the breakdown condition for a gas discharge.

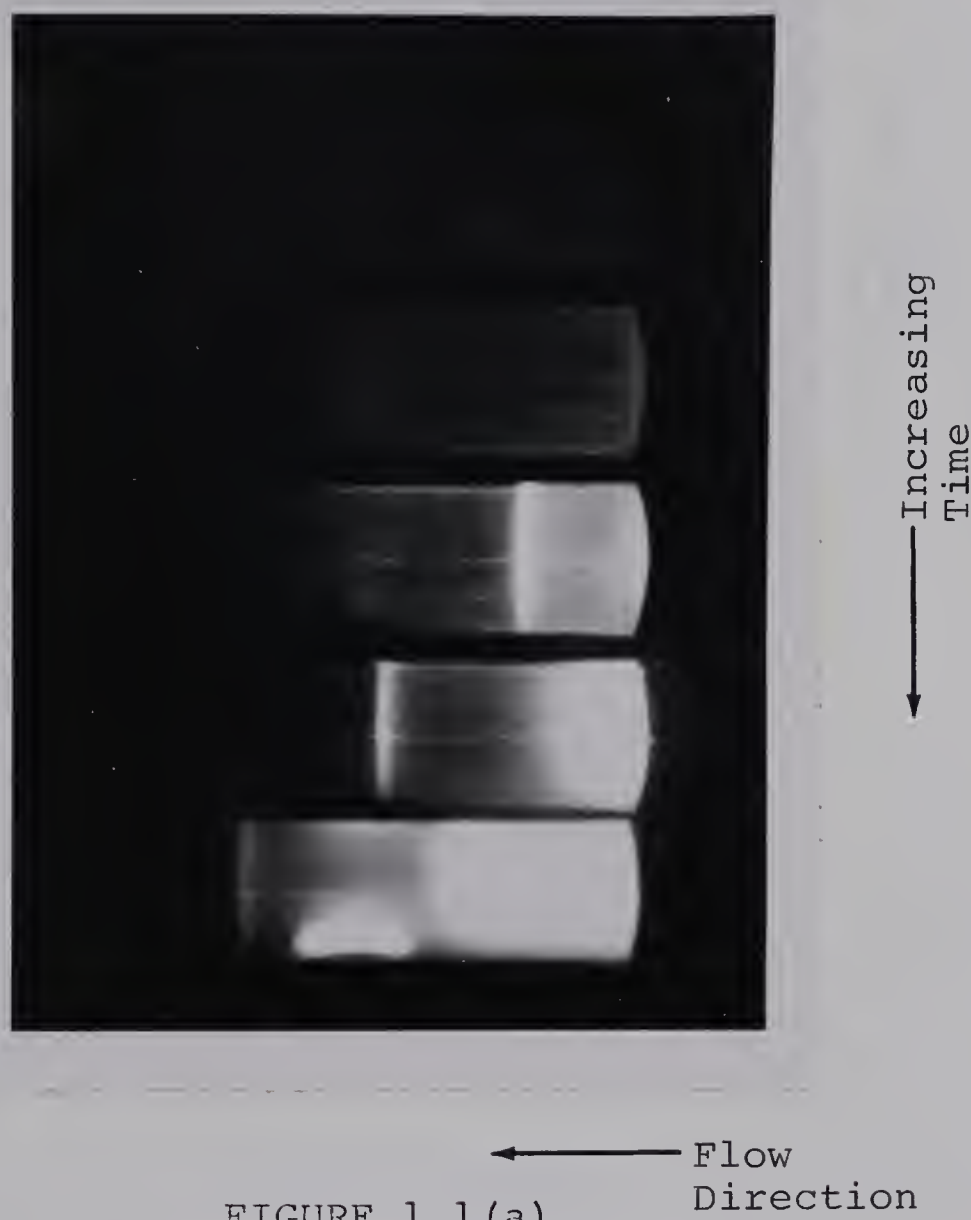


FIGURE 1.1(a)

← Flow
Direction

Photograph of discharge
without transverse magnetic field

($B=0$, $E_y=40$ v./cm.; produced by applied potential;
 $I \approx 6000$ amps. (frame 5); 10 μ sec. interframe delay;
exposure times per frame are 0.5, 0.5, 0.5, 0.2,
0.1 μ sec. respectively.)



Figure 1.1(b)

Photograph of Discharge

with Transverse Magnetic Field

($B = 1.63 \text{ w/m}^2$; E_y produced by motion through magnetic field; $u_2 B \approx 50 \text{ v/cm}$; $I \approx 1000 \text{ amps}$; 2 μsec interframe delay; 0.2 μsec exposure time per frame)

The instability behavior in a flow of gas was investigated by Gilpin and Zukoski^{27,126}, Kerrebrock and Dethlefsen⁵², Riedmüller⁸⁷, Vitshas, Golubev and Malikov¹¹⁷, Shipuk and Pashkin¹⁰², Golubev et al³¹, and Malikov⁶⁶.

Gilpin and Zukoski, Riedmüller, Vitshas et al, and Shipuk and Pashkin observed regular streamers oriented at an angle to the main current. The effects of Hall voltage saturation and increase in turbulence and amplitude of fluctuations with increase in magnetic field were also observed.

Golubev et al³¹ and Malikov⁶⁶, using a sodium seeded argon flow observed a number of plasma streamers forming in the presence of a magnetic field. Because the streamers were oriented primarily along the Faraday or $\vec{v} \times \vec{B}$ direction rather than at an angle to the Faraday direction, the authors were reluctant to attribute the filamentary structure to the presence of the ionization instability, despite commonly observed behavior such as the increase in fluctuation amplitude with Hall parameter and saturation of the Hall field with increasing Hall parameter. However, it is shown in this work (Chapter 3) that, during the formation period of the current streamers, they are inclined at the characteristic angle to the $\vec{v} \times \vec{B}$ direction but that, due to constraints on the current

flow (constrained to flow primarily in the $\vec{v} \times \vec{B}$ direction), the fully developed filaments must be aligned primarily in the $\vec{v} \times \vec{B}$ direction.

Zauderer^{121,124} has observed current pinches in a linear MHD channel which persisted in the absence of a magnetic field. No increase in turbulence and no saturation of Hall voltage were observed. It thus appears that the current pinching was due to the thermal pinch mechanism that occurs in a classical high pressure arc, and not to the magnetically induced instability investigated here.

Klingenber⁵⁵ observed current pinches in shock heated gas in the presence of a magnetic field. He attributed their formation to electrode effects and did not consider the role of the magnetic field in producing a current instability. The value of Hall parameter in his experiment was less than or just equal to the minimum value for appearance of the instability. Under these conditions, small variations in Joule heating rate introduced by varying the electrode arrangement may serve to suppress the instability. Another factor is the role played by impurities in his experiment. His test section was constructed of plexiglass and the interaction of

the hot gas with this plastic surface almost certainly contaminated the shock heated gas. It has been recognized¹¹ that a few tenths of a per cent of molecular impurity can absorb a large proportion of the electron energy and thus lower the electron temperature. This lowering of the electron temperature will damp out the instability. In the present work, it has been observed that a high impurity level caused by the failure to flush the shock tube with clean gas before each test is sufficient to produce an overall brightening of the gas, masking the instability.

1.2 The Nature of the Present Work

All of the previous work, in which the authors recognized the existence of the magnetically induced instability, has been conducted in low temperature, seeded, atomic gases, in which the dominant particle interaction mechanism was electron atom collisions and the electron density was almost completely due to the ionization of the seed atoms. The purpose of the present work is to consider the behavior of the instability

in the much more general and widely applicable case of an unseeded, partially ionized, Coulomb collision dominated plasma in which the electron density is due directly to the ionization of the atomic gas.

The partially ionized gas is produced by shock heating argon as described in Chapter 2. The magnetic field is perpendicular to the flow direction of the gas and the electric field is produced by the motional interaction between the gas flow and the magnetic field.

In Chapter 3, the theory of the ionization instability is extended to the Coulomb collision dominated case. The presence of multiply charged ions is accounted for by the use of an approximate method of calculation due to Raizer⁸². Expressions for the dependence of the onset of the instability on Hall parameter and directional dependence of the growth rate on Hall parameter are derived. Numerical calculations are made, for the case of shock heated argon, of the temperature nonequipartition, the instability onset and growth rate, and the angular dependence of the growth rate. The observed experimental behavior of the streamers shows good agreement with the calculations. The breakup of the streamers into smaller, secondary filaments is related to the angular dependence of the growth rate.

In Chapter 4, the behavior of the fully developed current streamers is examined. An enhanced interaction between the plasma streamer and the flow of shocked argon is observed, based on a consideration of the force balance on the streamer. It is suggested that this large interaction is due to turbulence produced in both the streamer and argon flow by the instability mechanism of Chapter 3. This theory is supported by an observed correlation between the degree of interaction and the Hall parameter.

A rotation of the plasma streamers to form a helical structure is observed. The formation of this structure is explained by the existence of a component of magnetic field parallel to the axis of the helix. The angle of pitch and the diameter of the helix are predicted on the basis of a simple minimum energy consideration. The predicted values show good agreement with experiment.

In Chapter 5, suggestions are given for possible applications of the present work. Possible future areas of research are indicated.

CHAPTER 2 DESCRIPTION OF THE EXPERIMENTAL APPARATUS AND DIAGNOSTIC TECHNIQUES

2.1 Method of Production and Properties of the Shock Heated Gas

The shock wave was produced by a pressure driven, diaphragm shock tube with helium heated by an electric discharge as the driver gas. The electric discharge was produced by a 20,000 volt, 8700 Joule capacitor bank.

The driver section consisted of a 5 cm. length of 5 cm. diameter by 1 cm. thick stainless steel tube. A stainless steel flange, "o"-rings, and mechanical clamps were attached to one end of the tube to accomodate a mylar polyester film (1.5×10^{-3} inch thickness) diaphragm. A flange, "o"-rings, and a 1 inch thick plexiglass insulator were fastened to the other end of the tube. The discharge occurred between a brass electrode passing through the center of the insulator

and the inner wall of the stainless steel tube. The driver was flushed with helium and filled to 5 p.s.i. above atmospheric pressure before each test.

The shock tube consisted of a 5 cm. diameter stainless steel tube in which the shock wave was allowed to flow for a distance of about 3 meters before reaching the magnetic interaction region. The unshocked gas was at a pressure of 0.5 torr and room temperature. Shocks of up to Mach 15 with a sample of shock heated gas 5 to 6 cm. long were produced 3 meters from the driver.

The equilibrium properties of the shock heated gas were calculated by de Leeuw⁵⁹. Appendix 1 gives properties of shock heated argon, derived from de Leeuw, for the pressure and Mach number range used in this experiment. A shock tube of similar design operated under similar experimental conditions was studied by Phillips⁸¹. He experimentally verified that the properties of the shock heated gas are well described by the usual Rankine-Hugoniot shock jump equations. He also showed that, at the initial pressures and Mach numbers used here, the shock heated sample had uniform properties over the 5 to 6 cm. sample length, within the limits of his diagnostic methods. Phillips also showed that the thickness of the ionization relaxation region is much less than the total thickness of the shock heated gas.

2.2 Description of the Magnetic Interaction Region

The shock tube in the interaction region consisted of a 60 cm. length of 5 cm. diameter pyrex tubing, beside which two large magnetic field coils were placed. The transverse magnetic field was produced by discharging a 5000 volt, 21,000 Joule capacitor bank through the two coils, series connected and arranged in the Helmholtz pair configuration. The period of the discharge was about 800 μ sec., much longer than the duration of passage of the shock heated gas. The coils consisted of 0.5 mm. by 1.5 cm. brass strip spirally wound and embedded in epoxy resin. A 5 cm. diameter hole was provided in the center of the coils to permit viewing of the passage of the shock heated gas. Magnetic fields of up to 2 w./m.^2 were produced over the 5 cm. electrode region. The field was spatially uniform to within 15 % over the area of the viewing port and was constant in time to within 10% for the duration of passage of the shock heated gas.

Figure 2.1 shows details of the experimental arrangement in the magnetic interaction region. Brass electrodes, 2.5 cm. in diameter, were machined and mounted flush with the interior wall of the pyrex section of the shock tube. The electrodes were connected together by a 20 cm. length of 0.15 mm. by 1 cm. brass strip.

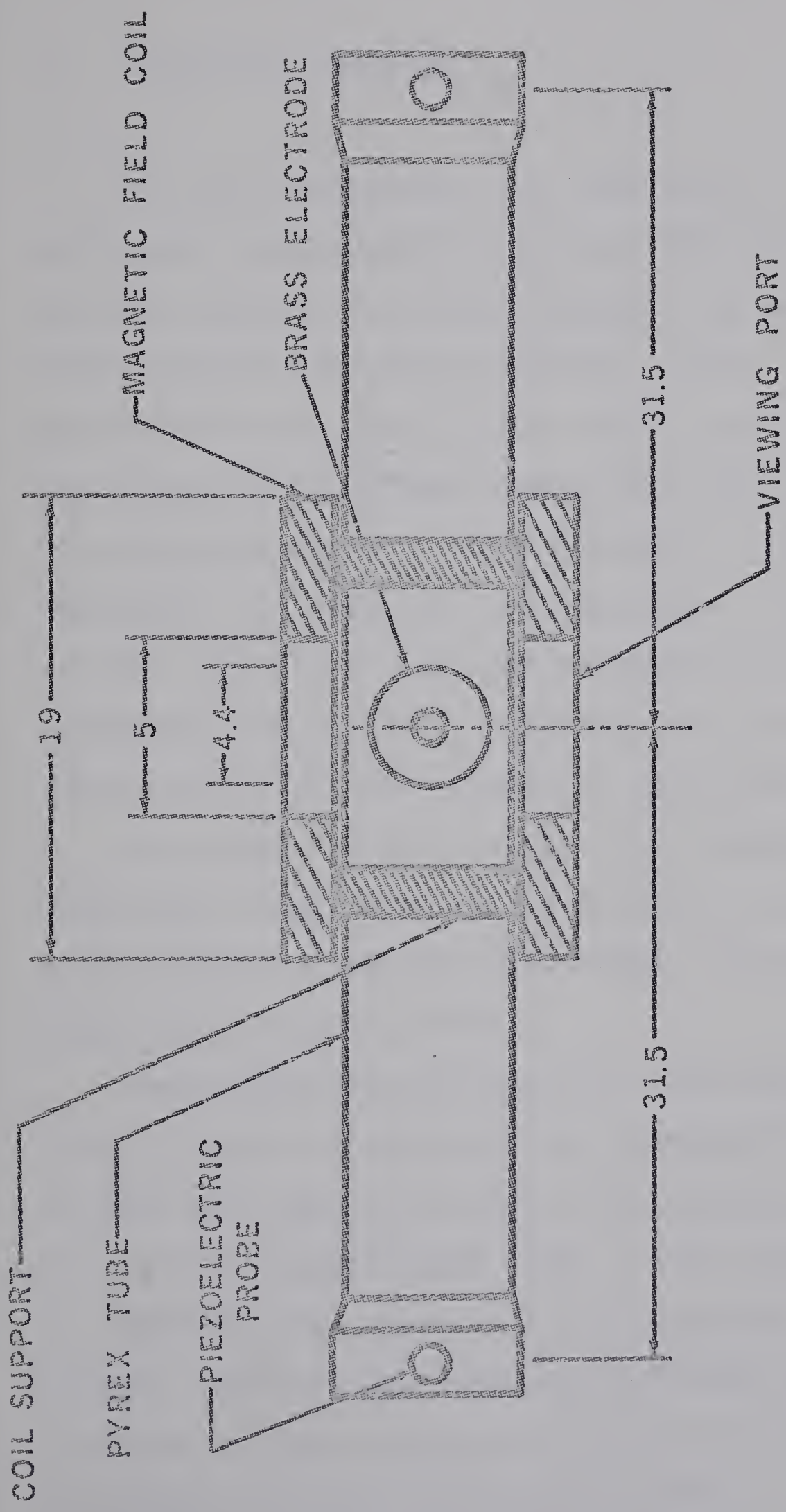


Figure 2.1
Experimental Arrangement of Magnetic Interaction Region
(all dimensions in cm.)

2.3 Diagnostic Methods

The main diagnostic tool used was an electronically shuttered, image converter camera (TRW Model 1D), permitting observations of the temporal and spatial development of the discharge structure. Using the camera, measurements were made of the growth rate of the streamers, the direction of maximum growth rate, and the effect of increasing magnetic field strength on the streamer structure. In addition, the velocities of the streamers and the luminosity front and the dimensions of the streamers were measured. Piezoelectric pressure transducers were also used to measure shock speed.

The total electrode current was determined by measuring the voltage drop across a section of the brass strip connecting the two electrodes, the resistance of which was accurately known.

Much electronic equipment for the amplification and delay of high voltage pulses was developed in order to trigger the capacitor banks, oscilloscopes, and electronic camera at the appropriate times. This equipment will not be described here since it is of reasonably standard design. However, one technique developed here is of broad interest to many workers in experimental investigations of plasmas and will be described below.

One problem frequently encountered in plasma research is due to the large amount of electromagnetic radiation produced whenever a high energy discharge occurs, for instance, whenever a high voltage arc is struck or whenever an energy storage capacitor bank is discharged. This radiation invariably activates the low level trigger circuitry on any nearby oscilloscopes. Frequently, such as in the operation of an electrically driven shock tube or an electrically excited laser, the operation of the oscilloscope must be delayed for a short period of time in order to observe the phenomena of interest. Although one delayed time base can be obtained with a dual-time base oscilloscope, in many cases it is necessary to have two or more delayed time bases to observe phenomena of short duration. This is impossible to accomplish unless some method is found to prevent the unwanted triggering of the primary time base.

One modification to accomplish this purpose will now be described. It is directly applicable to a Tektronix 555 oscilloscope but the same principle may be used on any oscilloscope of similar design.

The time base generators incorporate a "lockout multivibrator" (Figure 2.2) which prevents operation

of the time base under certain conditions; it is the circuit which permits single sweep operation and the delayed sweep of the secondary time base. Figure 2.2 shows a circuit modification designed to prevent the operation of the primary time base (time base "A") until an external high level pulse (-30 volts) is applied. This external pulse either causes the time base to sweep immediately or removes the lock-out and permits the next low level trigger signal to trigger the time base.

When switch S_1 is closed, the time base triggers immediately upon application of the -30 volt pulse (note that the "sweep function" switch must be set at "single sweep"; if it is in any other position, the sweep free-runs and cannot be synchronized or triggered).

When S_1 is open, the time base is enabled (the ready light comes on) by the -30 volt pulse. The time base may then be triggered by the usual means. When S_1 is open, the time base also operates normally in every position of the "sweep function" switch, provided no -30 volt pulses are applied.

The delayed -30 volt pulse can be obtained, for instance, from a thyratron delay unit, which can be made relatively insensitive to electromagnetic interference.

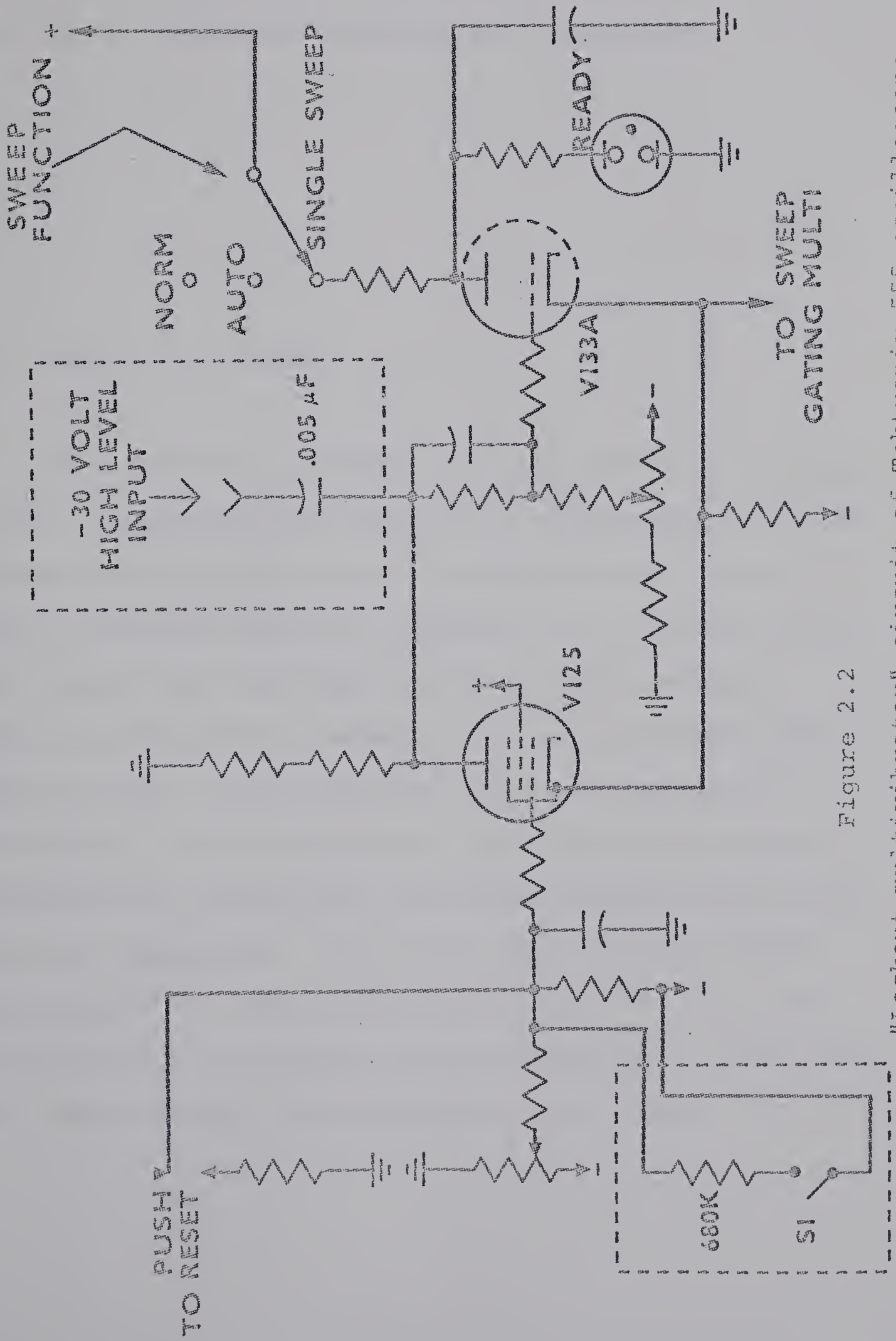


Figure 2.2

"Lockout multivibrator" circuit of Tektronix 555 oscilloscope showing modifications for delayed trigger operation (--- indicates modifications.)

CHAPTER 3 ONSET OF THE IONIZATION INSTABILITY

3.1 Outline of Theory

In a partially ionized gas subjected to an electric field, the possibility exists of a non-equipartition of energy between electrons and heavy particles. Specifically, we would expect an excess of the electronic thermal energy over the heavy particle thermal energy, where the electronic thermal energy is essentially determined by gain in the electric field and loss due to collisional processes, and the electron concentration is determined by approximate ionization equilibrium at the electron temperature. As in the work of Zauderer¹²³, Kerrebrock^{49,51}, and Zukoski and Gilpin^{27,126}, we rely on convection to maintain the gas temperature nearly constant while the gas flows through a test region.

Thus, we consider a situation where the electrons comprise a gas that is weakly coupled thermally to the heavy particle gas, but very strongly coupled to the valence electrons of the gas, and exhibiting a Maxwellian distribution of energies. One more parameter, then, is required, in addition to the thermodynamic variables of the gas, in order to determine the state of the plasma. The electron temperature is, of course, the fundamental variable that must be added. In the following sections, a method of calculation of the electron temperature is given.

The question of the stability of this non-equilibrium state will be considered in detail. In particular, the theories of Velikhov and Dykhne¹¹³, and Kerrebrock⁴⁹ indicate that a unique mechanism of ionization instability exists in a non-equilibrium plasma placed in crossed electric and magnetic fields. This instability manifests itself as a constriction of the discharge into current streamers. The theory is extended to the high temperature, multiply ionized, Coulomb collision dominated regime. The predictions of the extended theory will be compared with the experimental results obtained in partially ionized argon subject to crossed electric and magnetic fields.

3.1.1 Calculation of the Electron Temperature

The rate at which energy is gained by the electrons is the scalar product of the electron current \vec{j} and the electric field in the frame of the moving gas, \vec{E} . Ohm's law, neglecting diffusion and electron inertia effects, is⁹²:

$$\vec{j} = \sigma \vec{E} - \omega \tau \vec{j} \times \frac{\vec{B}}{B} \quad \dots (3.1)$$

where σ is the electron scalar conductivity, ω is the electron cyclotron frequency, and τ is the electron mean free time or the reciprocal of the electron collision frequency.

In a coordinate system as shown in Figure 3.1, Ohm's Law is:

$$j_x = \sigma_0 E_x - \omega \tau j_y$$

$$j_y = \sigma_0 E_y + \omega \tau j_x$$

$$j_z = \sigma_0 E_z$$

or, for $j_x = 0$, (no Hall current flows),

$$\sigma_0 E_x = \omega \tau j_y$$

$$j_y = \sigma_0 E_y$$

Thus,

$$\vec{j} \cdot \vec{E} = j_y E_y = \sigma_0 E_y^2 = j_y^2 / \sigma_0 \quad \dots (3.2)$$

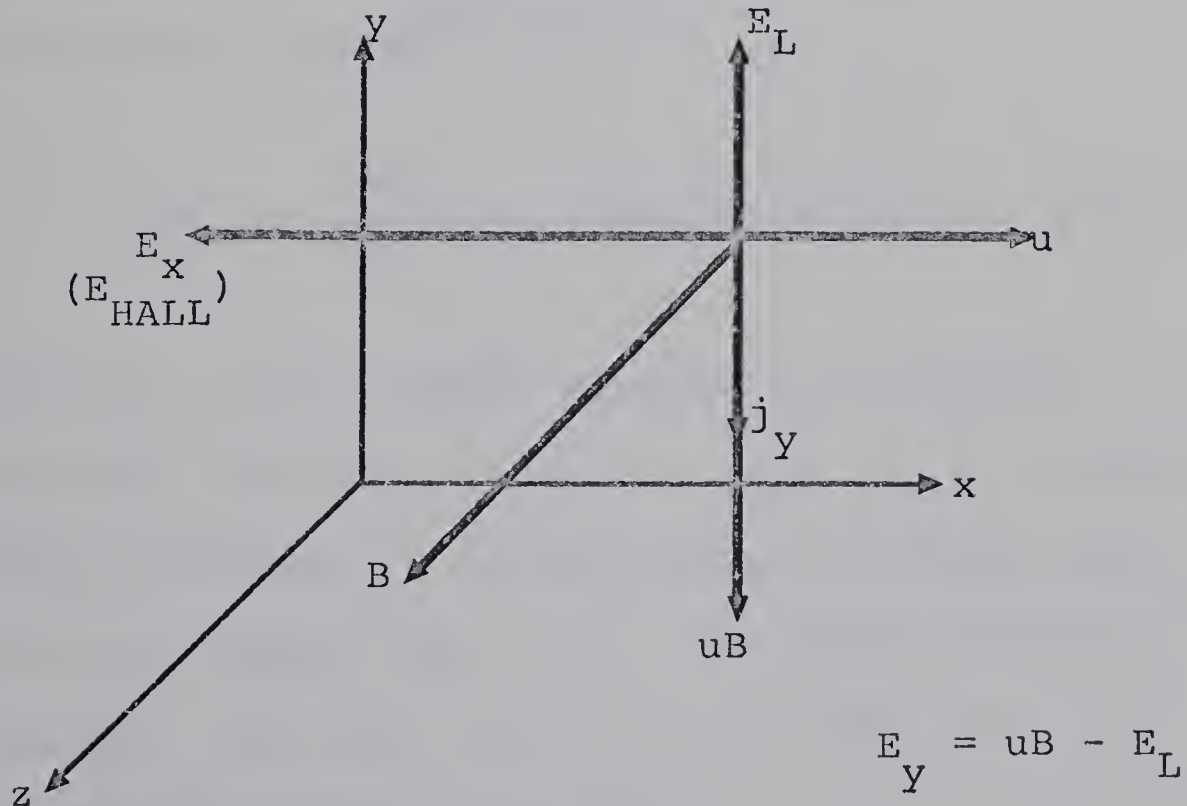


Figure 3.1

For a Maxwellian electron distribution function, the energy loss of the electrons per elastic collision with heavy particles is $2m_e/m_K$ times the difference in energy of electrons and heavy particles^{39,49,51,16}, where m_e is the electron mass and m_K is the mass of the K'th species of heavy particles. To account for possible inelastic collisions, a correction factor δ_K is introduced which is close to unity for monatomic gases (elastic collisions) but which is 10 to 10^3 for diatomic and polyatomic molecules in which vibrational and rotational modes may be excited^{39,92}. The energy balance of the electrons is then^{39,92,49,51}

$$\sigma_0 E_Y^2 = \sum_K (n_e v_{eK}) (2m_e/m_K) \delta_K (3k/2) (T_e - T_K) \quad \dots (3.3)$$

where n_e is the number density of electrons, v_{eK} is the electron collision frequency with the K'th species of heavy particles, k is Boltzmann's constant, T_e is the electron temperature, T_K is the temperature of the K'th species. The T_K 's are generally identical and are equal to the gas temperature T_g ³⁹.

In the plasma of interest here, (partially ionized argon), there are two species of heavy particles, argon atoms and argon ions. Thus, the energy balance equation becomes:

$$\sigma_0 E_y^2 = n_e (2m_e/m_a) (3k/2) (T_e - T_g) (v_{ei} + v_{ea}) \dots (3.4)$$

since δ_K is equal to unity for both species of heavy particles^{49,92}.

Now¹⁰⁶,

$$\sigma_0 = \frac{n_e e^2}{m_e (v_{ei} + v_{ea})} \dots (3.5)$$

So, the energy balance equation is:

$$E_y^2 = (3km_e^2/m_a e^2) (T_e - T_g) (v_{ei} + v_{ea})^2 \dots (3.6)$$

Thus, given an E_y (electric field in the frame of the gas) and given v_{ei} and v_{ea} , we can calculate the electron temperature.

In the temperature regime of interest here, (Mach 8 to Mach 16 argon shocks), v_{ei} is much greater than v_{ea} ⁶⁰; Coulomb collisions are the dominant collision process.

v_{ei} is given by Rose and Clarke⁹⁰ as:

$$v_{ei} = \frac{Z n_e \ln \Lambda}{1.51 \times 10^6 T_e^{3/2}} \quad \dots (3.7)$$

Now, we also need a relation between n_e , the electron density, and T_e , the electron temperature or mean thermal energy. This relation is given by the ionization equilibrium relation or Saha's equation.

3.1.2 Equilibrium of Electrons

As noted in the introduction to this chapter, we may think of the free and valence electrons as comprising a single gas. Electron-electron collisions tend to force this gas toward a Boltzmann distribution, whereas collisions of electrons with atoms or ions and radiation, in general, tend to perturb it. As noted by Kerrebrock^{49,51} and Ben Daniel and Tamor⁹, there is a value of electron density or ionization fraction below which the electrons are influenced more by energy exchange with heavy particles than by mutual energy exchange. At electron densities sufficiently far above this critical value, Coulomb collisions between electrons override all other processes and lead to a Maxwellian distribution.

Following Kerrebrock⁴⁹, the condition for a Maxwellian distribution of electron energies is:

$$n_e^2 \sigma_{ee} \gg (2 m_e/m_a) (n_e n_n \sigma_{en} + n_e n_i \sigma_{ei}) \dots (3.8)$$

where σ_{ee} , σ_{en} , σ_{ei} are the cross sections for electron-electron, electron-neutral, and electron-ion collisions respectively; n_e , n_n , and n_i are the electron, neutral, and ion number densities respectively; m_e and m_a are the electron and atom (ion) masses.

Using $n_e = Z n_i$ and dividing by $n_e n_n \sigma_{ee}$, we have:

$$\frac{n_e}{n_n} \gg 2 \frac{m_e}{m_a} \left(\frac{\sigma_{en}}{\sigma_{ee}} + \frac{n_e \sigma_{ei}}{Z n_n \sigma_{ee}} \right)$$

or,

$$\frac{n_e}{n_n} \left(1 - 2 \frac{m_e}{m_a} \frac{1}{Z} \frac{\sigma_{ei}}{\sigma_{ee}} \right) \gg 2 \frac{m_e}{m_a} \frac{\sigma_{en}}{\sigma_{ee}}$$

Now, since $m_e \ll m_a$ and $(\sigma_{ei}/\sigma_{ee}) \approx 1$ (ref. 90), we have:

$$(n_e/n_n) \gg 2 (m_e/m_a) (\sigma_{en}/\sigma_{ee})$$

Now, $\sigma_{en} \approx 10^{-20} \text{ m}^2$ (ref. 20), $\sigma_{ee} \approx 5 \times 10^{-17} \text{ m}^2$ (ref. 90), and $m_e/m_a \approx 1.36 \times 10^{-5}$. Using these numerical values, we expect the electrons to have a Maxwellian distribution at the electron temperature whenever

$$(n_e/n_n) \gg 5 \times 10^{-9} \quad \dots (3.9)$$

Thus, for the range of temperatures and densities encountered in this experiment, we would expect the electrons to have a Maxwellian distribution of energies about the electron temperature.

It remains to consider the effects of radiation from the electron gas on the electron energy balance.

3.1.3. Effect of Radiation Losses on the Electron Energy Balance and the Electron Temperature

The purpose of this section is to compare the rate of electron energy loss due to radiation with the rate of energy transfer to the heavy particles due to electron-heavy particle collisions.

Petschek et al⁸⁰ show that the main energy loss mechanism for shock heated argon in the temperature regime of interest here is continuum radiation due to free-bound electron transitions. By measuring the variation in light intensity versus distance behind the shock, the authors were able to show that this cooling of the gas was closely accounted for by the theory of continuum radiation from a partially ionized gas formulated by Unsöld¹⁰⁹. More recently, Horn, Wong, and Bershad³⁸ considered the contribution of emission from spectral lines to the total radiative emission energy loss. They found that the 4p4s and 3d4p Ar lines contributed rather large losses, with the result that the total loss is approximately equal for both continuum emission and line radiation.

In this section, we will consider only the continuum radiation. From ref. 38, the total radiative energy loss per unit volume per unit time for optically thin continuum radiation is:

$$Q = 6.86 \times 10^{-38} Z_{\text{eff}}^2 \frac{n_e^2}{T_e^{1/2}} \left(v_g + \frac{kT_e}{h} \right) \text{ ergs/cm}^3/\text{sec}$$

... (3.10a)

for n_e in cm^{-3} and T_e in $^{\circ}\text{K}$.

or,

$$Q = 6.86 \times 10^{-51} Z_{\text{eff}}^2 \frac{n_e^2}{T_e^{1/2}} \left(v_g + \frac{kT_e}{h} \right) \frac{\text{Joules}}{\text{m}^3 \text{ sec}} \dots (3.10b)$$

for n_e in m^{-3} , T_e in $^{\circ}\text{K}$.

The collisional loss rate is given by:

$$P_C = 2(m_e/m_a) n_e (3k/2) (T_e - T_g) v_{ei}$$

Using eq. (3.7) for v_{ei} ,

$$P_C = 3.73 \times 10^{-34} Z \ln \Lambda \left(1 - \frac{T_g}{T_e} \right) \frac{n_e^2}{T_e^{1/2}} \text{ watts/m}^3 \dots (3.11)$$

Now, the ratio of the collisional loss rate to the radiative loss rate is:

$$\frac{P_C}{Q} = \left(\frac{5.44 \times 10^{16}}{v_g + (kT_e/h)} \right) \frac{Z}{Z_{\text{eff}}^2} \ln \Lambda \left(1 - \frac{T_g}{T_e} \right) \dots (3.12)$$

Following Horn et al³⁸, we take $Z_{\text{eff}}^2 = 1.5$, and $h\nu_g = 2.85 \text{ eV}$. In addition, we take $Z = 1$, $\ln \Lambda = 6$, $kT_e \approx 1 \text{ eV}$, and $(1 - (T_g/T_e)) \approx 0.5$, as typical values for the experimental conditions.

We then have:

$$P_C/Q \approx 1.2 \times 10^2 \dots (3.13)$$

We see that the collisional loss rate is about two orders of magnitude larger than the radiation energy loss rate, and we are justified in neglecting the effect of radiative energy loss on the electron temperature. Including the contribution of line emission to the total radiative loss as described by Horn et al³⁸ does not invalidate this conclusion.

3.1.4. Calculation of the Electron Density

The calculation of the electron density, assuming ionization equilibrium at the electron temperature, proceeds from Saha's equation:

$$\frac{n_e n_i}{n_a} = A \frac{g_+}{g_a} T_e^{3/2} \exp(-I/kT_e) \quad \dots (3.14)$$

where

$$A = 2 \left(\frac{2\pi m_e k}{h^2} \right)^{3/2},$$

I is the ionization potential, g_+/g_a is the ratio of statistical weights, T_e is the electron temperature, n_e , n_i , and n_a are the electron, ion, and neutral number densities, respectively.

As we shall see, under the conditions of this experiment, electron temperatures will be high enough to ionize the second and perhaps third levels of the argon ions. Under these conditions, we must use the system of Saha equations¹²⁵:

$$\frac{n_{m+1} n_e}{n_m} = A \frac{u_{m+1}}{u_m} T_e^{3/2} \exp(-I_{m+1}/kT_e) \dots (3.15)$$

where n_{m+1} , n_e , and n_m are the $m+1$ multiply ionized ion, electron, and m multiply ionized ion number densities respectively. u_{m+1}/u_m is the statistical weight ratio for the electronic states of the ions. I_{m+1} is the ionization potential for the m 'th ion.

One can readily appreciate that the calculations for electron density based on this non-linear system of equations are extremely involved and time consuming. For each pair of temperature and density values, a non-linear system of algebraic equations must be solved to determine the concentrations of ions of different charge and hence the electron concentration. In addition, the incorporation of the full system of Saha equations in the calculation of the dispersion relation for ionization

instability (see following sections) would cause the resulting expression to become very involved and greatly complicate its derivation.

For these reasons, we will use an approximate method of calculation of the electron density due to Raizer⁸² and described in detail in Appendix 2. This approximation rests on two assumptions. The first is the assumption that the ion number density n_m and the ionization potentials I_{m+1} are considered to be continuous functions of the ionic charge multiplicity m , obtained by connecting the discrete values of n_m and I_{m+1} by continuous curves. We denote these two continuous functions by $n(m)$ and $I(m)$ respectively. The second assumption is the approximation that the average value of the ionic charge multiplicity, also the average number of free electrons per original atom

$$\bar{m} = \frac{\int_m n(m) dm}{\int n(m) dm} = \frac{n_e}{n_g} \quad \dots (3.16)$$

is exactly equal to that value of m for which the ion distribution function $n(m)$ has a maximum. (In the above equation, \bar{m} is the average value of m , n_e is the electron density, n_g is the total heavy particle density).

As shown in Appendix 2, the above assumptions lead to the following simple transcendental equation in \bar{m} :

$$\bar{m}_g = A T_e^{3/2} \exp \left(- \frac{I(\bar{m} + \frac{1}{2})}{kT_e} \right) \quad \dots (3.17)$$

or,

$$\bar{I}(m) = I(\bar{m} + \frac{1}{2}) = kT_e \ln \left(\frac{A T_e^{3/2}}{\bar{m} n_g} \right) \quad \dots (3.18)$$

where

$$A = 2 \left(\frac{2\pi m_e k}{h^2} \right)^{3/2}$$

Because the right hand side is a logarithmic function of \bar{m} , two or three successive approximations are sufficient to obtain a fairly accurate value of \bar{m} , given the function $I(m)$. As shown in Appendix 2, the function $I(m)$ may be approximated quite accurately for the first four or five levels of argon by the expression

$$I(m) = 15 m \text{ electron-volts} \quad \dots (3.19)$$

3.1.5 System of Equations for Ionization Instability

In this section, we will present the equations necessary to derive the dispersion relation for ionization instability. Three equations are necessary, a generalized Ohm's Law or equation of motion, an energy conservation

or energy balance law for the electrons, and a relationship between n_e and the mean electron thermal energy (T_e), i.e., Raizer's approximation to the set of Saha equations.

i) Generalized Ohm's Law:

Spitzer¹⁰⁴ derives the following generalized Ohm's Law from the equations of motion for ions of charge +Z and electrons:

$$\frac{m_i m_e}{Z \rho e^2} \frac{\partial \vec{j}}{\partial t} = \vec{E}' + \vec{v} \times \vec{B} - \eta \vec{j} + \frac{1}{eZ\rho} \left(m_i \vec{\nabla} P_e - Zm_e \vec{\nabla} P_i - (m_i - Zm_e) \vec{j} \times \vec{B} \right) \dots (3.20)$$

where $\rho = n_i m_i + n_e m_e$ and η is the electrical resistivity.

The $(\partial \vec{j} / \partial t)$ term is negligible for times greater than a small fraction of a microsecond, that is, inertial effects are negligible^{105,94}.

Now, for $\eta = (m_e v / n_e e^2)^{106}$, the term $(m_i - Zm_e) (\vec{j} \times \vec{B}) / eZ\rho$ becomes $\eta (\omega / v) \vec{j} \times \vec{B} / B$, where ω is the electron cyclotron frequency. So, Ohm's Law becomes:

$$\vec{E}' + \vec{v} \times \vec{B} + \frac{1}{eZ\rho} \left(m_i \vec{\nabla} P_e - z m_e \vec{\nabla} P_i \right) \\ = n \left(\vec{j} + \vec{j} \times (\omega/v) (\vec{B}/B) \right)$$

Now, $P_e = n_e k T_e$ and $P_i = n_i k T_i$. Thus, $\vec{\nabla} P_e = k(n_e \vec{\nabla} T_e + T_e \vec{\nabla} n_e)$ and $\vec{\nabla} P_i = k(n_e \vec{\nabla} T_i + T_i \vec{\nabla} n_e)$. So, the term $(m_i \vec{\nabla} P_e - z m_e \vec{\nabla} P_i)/eZ\rho$ becomes, using the fact that $m_e \ll m_i$, $(k/e)(\vec{\nabla} T_e + T_e (\vec{\nabla} n_e/n_e))$. Thus, Ohm's Law becomes:

$$\sigma_0 \left[\vec{E} + \frac{k}{e} \left(\vec{\nabla} T_e + T_e \frac{\vec{\nabla} n_e}{n_e} \right) \right] \\ = \vec{j} + \vec{j} \times \frac{\omega \vec{B}}{v B} \quad \dots (3.21)$$

where $\sigma_0 = 1/n = n_e e^2 / m_e v$, and $\vec{E} = \vec{E}' + \vec{v} \times \vec{B}$ is the electric field seen in the frame of the moving gas.

ii) Energy balance law for electrons:

The electronic energy balance is obtained as a moment of the Boltzmann equation^{49,16}. The result is:

$$\frac{d}{dt} \left(n_e \varepsilon_e + n_e \varepsilon_i \right) = \vec{j} \cdot \vec{E} - n_e \Delta \varepsilon_e \quad \dots (3.22)$$

where ε_e is the mean electron thermal energy $(3kT_e/2)$.

ε_i is the ionization energy $\bar{I} = I(\bar{m} + \frac{1}{2})$. $\vec{j} \cdot \vec{E}$ is the energy input rate due to Joule heating. $n_e \Delta \varepsilon_e$ is the energy loss rate from the electrons and is equal to $2(m_e/m_a)n_e v(\varepsilon_e - \varepsilon_i) + n_e \Omega_r$ (see Sect. 3.1.1). Ω_r is the radiation loss which we have shown, in Section 3.1.3, to be negligible. v is the collision frequency for electron-ion collisions. So, the energy balance equation becomes:

$$\begin{aligned} (3k/2) (d(n_e T_e)/dt) + (n_e/n_g) (d\bar{I}/d\bar{m}) (dn_e/dt) \\ + \bar{I} (dn_e/dt) = \vec{j} \cdot \vec{E} - 2(m_e/m_a)n_e v(3k/2)(T_e - T_g) \end{aligned} \quad \dots (3.23)$$

iii) Raizer's approximation: relationship between n_e and the mean thermal energy.

Raizer's approximation gives (Section 3.1.4):

$$n_e = \bar{m} n_g = A T_e^{3/2} \exp \left(- \frac{I(\bar{m} + \frac{1}{2})}{kT_e} \right) \quad \dots (3.24)$$

We express this relation in differential form as follows:

$$d\bar{m} = (A/n_g) \exp(-\bar{I}/kT_e) \left(3T_e^{1/2}dT_e/2 + \bar{I}dT_e/kT_e^{1/2} - T_e^{1/2}d\bar{I}/k \right)$$

Dividing by the original expression and rearranging:

$$\left(1 + \frac{\bar{m}}{kT_e} \frac{d\bar{I}}{dm} \right) \frac{dm}{\bar{m}} = \left(\frac{3}{2} + \frac{\bar{I}}{kT_e} \right) \frac{dT_e}{T_e}$$

or, in terms of n_e :

$$\left(1 + \frac{n_e}{kT_e} \frac{d\bar{I}}{n_g dm} \right) \frac{dn_e}{n_e} = \left(\frac{3}{2} + \frac{\bar{I}}{kT_e} \right) \frac{dT_e}{T_e} \quad \dots (3.25)$$

3.1.6 Growth Rate of the Ionization Instability

In this section, we calculate the growth rate and the angular dependence of the growth rate of the ionization instability. We assume that small initial perturbations in the quantities n_e , \vec{E} , \vec{j} , and T_e are described as follows:

$$n_e = n_{eo} + n_{el} \exp(i\vec{k} \cdot \vec{r} + i\tilde{\omega}t) \quad \dots (3.26a)$$

$$\vec{E} = \vec{E}_0 + \vec{E}_1 \exp(i\vec{k} \cdot \vec{r} + i\tilde{\omega}t) \quad \dots (3.26b)$$

$$\vec{j} = \vec{j}_0 + \vec{j}_1 \exp(i\vec{k} \cdot \vec{r} + i\tilde{\omega}t) \quad \dots (3.26c)$$

$$T_e = T_{e0} + T_{el} \exp(i\vec{k} \cdot \vec{r} + i\tilde{\omega}t) \quad \dots (3.26d)$$

We assume that there is no component of \vec{j} or \vec{E} or variation of properties in the direction parallel to \vec{B} ; i.e., we assume that \vec{E} , \vec{j} , and all variations are co-planar and that \vec{B} is perpendicular to this plane. We neglect terms higher than first order. We take the electron collision frequency, ν , as given by equation (3.7). We take Z as the average ionic charge multiplicity, \bar{m} , defined in Section 3.1.4.

Inserting the assumed form of the perturbation, we have, to first order:

$$\tau = \nu^{-1} = \tau_0 + (3/2)\tau_0(T_{el}/T_{e0}) - \tau_0(n_{el}/n_{e0}) \quad \dots (3.27)$$

$$\nu = \tau^{-1} = \tau_0^{-1} + \tau_0^{-1}(n_{el}/n_{e0}) - (3/2)\tau_0^{-1}(T_{el}/T_{e0}) \quad \dots (3.28)$$

Now, since $\sigma = (n_e e^2 / m_e \nu)$, $\sigma \propto T_e^{3/2}$, and, to first order,

$$\sigma = \sigma_0 + (3/2)\sigma_0(T_{el}/T_{e0})$$

The generalized Ohm's Law (equation 3.21), neglecting the diffusion terms for the moment, becomes

$$\sigma \vec{E} = \vec{j} + \left(\omega \tau \vec{j} \times (\vec{B}/B) \right)$$

To zero'th order,

$$\sigma_0 \vec{E}_0 = \vec{j}_0 + \left(\omega \tau \vec{j} \times (\vec{B}/B) \right) \quad \dots (3.29)$$

To first order, and subtracting the zero'th order equation,

$$\begin{aligned} \sigma_0 \vec{E}_1 + \sigma_0 \vec{E}_0 (3T_{e1}/2T_{e0}) &= \vec{j}_1 + \left(\omega \tau_0 \vec{j}_1 \times (\vec{B}/B) \right) \\ + \omega \tau_0 \left((3T_{e1}/2T_{e0}) - (n_{e1}/n_{e0}) \right) \left(\vec{j}_0 \times (\vec{B}/B) \right) \\ \dots (3.30) \end{aligned}$$

The energy balance equation, eq. (3.23), is

$$\begin{aligned} (3kT_e/2) (dn_e/dt) + (3n_e k/2) (dT_e/dt) \\ + (n_e/n_g) (\bar{d}\bar{I}/d\bar{m}) (dn_e/dt) + \bar{I} (dn_e/dt) \\ = \vec{j} \cdot \vec{E} - 3k(m_e/m_a) (n_e/\tau) (T_e - T_g) \end{aligned}$$

To zero'th order,

$$\vec{j}_0 \cdot \vec{E}_0 = 3k(m_e/m_a)(n_{e0}/\tau_0)(T_{e0} - T_g) \dots (3.31)$$

To first order, and subtracting the zero'th order equation,

$$\begin{aligned} i\tilde{\omega} \left\{ (3k/2)n_{el}T_{e0} + (3k/2)n_{e0}T_{el} + \bar{I}n_{el} \right. \\ \left. + (d\bar{I}/d\bar{m})(n_{e0}n_{el}/n_g) \right\} = \vec{j}_1 \cdot \vec{E}_0 + \vec{j}_0 \cdot \vec{E}_1 \\ - 3k(m_e/m_a) \left\{ \frac{n_{e0}}{\tau_0} \left[\frac{n_{el}}{n_{e0}} - \frac{3T_{el}}{2T_{e0}} \right] [T_{e0} - T_g] \right. \\ \left. + (n_{e0}T_{el}/\tau_0) + (n_{el}/\tau_0)(T_{e0} - T_g) \right\} \dots (3.32) \end{aligned}$$

Note that including the diffusion terms in Ohm's Law would add imaginary terms to Ohm's Law and thus on the right hand side of equation (3.32), through the Joule heating terms $\vec{j}_1 \cdot \vec{E}_0$ and $\vec{j}_0 \cdot \vec{E}_1$. These terms would not affect the growth rate but would introduce a finite phase velocity (see references 34 and 72).

The ionization equilibrium expression, equation (3.25), becomes:

$$\left(1 + \frac{n_{e0}}{kT_{e0}} \frac{d\bar{I}}{n_g d\bar{m}} \right) \frac{n_{el}}{n_{e0}} = \left(\frac{3}{2} + \frac{\bar{I}}{kT_{e0}} \right) \frac{T_{el}}{T_{e0}} \dots (3.33)$$

We note also, from equation (3.25), that

$$\frac{d \ln T_e}{d \ln n_e} = \frac{\left[1 + \frac{n_{e0}}{kT_{e0}} \frac{d\bar{I}}{n_g d\bar{m}} \right]}{\left[\frac{3}{2} + \frac{\bar{I}}{kT_{e0}} \right]} = \frac{(T_{el}/T_{e0})}{(n_{el}/n_{e0})} \dots (3.34)$$

We need two more conditions in order to eliminate the first-order quantities from the dispersion relation, equation (3.32). We shall exclude electromagnetic wave propagation from consideration and take the applied field, B , as being constant in time. Thus,

$$\text{curl } \vec{E} = 0 \dots (3.35)$$

We also make the plasma approximation that there is no net charge density and thus,

$$\text{div } \vec{j} = 0 \dots (3.36)$$

We now use equations (3.29), (3.30), (3.31), (3.33), (3.34), (3.35), and (3.36) to eliminate the first order quantities from the dispersion relation (see Appendix 3 for a detailed description). The expression for the growth rate as given in Appendix 3 is then:

$$\begin{aligned}
 \gamma \equiv \omega \tilde{\omega} = & \frac{j_0^2}{\sigma_0 n_{e0} \bar{I}} \left\{ \frac{3}{2} \frac{d \ln T_e}{d \ln n_e} (\sin^2 \phi - \cos^2 \phi) \right. \\
 & \left. + 2 \omega \tau_0 \sin \phi \cos \phi - 2 + \frac{3}{2} \frac{d \ln T_e}{d \ln n_e} - \frac{T_{e0}}{T_{e0} - T_g} \frac{d \ln T_e}{d \ln n_e} \right\} \cdot \\
 & \cdot \left\{ \frac{3}{2} \frac{k T_{e0}}{\bar{I}} \left[1 + \frac{d \ln T_e}{d \ln n_e} \right] + \frac{n_{e0}}{n_g} \frac{1}{\bar{I}} \frac{d \bar{I}}{d \bar{m}} + 1 \right\}^{-1} \quad \dots (3.37)
 \end{aligned}$$

where $(\pi/2) - \phi$ is the angle between the perturbed current, j_1 , and the unperturbed current, j_0 . $(d \ln T_e / d \ln n_e)$ is given by equation (3.34). $\bar{I} = I(\bar{m} + \frac{1}{2})$, where \bar{m} is the average ionic charge from equation (3.18). $(d \bar{I} / d \bar{m})$ is given by :

$$\frac{d \bar{I}}{d \bar{m}} = \frac{d \bar{I} (\bar{m} + \frac{1}{2})}{d \bar{m}} = \frac{d}{d \bar{m}} \left[15 \bar{m} + 7.5 \right] = 15 \text{ eV.}$$

for argon (see Section 3.1.4).

j_0^2/σ_0 is the Joule dissipation in the gas (see equation 3.2). $\omega\tau_0$ is the Hall parameter and σ_0 is the scalar conductivity calculated using the electron temperature T_{e0} and the average ionic charge multiplicity \bar{m} .

As shown in Appendix 3, the angle ϕ for which the growth rate is a maximum is given by:

$$\left[\frac{\pi}{2} - \phi \right] = \frac{1}{2} \tan^{-1} \left[\frac{\omega\tau_0}{\frac{3 \operatorname{dln} T_e}{2 \operatorname{dln} n_e}} \right] \quad \dots (3.38)$$

Using this value of ϕ in the growth rate expression, equation (3.37), one obtains:

$$\begin{aligned} \gamma_{\max} &= \frac{j_0^2}{\sigma_0 n_{e0} \bar{I}} \left\{ \sqrt{\left(\omega\tau_0 \right)^2 + \left(\frac{3 \operatorname{dln} T_e}{2 \operatorname{dln} n_e} \right)^2} - 2 \right. \\ &+ \left. \frac{3 \operatorname{dln} T_e}{2 \operatorname{dln} n_e} - \frac{T_{e0}}{T_{e0} - T_g} \frac{\operatorname{dln} T_e}{\operatorname{dln} n_e} \right\} \\ &\cdot \left\{ \frac{3 k T_{e0}}{2 \bar{I}} \left(1 + \frac{\operatorname{dln} T_e}{\operatorname{dln} n_e} \right) + \frac{n_{e0}}{n_g} \frac{1}{\bar{I}} \frac{d\bar{I}}{dm} + 1 \right\}^{-1} \end{aligned} \quad \dots (3.39)$$

We see that the growth rate increases with increasing $\omega\tau_0$ and also depends on the relation between equilibrium electron density and electron temperature through the term $(d\ln T_e)/(d\ln n_e)$.

We also note the dependence on the temperature difference between the electrons and heavy particles, through the term $T_{e0}/(T_{e0}-T_g)$. As T_{e0} approaches T_g , the growth rate becomes strongly negative, and any perturbation will be quickly damped.

3.1.7 Physical Mechanism of the Ionization Instability

The following physical explanation of the ionization instability is due to Nedospasov⁷³. The physical mechanism can be understood by considering the fluctuation of the Joule heating connected with the fluctuation of the plasma density.

Let us assume that in the shaded region of the figure (Figure 3.2), the electron density is larger than in the surrounding space by a small amount δn_e . We assume that the main current is directed along the y-axis and the magnetic field is perpendicular to the plane of the figure and directed out of the page.

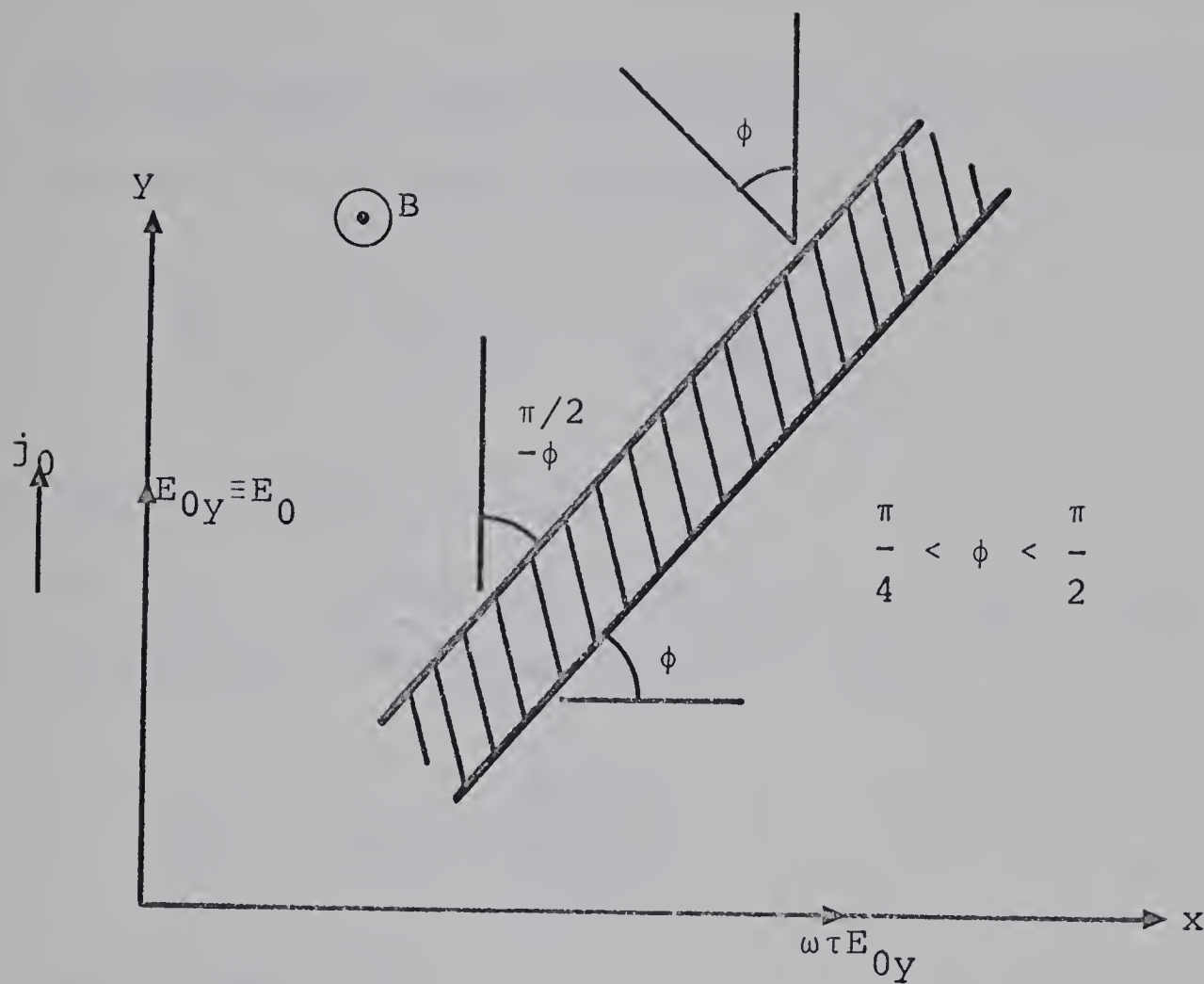


Figure 3.2

From the generalized Ohm's Law, we have:

$$\frac{E_{0x}}{E_{0y}} = \omega\tau$$

For simplicity, we neglect the fluctuations of τ . The component of current normal to the streamer is conserved⁸⁵ since we take $\text{div } \vec{j} = 0$. Therefore, electric charges appear on the boundary of the streamer and change the electric field inside the streamer. We note that the tangential field cannot change⁸⁶ since we take $\text{curl } \vec{E} = 0$

The additional power released in a unit volume of the streamer due to Joule heating is

$$\delta W_{jh} = \delta j_{||} E_{O||} + j_{O\perp} \delta E_{\perp} ,$$

since $\delta E_{||} = 0$ and $\delta j_{\perp} = 0$.

Now, $\delta j_{||} = j_{O||} (\delta n_e / n_e)$ since $j_{||} \propto n_e$ ($j_{||} = e n_e v_{||}$) and, from Figure 3.2, $j_{O||} = j_o \sin \phi$. So,

$$\delta j_{||} = j_o \sin \phi \left(\frac{\delta n_e}{n_e} \right).$$

Now, from Figure 3.2,

$$E_{O||} = E_{Oy} \sin \phi + \omega \tau E_{Oy} \cos \phi ,$$

and $E_{Oy} = j_o / \sigma$ from the generalized Ohm's Law in the absence of Hall currents. So,

$$E_{O||} = \frac{j_o}{\sigma} \left(\sin \phi + \omega \tau \cos \phi \right) .$$

From Figure 3.2, $j_{O\perp} = j_o \cos \phi$. Also, since $E_{\perp} \propto 1/\sigma$ for j_{\perp} constant and $\sigma \propto n_e$, then $E_{\perp} \propto 1/n_e$.

Thus, $\delta E_{\perp} = -E_{0\perp} (\delta n_e / n_e)$. From Figure 3.2,

$$E_{0\perp} = E_{0y} \cos \phi - \omega \tau E_{0y} \sin \phi$$

and $E_{0y} = j_o / \sigma$ as above. So,

$$E_{0\perp} = \frac{j_o}{\sigma} \left(\cos \phi - \omega \tau \sin \phi \right)$$

and

$$\delta E_{\perp} = \frac{j_o}{\sigma} \left(\omega \tau \sin \phi - \cos \phi \right) \frac{\delta n_e}{n_e}$$

Thus,

$$\begin{aligned} \delta W_{jh} &= \left(j_o \sin \phi \frac{\delta n_e}{n_e} \right) \frac{j_o}{\sigma} \left(\sin \phi + \omega \tau \cos \phi \right) \\ &+ \left(j_o \cos \phi \right) \frac{j_o}{\sigma} \left(\omega \tau \sin \phi - \cos \phi \right) \frac{\delta n_e}{n_e} \end{aligned}$$

Simplifying,

$$\delta W_{jh} = \frac{j_o^2}{\sigma} \left(\sin^2 \phi - \cos^2 \phi + 2 \omega \tau \sin \phi \cos \phi \right) \frac{\delta n_e}{n_e}$$

Now, the increase in the energy lost due to collisions with the gas atoms is

$$\delta W_C = \frac{j_0^2}{\sigma} \left(\frac{\delta n_e}{n_e} + \frac{\delta T_e}{T_e} \right) ,$$

since the loss rate is proportional to both n_e and $T_e - T_g$ or simply T_e if T_e is large, (again, we neglect the fluctuations of τ with δT_e and δn_e).

Thus, we see that in a streamer with $\delta n_e > 0$, the increase in the energy released due to Joule heating can exceed the increase in the energy lost to collisions with the heavy particles. This will occur for values of $\omega\tau$ above a certain value. The condition $\delta W_{jh} > \delta W_C$ also depends on the relation between $\delta n_e/n_e$ and $\delta T_e/T_e$. The greater the quantity

$$\frac{\delta n_e/n_e}{\delta T_e/T_e} \quad \text{or} \quad \frac{\delta \ln n_e}{\delta \ln T_e} ,$$

the more δW_{jh} exceeds δW_C . The angular dependence of the instability can also be seen. It is easily shown that δW_{jh} is a maximum for an angle ϕ of $\frac{1}{2}\tan^{-1}\omega\tau$ which approaches $\pi/4$ for $\omega\tau$ large.

In summary, we see that the instability occurs via the following mechanism: in a streamer with $\delta n_e > 0$, the increase in the electron energy due to Joule heating can exceed the increase in the energy lost due to collisions with the heavy particles. This in turn increases T_e and the degree of ionization, leading to a further deviation of the electron density from the equilibrium value.

The neglect of the fluctuations in collision frequency is not, strictly speaking, justifiable in the Coulomb collision dominated regime. However, the inclusion of the collision frequency fluctuations leads to the same qualitative result.

3.2 Application of Theory to Experiment

3.2.1 Calculation of the Plasma Parameters for Partially Ionized, Shock Heated Argon

To obtain the steady state plasma parameters (n_e , T_e , $\omega\tau$, σ , $(d\ln T_e)/(d\ln n_e)$) needed to calculate the growth rate and critical angle, ϕ_{\max} , the following equations were solved numerically:

$$\sigma_0 \vec{E}_O = \vec{j}_O + \omega\tau_0 \vec{j}_O \times (\vec{B}/B) \quad \dots (3.29)$$

$$\vec{j}_O \cdot \vec{E}_O = 2 \frac{m_e}{m_a} \frac{n_{eo}}{\tau_0} \frac{3k}{2} (T_{eo} - T_g) \quad \dots (3.31)$$

$$n_{eo} = \bar{m} n_g = A T_{eo}^{3/2} \exp \left[- \frac{I(\bar{m} + \frac{1}{2})}{kT_{eo}} \right] \quad \dots (3.24)$$

$$\vec{j}_O \cdot \vec{E}_O = \sigma_0 E_Y^2 = j_O^2 / \sigma_0 \quad \dots (3.2)$$

If one neglects electrode loss and the potential drop across the (very small) external resistance, E_Y , the electric field in the gas (see Figure 3.1) should be equal to $u_2 B$. However, electrode losses can be appreciable. To eliminate this inaccuracy, the measured values

of E_y were used in the calculations. Specifically, it was found that the measured values of E_y were closely approximated by the function

$$E_y = u_2 B \exp \left[-\frac{B}{B_1} \right] \quad \dots (3.40)$$

where $B_1 = 0.812 \text{ w/m}^2$ (see Figure 3.3).

The initial values of plasma density, n_g , and temperature, T_g , of the shock heated gas were taken from de Leeuw⁵⁹ and are given in Table 3.1.

Figure 3.3(a) shows calculated curves of electron temperature versus magnetic field strength. The maximum in T_e and the subsequent decrease with increasing B is due to the decrease in the measured values of E_y with increasing magnetic field (Figure 3.3). This has the effect of introducing a maximum in the Joule heating rate and consequently a maximum in the electron temperature through equation (3.31).

The steady state temperature was not measured directly in this work, partly because the onset of the instability is so rapid as to render very difficult any observation of the steady state conditions. However, Vasil'eva et al^{111,112} have measured the electron temperature in shock heated argon moving into a magnetic field. They used a Mach 8.5 shock propagating into argon at 10 mm Hg

initial pressure and in the presence of a magnetic field of from 3000 to 6000 gauss. Due to the higher gas pressures used, their Hall parameter was below the critical value for instability. They were thus able to observe a steady state electron temperature and their measurements are shown in Figure 3.3(a). Their measured values lie below the calculated curves; however, they observe substantial nonequilibrium. The reason for the lower measured values is the larger collision frequency (due to higher pressure) under the conditions of their experiment. Thus, the transfer of energy from electrons to ions is more efficient and, for a constant Joule heating rate, the gas cannot support as large an energy non-equipartition.

3.2.2 Variation of Hall Parameter with Applied Magnetic Field

Calculations based on equations (3.29), (3.31), (3.24), (3.2), and (3.40) give the change in the plasma parameters with increasing magnetic field. Figure 3.4 gives the variation of the Hall parameter, $\omega\tau$, with magnetic field. We see that $\omega\tau$ increases with increasing B . Thus, from equation (3.39), the growth rate of the ionization instability will increase with increasing B . We also note that

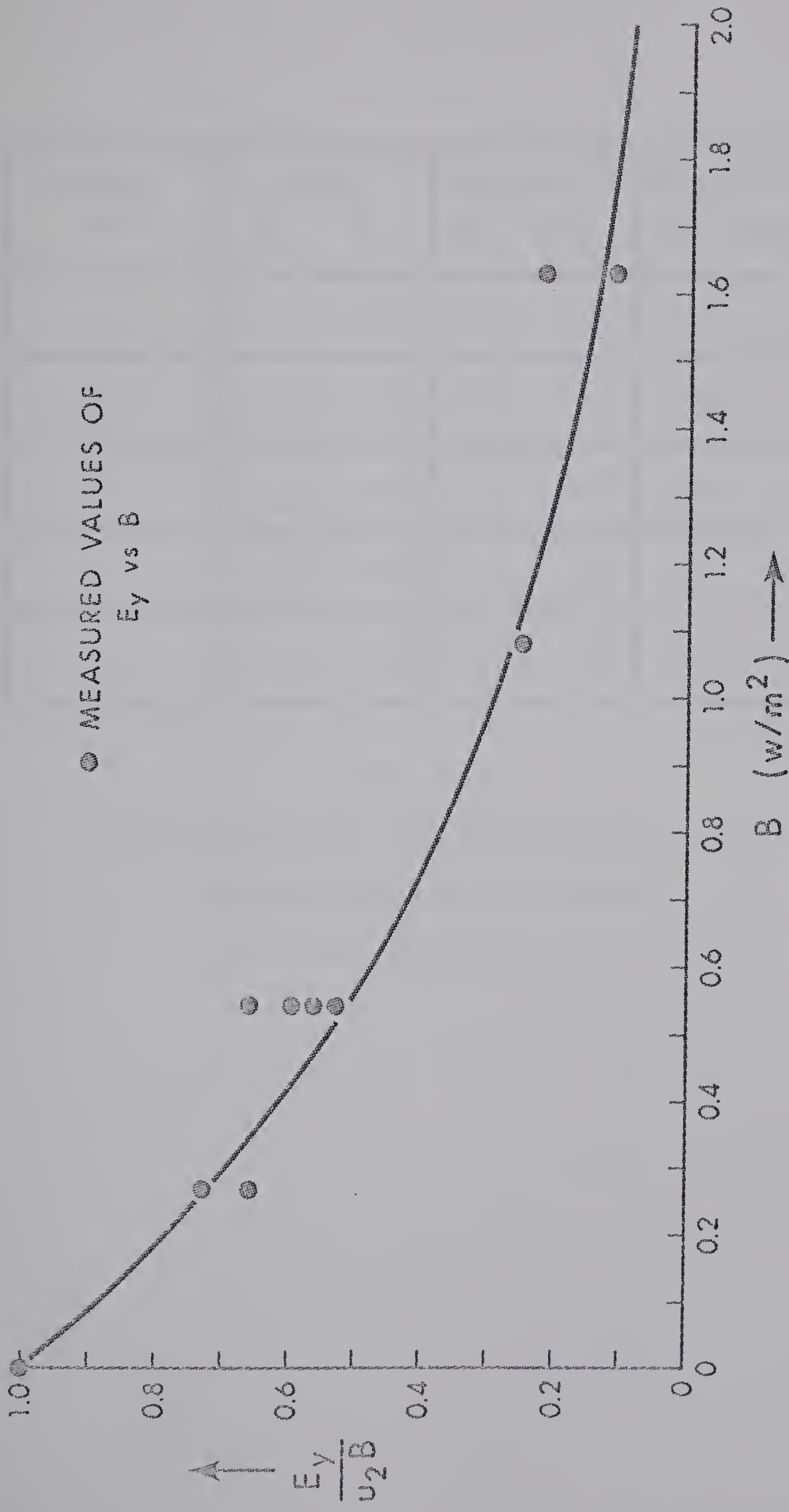


Figure 3.3
 Variation of E_y with Applied Magnetic Field

MACH NO.	TEMP. T_G , °K	DENSITY N_G , M^{-3}	VELOCITY U_2 , M/SEC
8	6.24×10^3	6.16×10^{22}	1.95×10^3
10	8.64×10^3	7.18×10^{22}	2.56×10^3
12	9.90×10^3	9.22×10^{22}	3.27×10^3
14	1.08×10^4	1.14×10^{23}	3.97×10^3
16	1.15×10^4	1.36×10^{23}	4.66×10^3

Table 3.1
Plasma Parameters for Shock Heated Argon
(thermal equilibrium assumed;
initial Ar pressure is 0.5 torr)

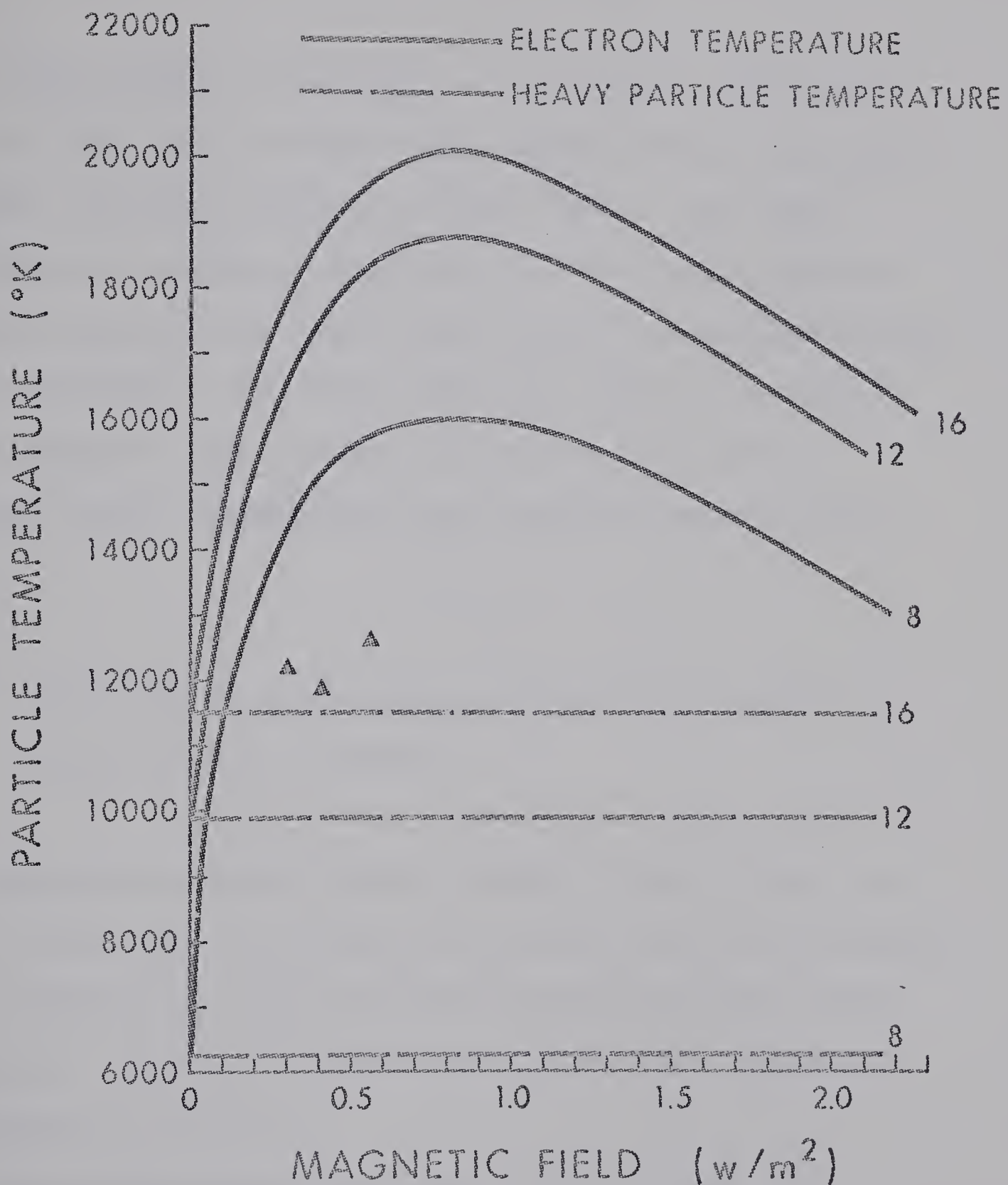


Figure 3.3(a)

Electron Temperature vs.
Magnetic Field Strength for
Various Shock Mach Numbers

(▲ Measurements of Vasil'eva et al)

as the Mach number is reduced, $\omega\tau$ increases. This reflects the fact that at lower Mach numbers, the temperature is lower, electron density is lower, and τ , the mean free time for electron collisions, is then much greater. Thus, we see that the growth rate of the ionization instability increases as the Mach number is reduced, at least in the range of Mach numbers considered here, for a constant initial temperature and pressure ahead of the shock.

3.2.3 Variation of Growth Rate with Applied Magnetic Field and Hall Parameter

Equations (3.29), (3.31), (3.24), (3.2), (3.40), and (3.39) allow one to calculate the growth rate of the ionization instability versus magnetic field and versus Hall parameter. Results of these calculations are presented in Figures 3.5 and 3.6.

We see from Figures 3.5 and 3.6 that there is a critical magnetic field and a critical Hall parameter above which the growth rate for the instability is positive. The critical magnetic field is between 0.4 and 1.4 webers/ m^2 and increases with the Mach number of the argon shock wave. The reason for the increase of the critical field

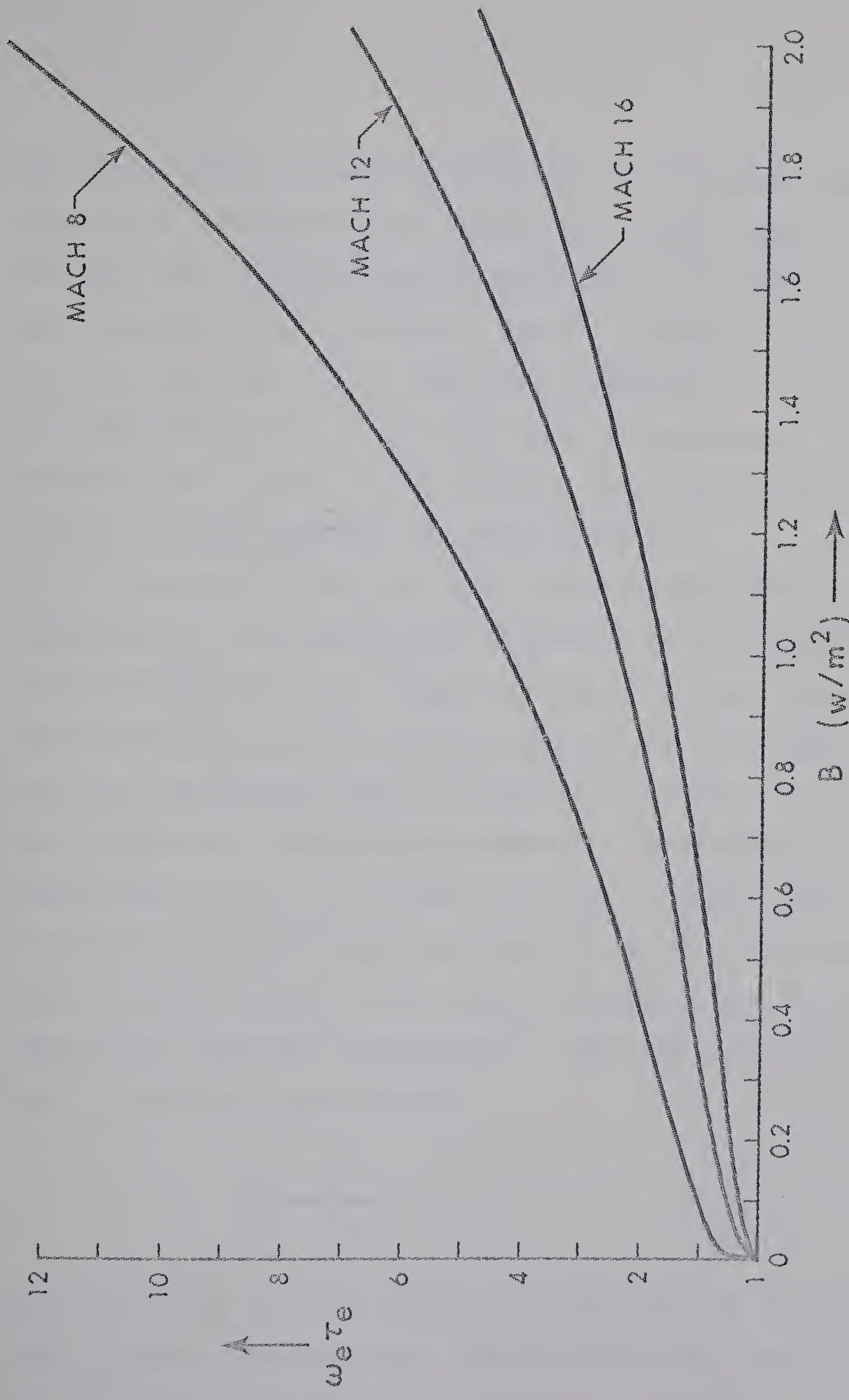


Figure 3.4
Variation of Hall Parameter with Magnetic Field Strength

with Mach number is that at the higher Mach numbers, the equilibrium temperature and density are higher, thus τ , the mean free time for electron collisions, is lower and a greater value of magnetic field is needed to produce the same value of $\omega\tau$, the Hall parameter.

From Figure 3.6, we see that the critical Hall parameter has a value in the range of two to three and is only slightly dependent on shock velocity.

In Figures 3.7 and 3.8, the e-folding time (the reciprocal of the growth rate) is plotted versus magnetic field strength for argon heated by a Mach 12 shock wave. Measurements were made of the e-folding time from image converter photographs made as described in Chapter 2. The length of an individual streamer was assumed to be proportional to $\exp(t/\chi)$ where χ is the e-folding time. The length of the streamer was measured at two different times (corresponding to two adjacent frames of the five-frame image converter photographs). Then the e-folding time is given by the expression

$$\chi = \frac{t_2 - t_1}{\ln(L_2/L_1)}$$

where L_2 and L_1 are the streamer lengths measured at the times t_2 and t_1 respectively. Measurements made in this

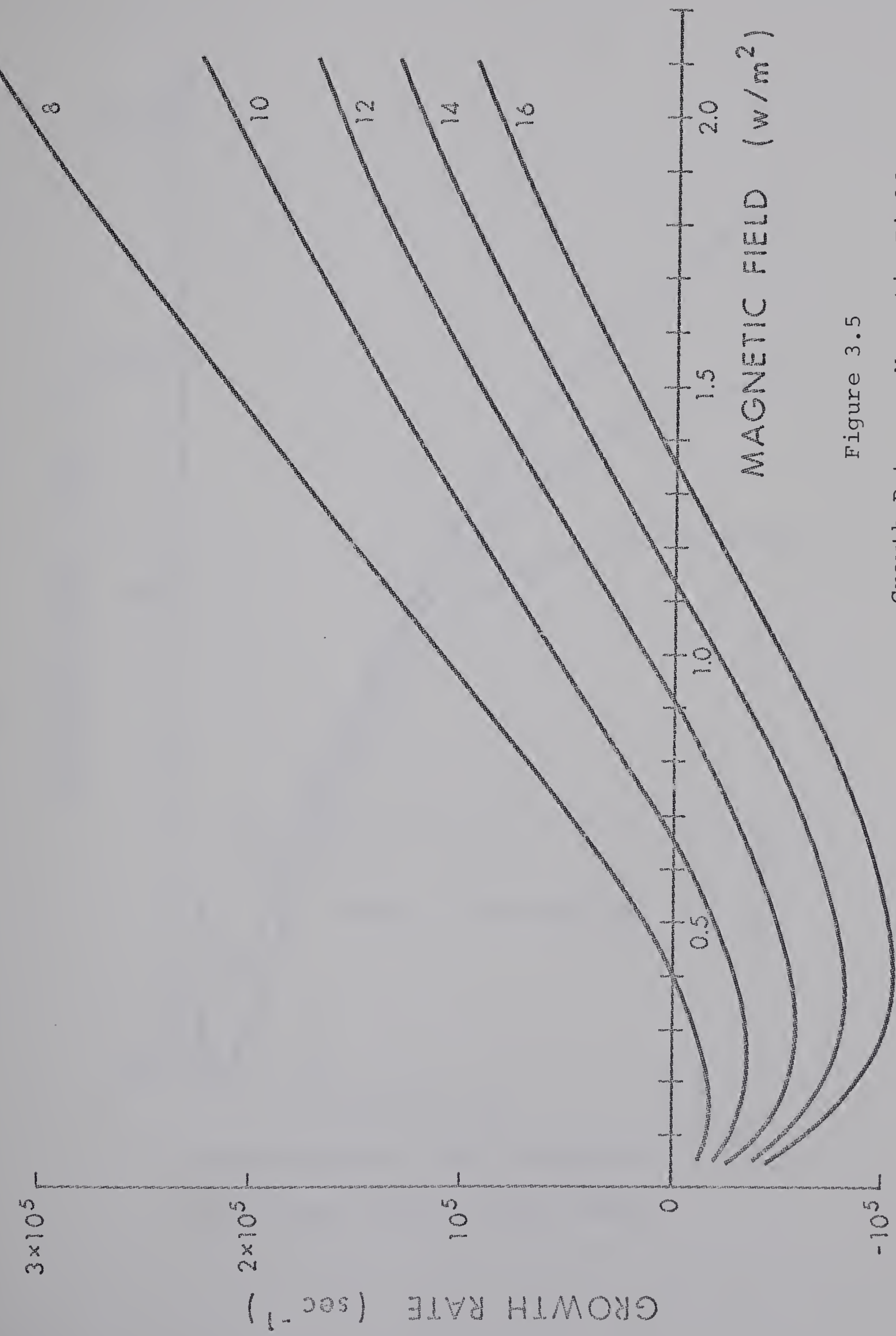


Figure 3.5

Growth Rate vs. Magnetic Field
for Various Values of Mach Number

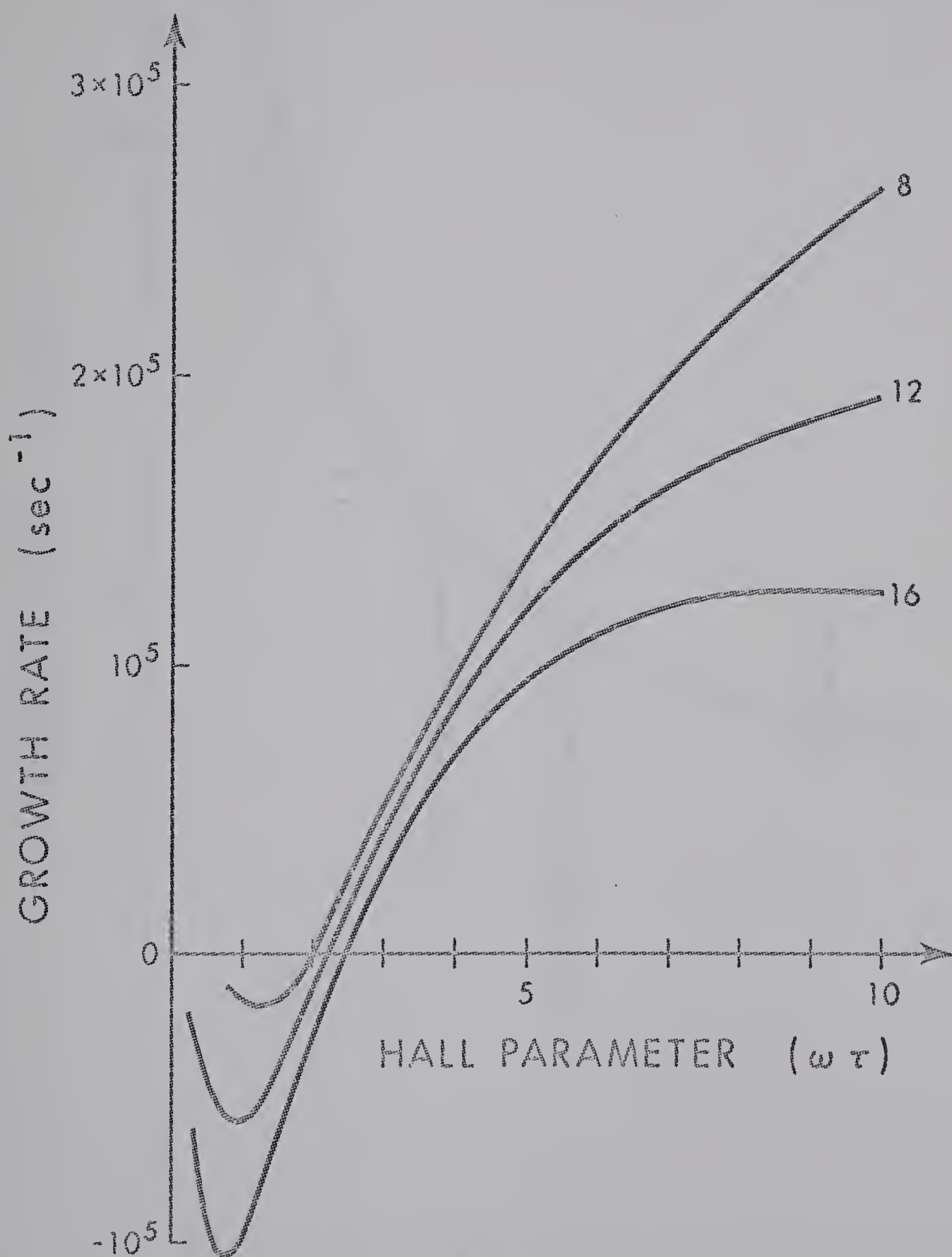


Figure 3.6
Growth Rate vs. Hall Parameter
for Various Values of Mach Number

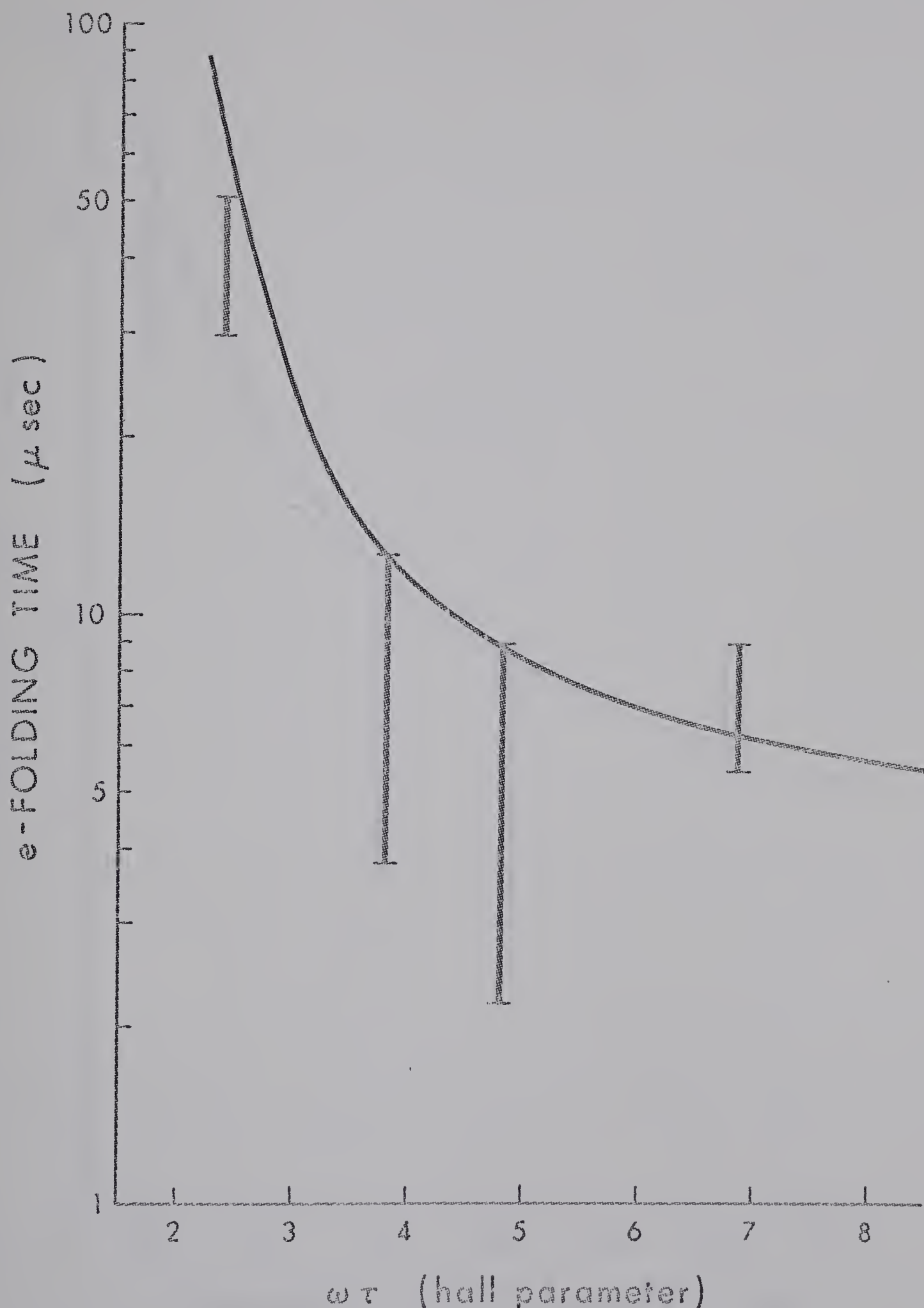


Figure 3.7

e-Folding Time vs. Hall Parameter

for a Mach 12 Argon Shock

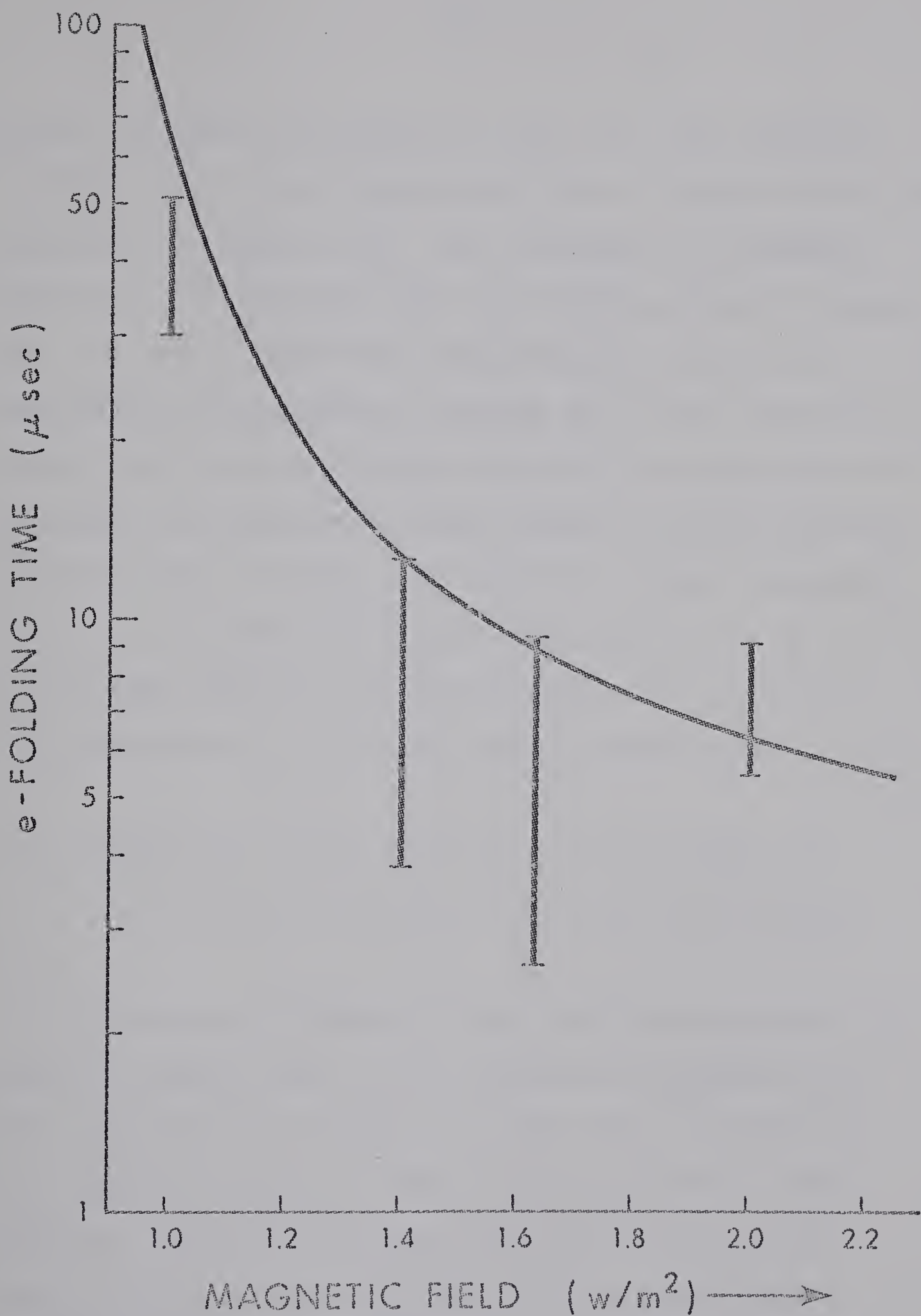


Figure 3.8
e-Folding Time vs. Magnetic Field Strength

for a Mach 12 Argon Shock

manner are shown on Figures 3.7 and 3.8. The measured e-folding time is well within an order of magnitude of the predicted e-folding time. This agreement is somewhat fortuitous in the sense that the theory predicts a growth rate for small, plane wave perturbations whereas the experimental measurements are made on a large amplitude, highly non-linear disturbance wherein the growth rate is certainly influenced to a large extent by such things as convective heat transfer and radiative energy transport. However, one would still expect the growth rate to be of the same order as that predicted by the theory and this expectation is borne out by the measurements.

3.2.4 Variation of the Critical Magnetic Field and Critical Hall Parameter with Shock Mach Number

The values of magnetic field and Hall parameter for which the growth rate of the ionization instability is zero are plotted in Figures 3.9 and 3.10. In addition, the values of magnetic field and Hall parameter which produce a positive e-folding time equal to the flow duration time of the shock heated gas are plotted.

Data obtained from the experiments with shock heated argon as described in Chapter 2 are also plotted. Figures 3.9 and 3.10 show clearly that the theory correctly predicts the onset of the instability.

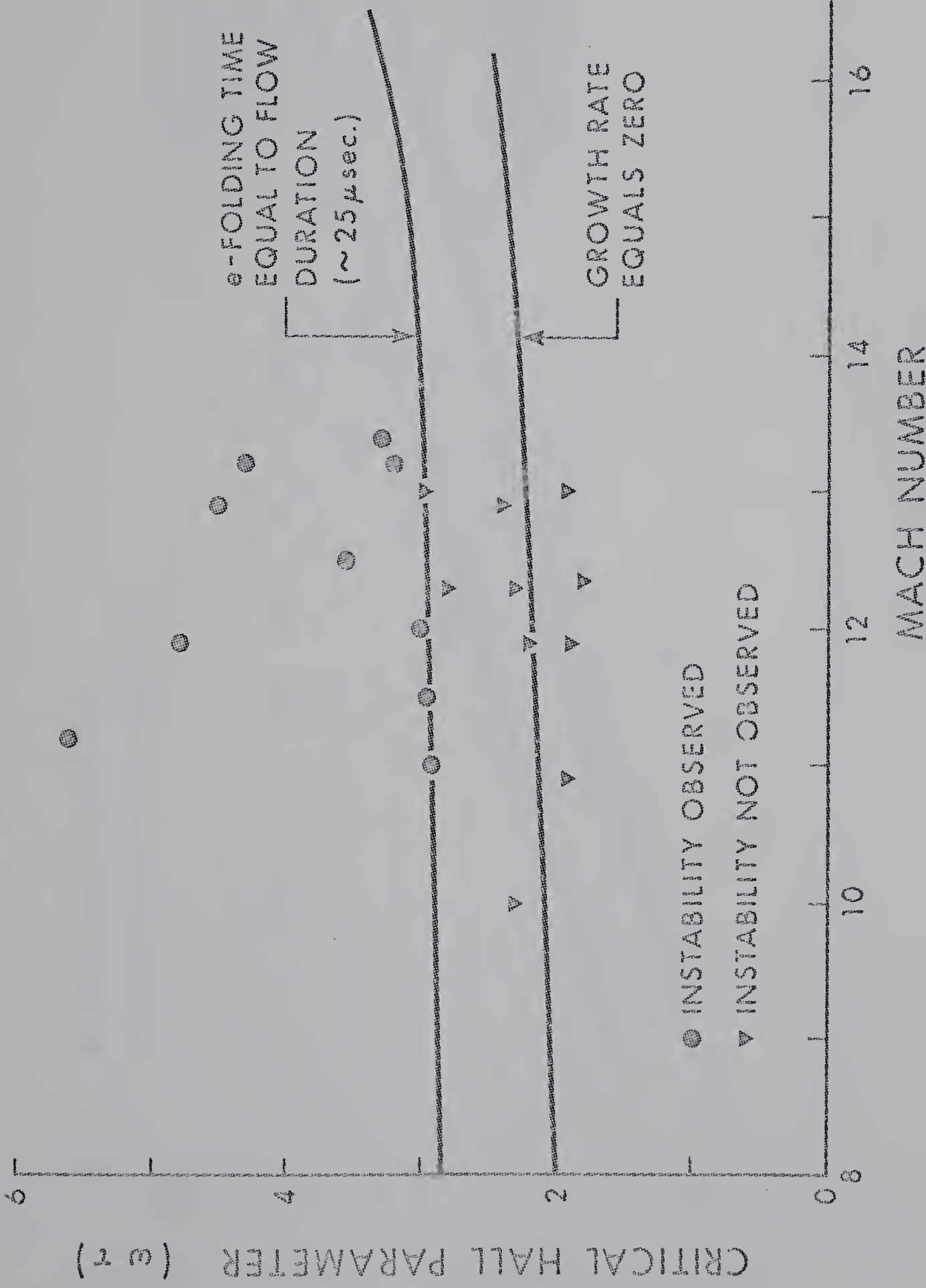


Figure 3.9
Critical Hall Parameter for Instability Growth

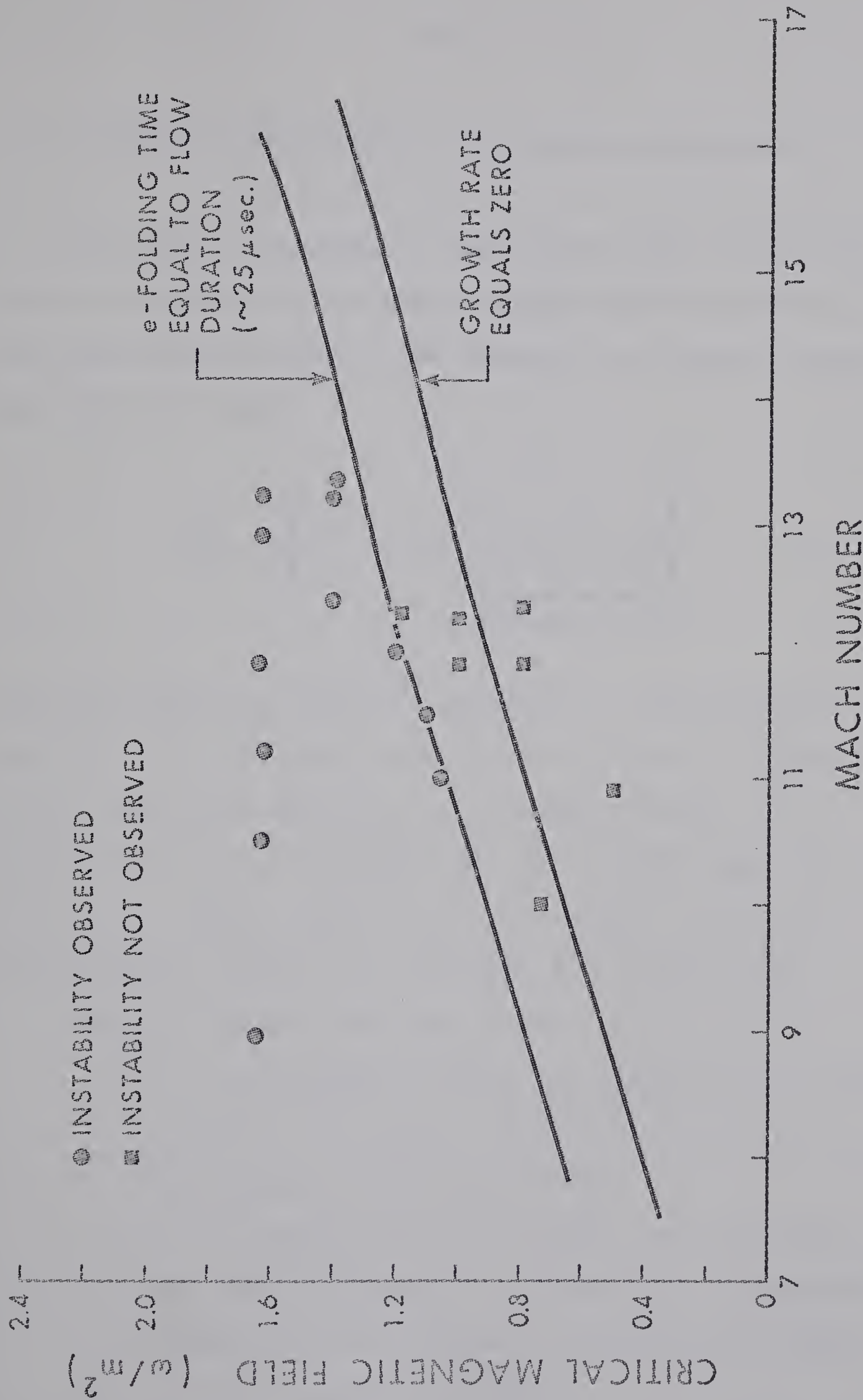


Figure 3.10 Critical Magnetic Field for Instability Growth

3.2.5 Angular Dependence of the Streamer Formation

As shown in Appendix 3, the growth rate of the ionization instability has an angular dependence relative to the unperturbed current. The direction of maximum growth rate is at an angle

$$\alpha \equiv \left(\frac{\pi}{2} - \phi \right) = \frac{1}{2} \tan^{-1} \left[\frac{\omega \tau_0}{\frac{3 d \ln T_e}{2 d \ln n_e}} \right] \quad \dots \text{(A.3.36)}$$

where the value of the \tan^{-1} function is taken between 0 and $\pi/2$. α is the angle between the average or unperturbed current and the instability or streamer current. In Appendix 3, it is also shown that the streamer may be produced on either side of the main current j_o at the characteristic angle α (see Figures A.3.1 and A.3.2).

Thus, the theory indicates that:

- 1) the streamers should be oriented at an angle α to the main current (the main current is in the Faraday or $\vec{v} \times \vec{B}$ direction).
- 2) as pointed out by Gilpin²⁸, the streamers will tend to break up at higher Hall parameters, forming smaller streamers inclined at an angle α to the original streamer.

Using the experimental arrangement described in Chapter 2, photographs were made of the discharge structure in the center of the magnetic field region as the shock heated gas passed through the magnetic field. Figure 3.11(a), a sequence of photos separated in time by 2 μ sec., shows the structure formation. In particular, the third frame shows a number of parallel streamers oriented at an angle of about 40 degrees to the $\vec{v} \times \vec{B}$ direction. This agrees with the theoretically calculated behavior (see Figures 3.13 and 3.14). As the structure develops, one streamer appears to predominate, conducting most of the current in one channel or arc (see frames 4 and 5 of Figure 3.11(a)). The structure of the streamers then becomes oriented primarily along the Faraday or $\vec{v} \times \vec{B}$ direction, (see Figure 3.11(b)). This orientation has been observed previously^{31,66} by workers at the Kurchatov Institute in the USSR using a low temperature, seeded plasma. This change in orientation as the structure develops is very likely due to the imposition of boundary conditions on the plasma in the experimental configuration, i.e., to the fact that the streamer current is constrained to flow primarily in the $\vec{v} \times \vec{B}$ direction because of the electrode configuration. This fact is not taken

into account in the theory presented in Section 3.1, since the streamers are assumed to be small perturbations to the main, uniform $\vec{v} \times \vec{B}$ current. The theory will cease to describe the exact physical situation when the perturbation or streamer current becomes large compared to the main current.

Figure 3.11(b) clearly shows the breakup of the current filaments or streamers, forming smaller streamers at an angle to the original, as predicted by Gilpin²⁸. As shown in Figure 3.12, the smaller streamers form at an angle to the main streamer of about 40 degrees.

The angle α , between the perturbed current and the original current, was calculated as described in Section 3.2.1. Figure 3.13 gives curves of the angle versus magnetic field for various shock Mach numbers. Figure 3.14 shows data taken from a large number of image converter photographs of the streamer structure. The solid curve is the theoretical curve for initial gas conditions produced by a Mach 12 shock wave propagating into argon at 0.5 torr initial pressure.



Figure 3.11(a)

Image Converter Photographs
of the Discharge Structure
in the Center of the Magnetic Field Region

Exposure duration = 0.2 μ sec.

Time between exposures = 2 μ sec.

Shock Mach No. = 12

Magnetic Field Strength = 1.6 w/m²

Hall Parameter = 4.8



Figure 3.11(b)

Image Converter Photographs

of the Discharge Structure

in the Center of the Magnetic Field Region

Exposure duration = 0.1 μ sec.

Time between exposures = 1 μ sec.

Shock Mach No. = 12

Magnetic Field Strength = 1.6 w/m²

Hall Parameter = 4.8

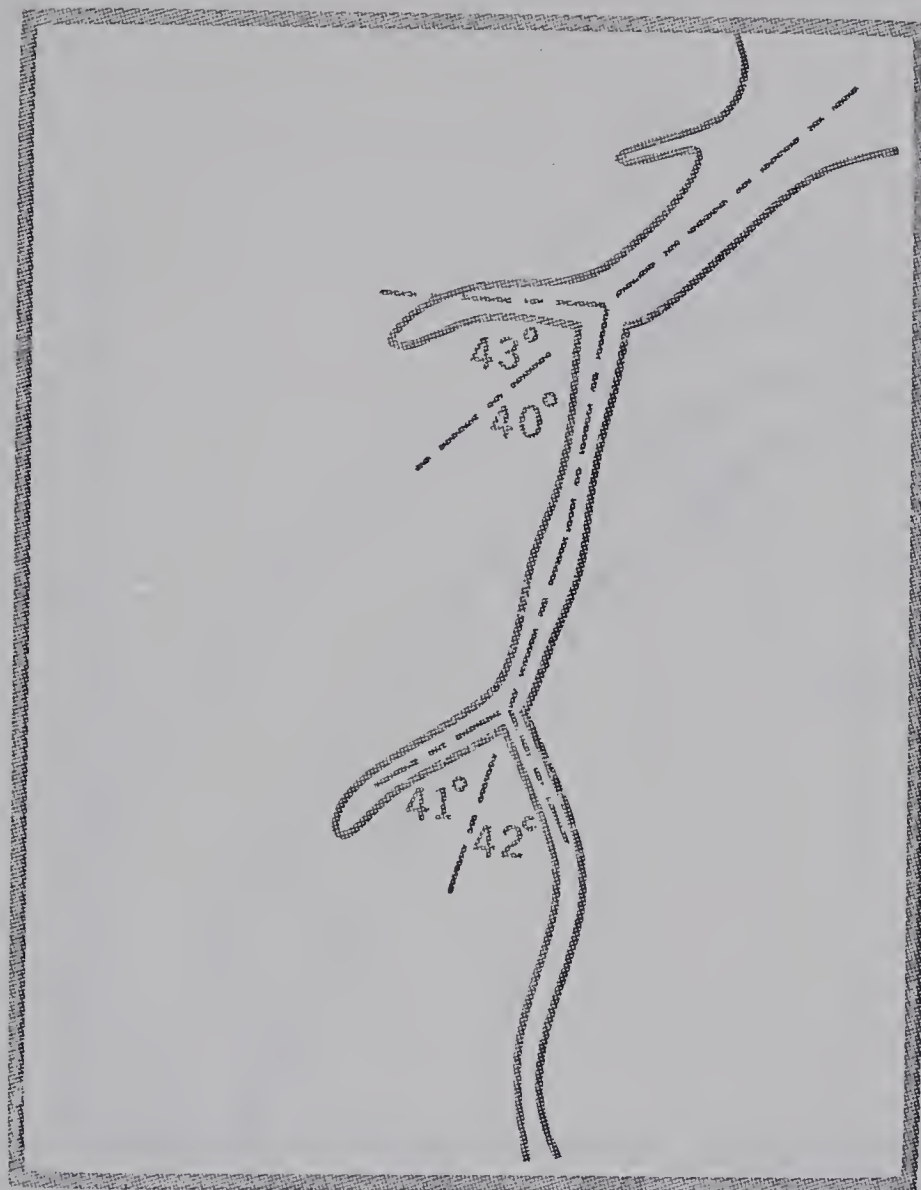


Figure 3.12

Drawing of Frame #1 of Figure 3.11(b),
taken from the original Polaroid photograph

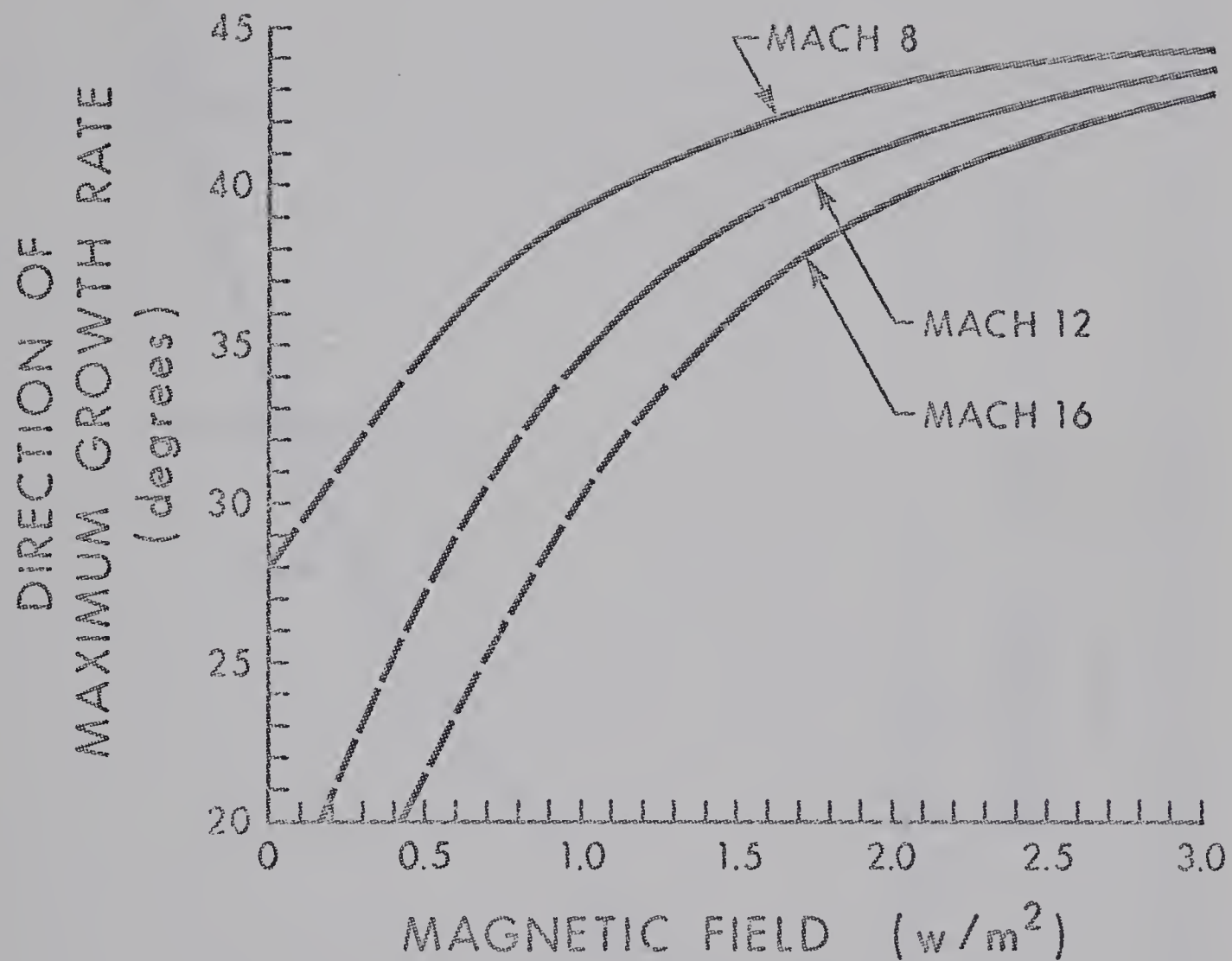


Figure 3.13
Angle between Perturbation Current
and Original Current
vs. Magnetic Field

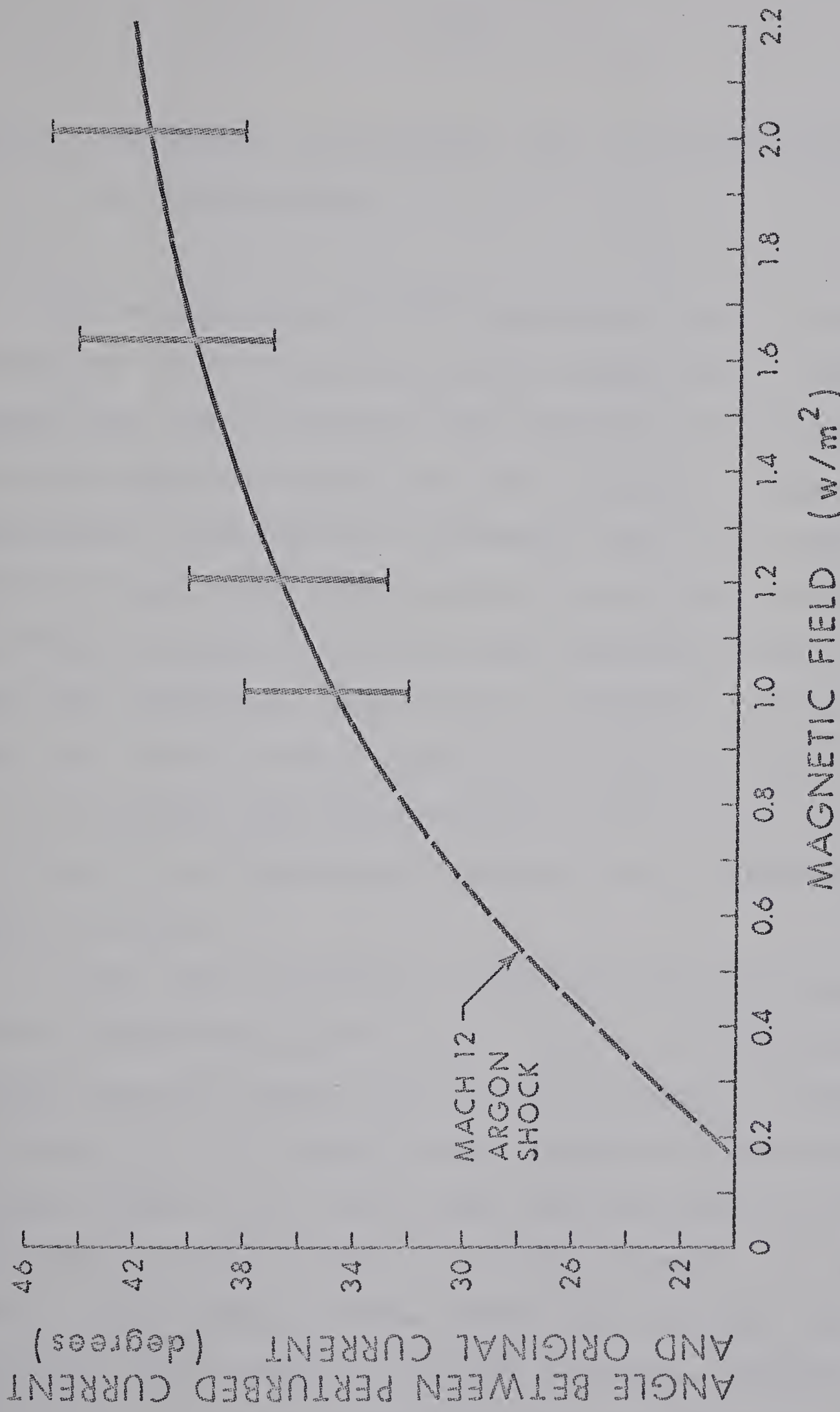


Figure 3.14
Angle between Perturbation Current and Original Current vs. Magnetic Field

3.2.6 Development of Turbulence with Increasing Values of Hall Parameter

It has been observed^{7,101} by workers using a pulsed discharge in low temperature argon seeded with an alkali metal that, with increasing Hall parameter, the discharge becomes highly structured and very turbulent. Workers observing a discharge in a supersonic flow of low temperature argon seeded with traces of sodium have reported^{31,66} a similar increase in structure and turbulence with increasing Hall parameter. Specifically, Malikov⁶⁶ has observed that for small $\omega\tau$ two or three broad pinches develop. As $\omega\tau$ is increased, the characteristics become finer and for $\omega\tau$ from 15 to 20 each pinch decomposes into a system of finer filaments.

A very similar behavior is observed under the experimental conditions reported here. Figure 3.15 shows photographs taken for three values of Hall parameter. Figure 3.15(a), ($\omega\tau \approx 3$), shows a single somewhat diffuse pinch. Figure 3.15(b), ($\omega\tau \approx 4.8$), shows the main pinch or streamer splitting up into a number of smaller streamers. In addition, two secondary pinches extend from the upper electrode and split into a number of smaller streamers. Figure 3.15(c), ($\omega\tau \approx 6.8$), shows a great deal of internal

structure to the main streamers. The turbulence inside the main streamer causes the streamer to broaden. The last frame of Figure 3.15(c) shows a general turbulence and brightening extending into the background gas. Thus, it can be seen that an increase in Hall parameter is correlated with an increase in structure and turbulence of the discharge.

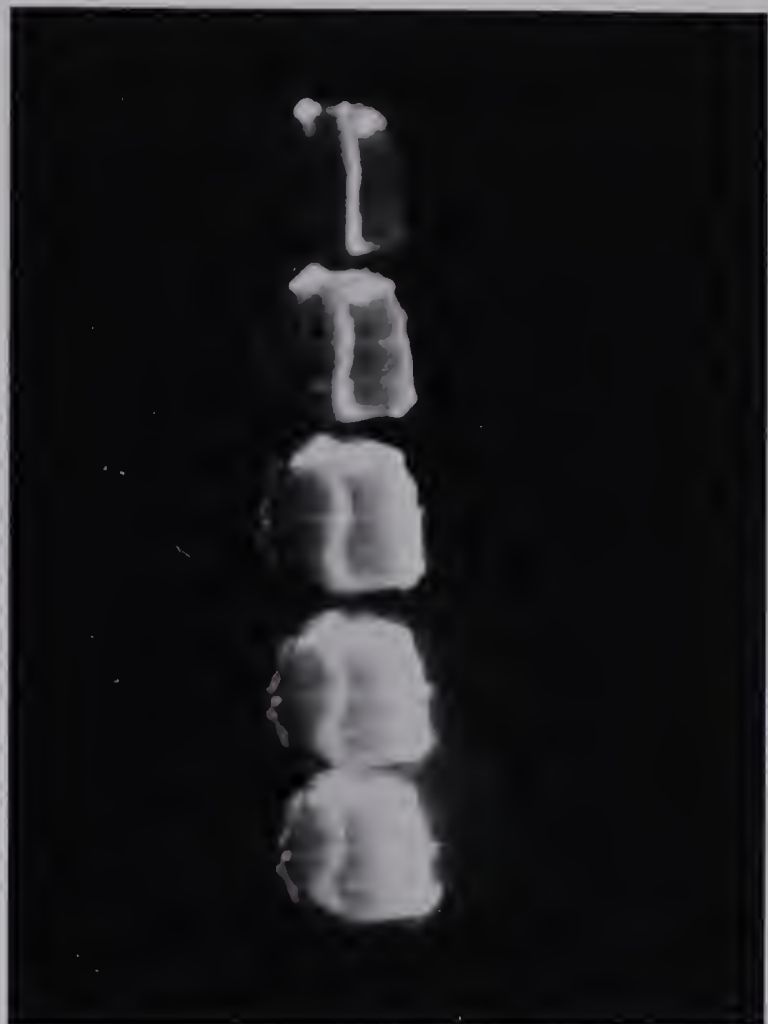


Figure 3.15 (a)

Variation of the Discharge Structure
with Hall Parameter

Hall parameter = 3

Exposure time = 0.2 μ sec.

Interframe delay = 2 μ sec.



Figure 3.15 (b)

Variation of the Discharge Structure
with Hall Parameter

Hall parameter = 4.8

Exposure time = 0.1 μ sec.

Interframe delay = 1 μ sec.

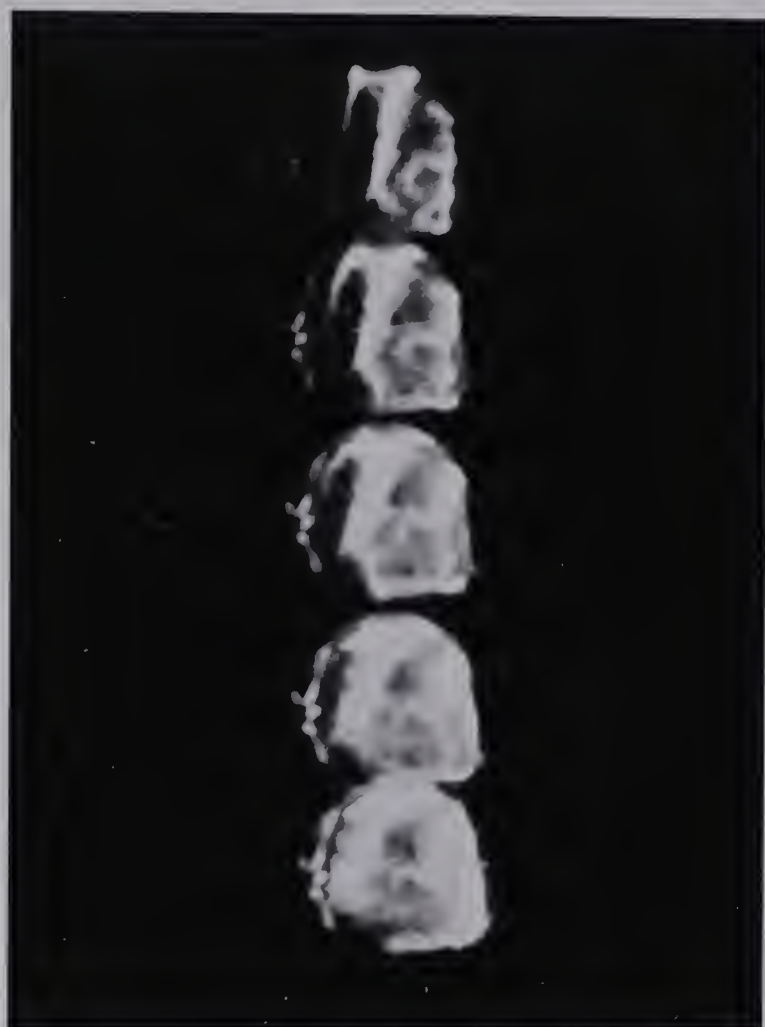


Figure 3.15 (c)

Variation of the Discharge Structure
with Hall Parameter

Hall parameter = 6.8

Exposure time = 0.2 μ sec.

Interframe delay = 2 μ sec.

CHAPTER 4 BEHAVIOR OF THE CURRENT STREAMERS AFTER FORMATION

4.1 Sequence of Events after Formation

As shown in Figure 3.11(a), the first noticeable feature is the appearance of a number of luminous striations (frames 2 and 3 of Figure 3.11(a)) at an angle close to that predicted by equation A.3.36. As the striations develop, one or two of them tend to carry most of the current and these striations expand to become highly luminous streamers oriented primarily along the $\vec{v} \times \vec{B}$ or Faraday direction. The secondary striations then become less luminous and appear to disintegrate (frames 4 and 5 of Figure 3.11(a)). The primary streamers then continue to increase in luminosity and break up into secondary streamers at a characteristic angle to the primary streamer as described in Section 3.2.5. As the current through the primary streamers increases, the $\vec{j} \times \vec{B}$ force on the streamers also increases, decelerating them. This deceleration is dealt with in the next section.

Further development of the current structure is limited by the flow duration time of the shock heated gas. When the highly conductive, luminous driver gas reaches the electrode region, the $\vec{v} \times \vec{B}$ or Faraday current will be conducted by the driver gas, thus removing the energy source needed to maintain the streamers in the shock heated gas. This is clearly shown in Figure 4.1. The driver gas (the very luminous region at the right hand side) begins to intrude into the electrode region by the third frame. The process continues in the fourth frame and the streamers begin to decrease in luminosity. By the fifth frame, the streamers have almost completely disappeared.

There is some evidence to suggest that the streamers are initiated from a region of high luminosity. Figure 4.2 shows photos taken at right angles and slightly closer to the driver compared to Figure 4.1. The shock heated gas flows from right to left. The highly luminous region on the right is the driver gas. The two shadows in the middle are the supports for the magnetic field coils. An expanding luminous region is seen just behind the shock front. This luminous region is produced by the focussing effect of the applied magnetic field. The charged particles will tend to follow the field lines and the gas will be compressed as the field lines converge.

Referring again to Figure 4.1, it can be seen that most of the streamers appear to emanate from this luminous region. It can also be seen that streamers emanate from electrode spots on the upper electrode (cathode). It may be that these highly luminous regions provide the perturbation to trigger the instability. More investigation is required to fully understand the role of these luminous regions in the formation of the streamers.

4.2 Force Balance on the Current Streamer and the Interaction of the Streamer with the Gas Flow

In this section, we will consider the balance of forces acting on the current streamer. The first major force is the magnetic interaction or $\vec{j} \times \vec{B}$ force which acts in an upstream direction and tends to decelerate the streamer. The second force which must be considered is the hydrodynamic or convective drag force which acts downstream and tends to increase the velocity of the streamer towards the flow velocity of the shock heated gas. The third force is the inertia force due to the deceleration of the streamer.

There exists a substantial literature on electric arcs in a transverse gas flow in the presence of a magnetic field. References 10, 12, 13, 14, 15, 18, 24, 25, 30, 61,



Figure 4.1
Image Converter Photographs
Taken Through Center of
Magnetic Field Coils

Exposure duration: first frame, 0.5 μ sec.,
second to fifth frames, 0.2 μ sec.

Interframe delay: frames 1-2, 8 μ sec.
frames 2-3, 3-4, 4-5, 2 μ sec.

 $B = 1.63 \text{ w/m}^2$; Mach No. = 12

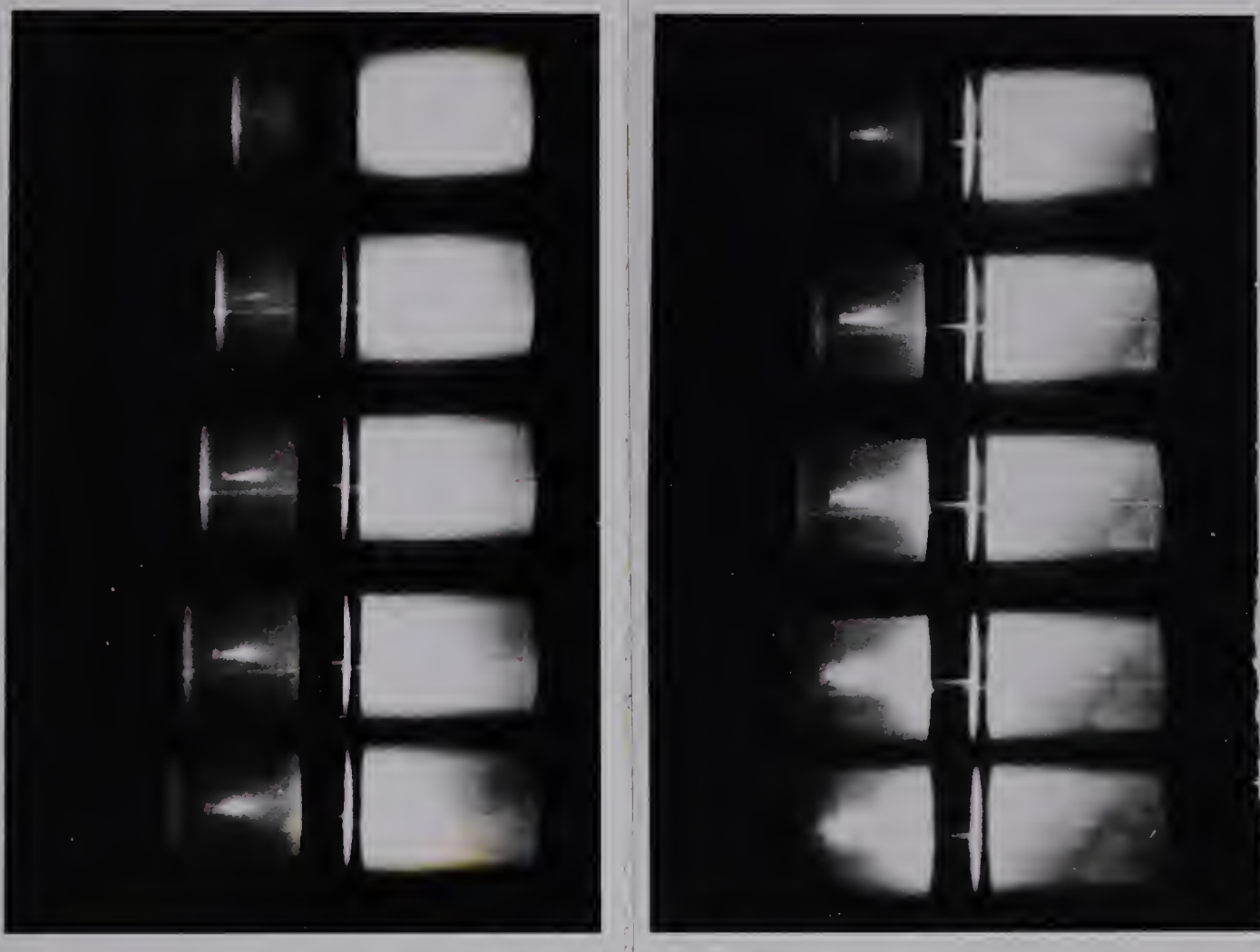


Figure 4.2

Photographs of Shock Heated Gas as Shock
Front Enters Magnetic Field Region.

Circular shadow at left of last two frames is
the shadow of the upper electrode (anode)

Exposure duration: 0.2 sec.

Interframe delay: 2 sec.

Magnetic Field Strength = 1.63 w/m^2

Mach Number = 12

69, 70, 77, 89, 95, 107, and 118 give a representative sample of some of the more recent papers in this area.

Roman and Myers⁸⁹, Winograd and Klein¹¹⁸, and Nicolai and Kuethe⁷⁷, among others, have shown that the arc behaves like a solid cylinder and is essentially impervious to the gas flow, under their experimental conditions.

Their experimental conditions consisted essentially of an arc subjected to a cross flow of air or nitrogen at room temperature. The drag force caused by the cross flow was balanced by the $\vec{j} \times \vec{B}$ force produced by an externally applied transverse magnetic field. The above authors^{77, 89, 118} found that the magnetic field, B , required to balance the arc is approximately proportional to the square of the transverse gas blowing velocity, V_∞ . This dependence is the same as that obtained by equating the aerodynamic drag force and the magnetic retarding force on a conducting cylinder of unit length:

$$B I_a = \frac{1}{2} C_D D_a \rho_\infty V_\infty^2 \quad \dots (4.1)$$

where I_a is the current flowing along the axis of the cylinder, D_a is the significant dimension (diameter), C_D is the drag coefficient⁴⁸, and ρ_∞ is the free stream gas density. The above authors^{77, 89, 118} found that the drag coefficient, C_D , defined by the above equation, is

very close to unity for a subsonic or near sonic cross flow. This is approximately the value^{32,35,64} for a solid cylinder in cross flow in the same range of Reynolds number. Figure 4.3 gives a graph of C_D versus Reynolds number for a solid cylinder.

The value of the drag coefficient, C_D , is a measure of the extent of interaction between the arc and the flow. Other workers have found higher values of C_D for a balanced cross flow arc. For instance, Myers et al⁷⁰, working with an argon arc in a flow velocity of up to 100 m/sec balanced by a magnetic field of up to 3 w/m^2 , found values of C_D approximately six times greater than that for a solid cylinder. Myers et al correctly point out that this indicates a much more pronounced arc-flow interaction than in the case of a solid cylinder of similar size. Bond and Wickersheim¹⁵, working with an arc in sulphur hexaflouride, also observed a more pronounced interaction. Their observed drag coefficient again ranges up to six times that for a solid cylinder. The authors¹⁵ observed a fine sawtooth structure to the arc column and suggest that the value of C_D and hence the degree of interaction are considerably affected by this arc structure.

The above discussion suggests that some idea of the degree of interaction between the current streamer and the shock heated gas flow may be obtained by investigating

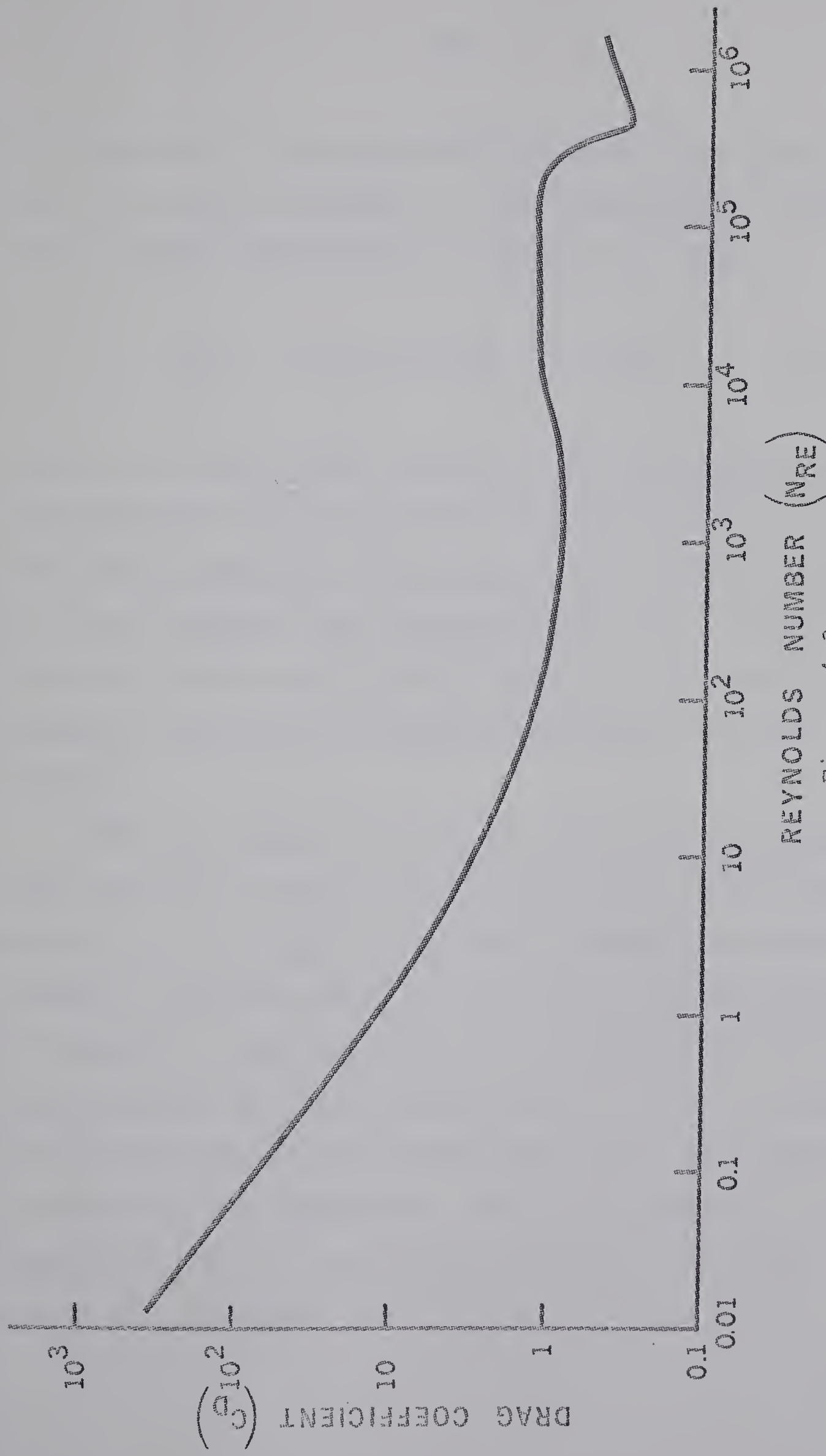


Figure 4.3
Drag Coefficient vs. Reynolds Number
for a Solid Cylinder (from refs. 35 and 48)

the magnitude of the drag coefficient of the streamer.

Since the current streamer is being decelerated, we must add an inertia force term to equation 4.1. Thus,

$$I_a B - \frac{1}{2} C_D \rho_\infty D_a V_\infty^2 = m_a \dot{u}_a \quad \dots (4.2)$$

where I_a is the streamer current, B is the applied transverse magnetic field, C_D is the drag coefficient, ρ_∞ is the shock heated gas mass density, D_a is the streamer diameter, V_∞ is the relative flow velocity between the streamer and the shock heated gas, m_a is the mass per unit length of the streamer, and \dot{u}_a is the measured deceleration of the streamer.

Table 4.1 gives values of the effective C_D calculated from equation 4.2 using the measured values of the parameters I_a , B , ρ_∞ , D_a , V_∞ , m_a , and \dot{u}_a shown in the table. Values of Reynolds number for flow past a solid cylinder of diameter D_a , and the value of C_D expected at this N_{RE} based on solid cylinder theory are also given. ρ_∞ was derived from the measured shock Mach number and undisturbed gas pressure and temperature, using the graphs given in Appendix 1. D_a , V_∞ , and \dot{u}_a were measured from image converter photographs taken of the current streamer.

MACH NO.	B_2 W/m^2	ωr	\bar{I}_a amps	u^2 m/s	u_3 m/s	V_∞ m/s	D_a m.	$\frac{\dot{V}_D}{\rho} \cdot$ kg/m^3	\dot{u}_a m/s^2	I_a^B nt/m	$\frac{\dot{V}_D}{\rho} \cdot$ m/s^2	\dot{u}_a m/s	C_D exp- ected	
12	1.0	2.4	700	$3 \cdot 2 \cdot 8 \cdot 10^3$	$2 \cdot 46 \cdot 10^3$	820	$6 \cdot 31 \cdot 10^{-3}$	$6 \cdot 11 \cdot 10^{-3}$	$1 \cdot 91 \cdot 10^7$	$1 \cdot 0 \cdot 10^7$	700	$13 \cdot 0 \cdot 10^7$	$1 \cdot 91 \cdot 54$	580 0.9
13.2	1.63	4.4	2800	$3 \cdot 69 \cdot 10^3$	$2 \cdot 73 \cdot 10^3$	970	$2 \cdot 67 \cdot 10^3$	$6 \cdot 96 \cdot 10^{-3}$	$3 \cdot 90 \cdot 10^{-3}$	$1 \cdot 26 \cdot 10^9$	$4560 \cdot 10^8$	$8 \cdot 75 \cdot 10^7$	$49 \cdot 1 \cdot 516$	340 1.0
13.6	1.63	4.2	2300	$3 \cdot 84 \cdot 10^3$	$3 \cdot 15 \cdot 10^3$	690	$3 \cdot 38 \cdot 10^3$	$7 \cdot 28 \cdot 10^{-3}$	$6 \cdot 54 \cdot 10^{-3}$	$4 \cdot 9 \cdot 10^8$	$3750 \cdot 10^8$	$5 \cdot 86 \cdot 10^7$	$32 \cdot 0 \cdot 634$	490 0.9
13.2	1.4	3.4	1100	$3 \cdot 72 \cdot 10^3$	$2 \cdot 83 \cdot 10^3$	920	$2 \cdot 24 \cdot 10^3$	$6 \cdot 96 \cdot 10^{-3}$	$2 \cdot 74 \cdot 10^{-3}$	$3 \cdot 75 \cdot 10^8$	$1540 \cdot 10^8$	$6 \cdot 60 \cdot 10^7$	$32 \cdot 0 \cdot 634$	490 0.9
13.3	1.4	3.4	880	$3 \cdot 74 \cdot 10^3$	$2 \cdot 94 \cdot 10^3$	800	$1 \cdot 92 \cdot 10^3$	$7 \cdot 08 \cdot 10^{-3}$	$2 \cdot 04 \cdot 10^{-3}$	$3 \cdot 45 \cdot 10^8$	$1230 \cdot 10^8$	$4 \cdot 35 \cdot 10^7$	$7 \cdot 04 \cdot 281$	260 1.0
13.3	1.4	3.4	720	$3 \cdot 74 \cdot 10^3$	$2 \cdot 88 \cdot 10^3$	860	$1 \cdot 71 \cdot 10^3$	$7 \cdot 08 \cdot 10^{-3}$	$1 \cdot 62 \cdot 10^8$	$1 \cdot 48 \cdot 10^8$	$1010 \cdot 10^7$	$4 \cdot 48 \cdot 10^6$	$2 \cdot 28 \cdot 225$	230 1.0

Table 4.1
Effective Drag Coefficient

m_a was assumed given by the relation

$$m_a = (\pi/4) D_a^2 \rho_\infty \quad \dots (4.3)$$

That is, we assume the mass density in the streamer to be the same as that of the shock heated gas. The effect of the temperature increase and resultant expansion will be to reduce m_a below the value given by equation 4.3. Thus, equation 4.3 specifies an upper bound for m_a and therefore, from equation 4.2, a lower bound for C_D . Also, the values of $m_a \dot{u}_a$ given in Table 4.1 are much less than the term $I_a B$. Errors in $m_a \dot{u}_a$ then have only a small effect on the values of C_D .

The values of effective C_D given in Table 4.1 show that C_D is from two to three orders of magnitude greater than the expected value for a solid cylinder. This shows that there is a marked degree of interaction between the shock heated gas flow and the current streamer. The possible reasons for this strong interaction will now be investigated.

One possibility is the existence of arc root or electrode phenomena, that is, the root of the arc may be tied to a specific point on the electrode, thus inhibiting the motion of the arc. Of course, the effect of this electrode phenomena would be to decrease the arc velocity and thus decrease the effective drag coefficient. Thus, arc root phenomena will not explain the observed large interaction.

A second possibility is that the measured luminosity width, D_a , of the streamer does not correspond to the actual diameter of the interaction region. The highly luminous region could correspond only to a small core and the region of high pressure could extend over a much larger diameter. This would have the effect of increasing the hydrodynamic pressure $\frac{1}{2}\rho_\infty D_a V_\infty^2$ proportionate to the increase in D_a . However, to increase the hydrodynamic pressure by the two to three orders of magnitude required to balance $I_a B$ would require that the effective D_a be larger than the dimensions of the plasma. This possibility is then ruled out.

Another possibility is the existence of a fine structure to the streamers, on a scale much smaller than that disclosed by the image converter photographs. One can conceive of the streamer being composed of a large number

of small streamers, each of which is impervious to the gas flow. The significance of this is the introduction of viscous effects to the flow around these much smaller impervious cylinders. The Reynolds number of the flow, $V_\infty D_a / \nu$, will be reduced proportionate to the reduction in D_a , where D_a is the diameter of the small impervious cylinders, and ν is the kinematic viscosity of the shock heated gas. As shown in Figure 4.3, the reduction in Reynolds number leads to a large increase in the drag coefficient, C_D , for flow around a solid cylinder, as the flow enters the viscosity dominated regime. Thus, if the streamer fine structure was of a small enough scale, the drag coefficient may be large enough to explain the results of Table 4.1. Now, from Figure 4.3, a drag coefficient of the order of 100 to 1000 implies a Reynolds number of about 0.01 to 0.1. This implies that the fine structure of the streamers would be of a scale three to four orders of magnitude smaller than the measured diameter of the streamers. From Table 4.1, the characteristic length of the fine structure would be of the order of 10^{-6} to 10^{-7} meters. Now, this is of the order of the electron mean free path which implies that the fluid model breaks down in this length regime. Thus, the possible existence of a fine structure to the streamers and the introduction of viscous effects to the flow do not appear to explain the

anomalously large drag coefficient.

Another possibility for explaining the large arc-flow interaction is the presence of turbulence in both the shock heated gas and in the streamer. Pert⁷⁹ has discussed the production of turbulence in shock heated gases. He found that the transition to turbulence can be expressed in terms of the hydrodynamic Reynolds number for pipe flow based on the properties of the shock heated gas. He found that under certain conditions, the energy of the turbulent field can be propagated to the shock front and can cause a disruption and instability in the front, thus preventing the formation of a region of shock heated gas. Under the conditions of this experiment, the Reynolds number for pipe flow based on the properties of the shock heated gas is about 1500 to 2000, well below Pert's critical Reynolds number for shock front instability of 9000. However, the value of Reynolds number for this experiment is close to the value for the sustenance of turbulence. Kaufmann⁴⁸ gives this value as about 2300. It is thus reasonable to expect that there will be some turbulence of the shock heated gas under the conditions of this experiment, based on hydrodynamic considerations alone. In addition, the results of Section 3.2.6 show that a large value of Hall parameter such as exists in this

experiment can induce additional large scale turbulence.

Thus, we can reasonably assume that there exists a fairly high degree of turbulence in the shock heated gas.

The problem of the interaction between an electric arc and a turbulent gas flow has been investigated by Garosi and Bekefi²⁵. They made experimental studies of the case of an arc discharge struck in a stream of flowing argon gas, the flow direction being parallel to the axis of the discharge. The Reynolds number was varied from zero to 6300; the flow then ranged from the laminar regime to the regime of fully developed pipe turbulence. The authors²⁵ found that turbulence in the flowing gas had a very profound effect on the properties and behavior of the discharge. Among the observed effects were high frequency, fine grained oscillations of the electron density, an enhanced loss of plasma particles, and an increase in electrical resistivity of the arc plasma. These effects begin to appear in the Reynolds number range of 1000 to 2000, similar to the Reynolds number range existing in this experiment.

The most important effect reported by Garosi and Bekefi, from the point of view of application to the present experiment, is the existence of a bulk motion of the arc, in which the entire column is displaced almost like a rigid cylinder. Under their experimental conditions,

with the flow along the axis of the arc, the authors reported that the displacement was quasiperiodic with a period of the order of one millisecond. The authors attribute this bulk motion to large scale fluctuations or eddies which appear in the flow above a Reynolds number of about 1000.

It thus appears reasonable, on the basis of Garosi and Bekefi's results, to expect an enhanced arc-flow interaction whenever turbulence is present in the flow. As discussed previously, there are two mechanisms acting to produce turbulence in the present experiment. The first is the production of turbulence by hydrodynamic means alone, whenever the Reynolds number for pipe flow is of the order of 2000 or greater. The second is the mechanism discussed in Section 3.2.6, where a large Hall parameter can produce large scale turbulence. We would then expect a correlation between an increase in arc-flow interaction, manifested by an increase in C_D , and an increase in flow velocity, u_2 , or Reynolds number, N_{RE} . We would also expect a correlation between an increase in C_D and an increase in Hall parameter or magnetic field strength.

Table 4.2 shows values of drag coefficient, C_D , from Table 4.1 along with corresponding values of Hall parameter and Reynolds number, derived from Table 4.1.

HALL PARAMETER	EFFECTIVE DRAG COEFFICIENT	REYNOLDS NO. FOR PIPE FLOW
2.4	54	4.6×10^3
3.4	232	6.5×10^3
3.4	281	6.6×10^3
3.4	225	6.6×10^3
4.4	516	6.5×10^3
4.2	634	7.3×10^3

Table 4.2
Correlation between
Effective Streamer Drag Coefficient
and Hall Parameter and Reynolds Number (pipe flow)
of Shock Heated Gas

It can be seen that there is a definite correlation between increasing Hall parameter and increasing drag coefficient. There is also a slight correlation between increasing drag coefficient and increasing Reynolds number, although the narrow range of Reynolds number available here makes it difficult to draw any definite conclusions.

In summary, it is proposed that the large arc-flow interaction is due to turbulence induced in the shock heated gas primarily by the mechanism discussed in Chapter 3. The experimental data presented in Tables 4.1 and 4.2 appears to support this proposition.

4.3 Helical Instability of the Current Streamers

In an attempt to maximize the resolution of the electronic camera and obtain maximum possible resolution of the discharge structure, single photographs were taken with the discharge imaged onto as large an area of the image converter tube photocathode as possible. The resulting photographs showed a definite helical structure to the discharge. Figure 4.4 shows two typical photographs taken as described. A "double helix" structure can be seen, with both secondary filaments forming



Figure 4.4
Photographs Showing Helical Structure
of the Current Streamers

Linear dimensions are approximately 0.7
of actual size.

Mach Number = 12; $B = 1.63 \text{ w/m}^2$; $\omega\tau \approx 5$

The shock front and background gas are not
visible in the photo on the right; the exposure
and development time were varied to bring out
the more intense portions of the image.

helices about the axis of the original streamer. In this Section, the behavior and the reasons for the formation of this helical structure will be investigated.

One very likely mechanism for a structure of this kind arises from the existence of a component of magnetic field in the direction of the streamer, parallel to the axis of the helix. It is easily seen that there exists a radial component of field, relative to the axis of the Helmholtz-pair field coils, due to incomplete flux linkage between the two coils. This radial field will then provide a component parallel to the axis of the streamer discharge, although the magnitude of this field will vary considerably over the interaction region.

An estimate of the magnitude of this radial field can be obtained in the following way. We assume a knowledge of the inductance of each coil separately and of the inductance of the coupled pair in place beside the shock tube, as shown in Chapter 2. The inductance of a single coil, L_1 , was measured to be 5.36×10^{-6} Henrys. The inductance of the coupled pair, L_M , was measured to be 12.2×10^{-6} Henrys.

Now, the total flux which links both coils is⁸⁴

$$\phi_{21} + \phi_{12} = 2IM \quad \dots (4.4)$$

where ϕ_{21} is the flux linking the 2nd coil due to a current I in the 1st coil, and ϕ_{12} is the flux linking the 1st coil due to a current in the 2nd coil. M is the mutual inductance of the two coils defined as⁸⁴

$$L_M = L_1 + 2M \quad \dots (4.5)$$

Now, the total flux which is produced by coil 1 but which diverges out of the interaction region without linking coil 2 is given by

$$\phi_1 - \phi_{21} = L_1 I - MI \quad \dots (4.6)$$

Similarly, the total flux produced by coil 2 which does not link coil 1 is

$$\phi_2 - \phi_{12} = L_2 I - MI \quad \dots (4.7)$$

We can consider the interaction region as being bounded by a circular cylinder with its axis coinciding with the

axis of the coils. The diameter of the cylinder is 5 cm., (the inner diameter of the coils), and the length is 6 cm. (the distance separating the two coils). Thus, the field in the direction parallel to the axis of the coils, averaged over the interaction region, is

$$B_T \approx \frac{\phi_{21} + \phi_{12}}{\pi \times (2.5 \times 10^{-2})^2} \text{ w/m}^2 \quad \dots (4.8)$$

Similarly, the average field in the radial direction, diverging from the interaction region, is

$$B_R \approx \frac{\phi_2 - \phi_{12} + \phi_1 - \phi_{21}}{\pi \times 5 \times 10^{-2} \times 6 \times 10^{-2}} \text{ w/m}^2 \quad \dots (4.9)$$

Expressing the radial field as a fraction of the (measured) transverse field, and using equations (4.4) to (4.9), we have

$$\frac{B_R}{B_T} \approx 0.208 \times \frac{L_M - L_1}{3L_1 - L_M} \quad \dots (4.10)$$

Using the measured values of L_1 and L_M , we have

$$\frac{B_R}{B_T} \approx 0.366 \quad \dots (4.11)$$

This value is only an approximate average value of B_R . B_R exhibits a considerable spatial variation, in particular, B_R vanishes on a plane parallel to and equidistant from the planes of the two coils.

The mechanism by which an axial magnetic field can lead to a helix structure can be explained qualitatively as follows: as discussed in Chapter 3 and Appendix 3, the current filament breaks up into two secondary filaments each at an angle α , given by equation (A.3.36), to the original. The secondary filaments then introduce a radial component of current with respect to the axis of the original filament. This radial current interacts with the axial or longitudinal magnetic field to produce a $\vec{j} \times \vec{B}$ azimuthal force which acts until the radial current vanishes, that is, until the filament is twisted into a helical shape such that the former radial component now flows completely in the azimuthal direction.

We will now consider the question of the determination of the radius and pitch angle of the helix and the question of its stability. There is a considerable literature

(references 1, 3, 8, 26, 33, 36, 37, 43, 44, 65, and 108, for example) on the existence of a helical instability in the positive column and the resulting enhanced diffusion due to this instability. The theoretical papers (ref. 44, for example) start from the equations of continuity for ions and electrons and the electron equation of motion. A steady state solution is obtained and this solution is subjected to a perturbation of the form

$\exp [i(\omega t + m\theta + kz)]$ where θ is the azimuthal angle.

A critical magnetic field of the order of a few kilogauss³ is found for a given mode ($m = 1$). In addition, the frequency and wavelength of the helix at the critical magnetic field are found⁴³. However, this theory does not fit the experimental conditions encountered here, for the following reasons: first, the positive column was considered to be in the Schottky diffusion state^{23,98}; that is, the particle loss is due to ambipolar diffusion and the electron and ion concentrations are taken to be zero at the wall of the discharge tube. It is also assumed that the temperature is constant throughout the positive column. This theory is only valid for low pressures below about 5 or 10 torr¹. Above this pressure the positive column gradually contracts; the thermal transport properties of the gas and radiation loss determine the

size of the column; a radial variation of temperature appears and increases the role of recombination processes in the loss of charged particles. In this experiment, where the ionization process is unstable, the temperature inhomogeneity is even more pronounced and, as we have seen, the current distribution is very non-uniform. For these reasons, the Kadomtsev instability theory⁴⁴ is not applicable to this experiment.

To deduce the radius of the helix, we make use of the idea that any conservative system will tend to assume a configuration of minimum energy. If we consider only the potential energy of the magnetic field, then this condition is that the integral⁹⁷

$$W = \int_v \frac{B^2}{2\mu_0} dv \quad \dots (4.12)$$

be a minimum, where B is the sum of the field B_R and the field due to the helical current filament.

We can approximate this situation by assuming B_R to be everywhere uniform in space and the "helix" to be made up of a number of circular current loops. We further assume that the field of each loop may be considered independently of the fields of the other loops. We thus consider a loop carrying a known current immersed in a

uniform field B_R , parallel to the axis of the loop. The problem then reduces to finding the radius of the loop which will minimize the quantity

$$W = \int_v \frac{(B_R + B_{lp})^2}{2\mu_0} dv \quad \dots (4.13)$$

where B_{lp} is the field due to a circular filament of current, as given by Jackson⁴¹. The field of such a current distribution is a very complicated function of position, especially close to the loop; thus the minimization of W is a rather involved problem and probably can only be achieved by numerical techniques. To simplify the problem even further, we note that the field close to the current filament gives the biggest contribution to W and hence we need only consider B_{lp} in this region. As the final approximation, instead of integrating B^2 over all space, we will minimize B^2 at one representative point, specifically, the point of intersection of the axis of the loop with the plane of the loop. The value of B_{lp} at this point is given simply by

$$B_{lp} = \frac{\mu_0 I_s}{2a} \quad \dots (4.14)$$

where I_s is the streamer current, and a is the loop radius.

The minimum of the quantity $B^2 = (B_R + B_{1p})^2$ is obviously $B_{1p} = -B_R$. Thus, the characteristic radius is given by

$$\frac{\mu_0 I_s}{2a} = B_R \quad \dots (4.15)$$

For the conditions of Figure 4.4 ($I_s \approx 10^3$ amps, $B_R \approx 0.366 \times 1.63 = 0.6 \text{ w/m}^2$),

$$2a \approx 2 \text{ mm.}$$

From Figure 4.4, the observed helix diameters are 3 to 5 mm., so the above rather gross approximations appear to predict the helix diameter fairly well.

The pitch angle of the helix is simply given by the angle α from equation (A.3.36), since this is the angle which the secondary filament makes with the primary filament or the axis of the helix. From Chapter 3, this angle should be about 40 to 45 degrees. From Figure 4.4, it is seen that the pitch angle of the helix is quite close to this value.

The question of the stability of the helix structure will be considered next. The structure is stable as long as B_R and I_s remain constant. However, if B_R increases or decreases, then the radius of the helix will decrease or

increase respectively. If I_s increases, then the radius will also increase. In some of the photographic observations made, the variation of the radius was observed as I_s increased. A pronounced increase of the radius was observed, up to 10 mm. or more. At this point, the filaments appeared no longer able to sustain themselves, became very diffuse, and were convected away by the flow of shock heated gas.

CHAPTER 5 APPLICATIONS AND SUGGESTIONS FOR FURTHER RESEARCH

5.1 Applications

The work reported here has a number of applications to practical problems. The first is to the design of a magnetohydrodynamic (MHD) generator of the closed cycle type. The proposal^{42,67} is to couple a nuclear reactor of the high-temperature, gas (helium) cooled type⁶⁷ to an MHD generator. However, due to constraints introduced by materials, safety, and economics, the maximum temperature of the gas at the outlet from a reactor is of the order of 1500 degrees Kelvin. This temperature is insufficient to obtain the thermal ionization ensuring the required electrical conductivity of the working fluid, even with the use of additives with a small ionization potential (alkali metals).

To overcome this difficulty, it is necessary to create a plasma in which preferential heating of the electrons yields the required conductivity. This separation between

the electron temperature and heavy particle temperature can be achieved by Joule heating of the electrons^{49,51,91}. The resulting nonequilibrium plasma is then subject to the ionization instability discussed in the preceding chapters. This instability has been found to lead to a turbulent plasma state with properties differing substantially from those predicted by simple theory. Specifically, the time-averaged conductivity has been found to decrease by as much as an order of magnitude below that predicted by uniform plasma theory^{7,52,101,103}. In addition, a non-uniform current distribution or the restriction of current flow to narrow filaments leads to the gas flow-magnetic field interaction being confined to only a small portion of the volume of the MHD channel, leading to highly inefficient operation.

It can be seen that an understanding of the onset conditions and the behavior of this instability is a most important prerequisite for the successful operation of a nonequilibrium MHD generator.

Proposals have been made⁹³ that the ionization instability may be suppressed by operating the MHD plasma at higher temperatures, where Coulomb collisions dominate or where the additive is almost fully ionized. The significance of the work reported in the preceding chapters is

that the instability will not be suppressed; it will occur in the Coulomb collision dominated regime and in the absence of an additive.

These plasma stability problems do not occur in combustion MHD generators since the required conductivity can be attained by using oxygen enrichment, air preheating, and seeding of the working fluid (natural gas, fuel oil) in the combustion chamber. Temperature nonequilibrium does not occur to any appreciable extent due to the much more efficient energy transfer to the organic molecules during electron-heavy particle collisions. Accordingly, considerable success has been achieved in the construction and operation of combustion MHD generators, for example⁴², the LORHO and AVCO Mark V generators in the USA and the U-02 installation in the USSR. Continuous operating times in excess of 50 hours and power outputs up to 43 KW were reported for the U-02 installation¹⁰⁰. The power was delivered through a solid state inverter system to the Moscow grid. The USSR is constructing a pilot plant of about 75 MW installed capacity; 25 MW is provided by the MHD generator. This installation, known as the U-25 located in Moscow, was scheduled to commence operation during 1970.

Success has been not nearly as impressive in the case of nonequilibrium closed cycle generators, due to the less than complete understanding of the processes which occur in the MHD generator duct. Recently, Decker, Hoffman, and Kerrebrock¹⁹ have described in detail the operation of a large, experimental nonequilibrium MHD generator, using helium seeded with cesium. Load currents at least five times those possible with frozen ionization were drawn but these were still far below those predicted by uniform plasma theory. The authors, although assuming in their analysis that a steady state exists in the generator duct, state this may well not be the case and that the nonequilibrium ionization may in fact occur by the formation of convected ionization instabilities.

Millionshchikov (vice-president of the Academy of Sciences, USSR) and his co-authors⁶⁷ calculate the relative costs of a helium-cooled high-temperature nuclear reactor coupled to an MHD generator, compared to the costs of a conventional organic fueled, steam powered plant, based on a power level of 1200 MW. They find that the specific yearly expenses are 1.5 to 2.5 times less for the helium cooled reactor and the cost of electric power is two to three times less, while the capital investments are approximately equal. The authors suggest that the combination

of a helium cooled reactor with both an MHD generator and a gas turbine unit would provide higher technical and economic efficiencies than any other known power plant system. Thus, the incentives for continued work on the problems of nonequilibrium MHD generators are great.

Another application of the work of the preceding chapters is to the extinguishing of a plasma arc such as occurs in a circuit breaker. As shown in Chapter 1, the effect of the magnetic field is to transform the current distribution from a uniform current flow to a current flow constricted in narrow filaments. An interesting question is whether an applied magnetic field of sufficient magnitude can have a similar effect on a steady arc. Temperatures in a typical circuit breaker arc are in a range of 1 to 2 eV⁵⁸, very close to the temperature range in this experiment. Thus, the degree of ionization would be approximately the same (5% to 20%). The non-equipartition between the electron and ion energies in an electric arc in atomic gases is well established^{40,57}, and the criterion $T_e > T_i$ is satisfied. The arc pressure would be somewhat higher and the magnetic field strength would have to be increased accordingly to obtain the appropriate Hall parameter. If similar phenomena are observed as were observed here, then the arc should become turbulent and

its effective conductivity should decrease considerably as noted in references 7, 52, 101, and 103. The simultaneous imposition of a longitudinal magnetic field of appropriate magnitude may then lead to a helical instability of the filaments with consequent increasing of the filament length and disintegration of the filaments as described in Chapter 4.

The enhanced gas flow-arc interaction discussed in Chapter 4 also has application to the circuit interruption problem. One common method of interrupting an arc is by the use of a blast of high pressure gas^{58,83}. The rapidity with which the arc plasma can be removed from the electrode region of the breaker depends on the degree of interaction between the gas flow and the plasma, specifically, on the magnitude of the effective drag coefficient, C_D . The large increase in the magnitude of C_D observed here (Section 4.2) may well provide a means whereby the ionized plasma may be removed more quickly from the circuit breaker.

Another application is to the development of high power lasers. It has been suggested⁷⁸ that the plasma properties typical of a nonequilibrium MHD generator may be exploited to produce a population inversion by MHD action in a molecularly loaded gas mixture.

Nighan et al⁷⁸ theoretically studied this possibility and showed that conditions favorable for the production of a vibrational population inversion in CO₂ can be achieved in a typical nonequilibrium MHD generator, for example, using helium seeded with cesium and combined with nitrogen and carbon dioxide. The ionization instability may well occur here, limiting the laser power obtainable. A knowledge of the onset conditions and behavior of the instability then becomes of considerable importance.

5.2 Further Research

In addition to the investigations into the possible applications discussed in the last section, there are opportunities for further research into the mechanism of the ionization instability, especially into an improvement of the theoretical description of the phenomena. The theory could be extended to the non-linear, large amplitude regime, perhaps extending the work of Gilpin and Zukoski^{27,126}. The theory presented in Chapter 3 assumes an infinite (unbounded) plasma. Boundary effects could be introduced, perhaps along with a consideration of the large amplitude regime, thus extending the work of Nelson⁷⁶. Velikov et al¹¹⁵ have done a computer

simulation of the instability under quite restrictive conditions (T_e constant, $T_e >> T_i$, diffusion and transport properties other than electric conductivity neglected).

This work could be generalized considerably.

The determination of the physical processes limiting the size of the current filaments is another area for investigation. Rough calculations of convective heat transfer from the filament to the flowing gas based on consideration of the filament as a solid cylinder provide reasonable agreement with measured Joule heating rates. However, assumptions had to be made regarding the filament density and temperature. Further calculations could be made in this area, perhaps including the effects of turbulence on heat transfer rates and including experimental data on properties of the hot filament. Radiation energy losses may also make an important contribution to the total loss. Glushov et al²⁹ suggest that a solution to the steady state equations (equations 3.29, 3.31, and 3.14) can lead to a current pinch, and derive a critical Hall parameter for the transition. However, the authors also suggest that allowance for energy transport will change the critical condition.

Various refinements can be introduced to the theoretical calculations. For example, the effects of energy

nonequipartition on the electron distribution function¹¹⁶ and on the transport properties^{6,17,68} can be taken into account. Also, the influence of the Ramsauer effect on the temperature nonequilibrium can be considered^{20,56}

The substitution of He for Ar as the shocked gas may produce some useful results, especially since helium is proposed as the coolant for the high temperature, gas cooled nuclear reactors under consideration as a heat source for MHD generators. The ionization potentials for He are 24 eV for HeI and 54 eV for HeII. Thus, the gas must reach slightly higher temperatures than in the case of argon for the instability to appear. In addition, the large energy difference between the two ionization potentials may produce a temperature region in which the instability is damped. There may be a temperature range centered about 30,000 degrees K where the first level is essentially fully ionized but where the second level has not started to contribute to the ionization to any extent. The large degree of coupling between temperature perturbations and electron density perturbations will then be substantially removed and the formation of the instability may be prevented.

An interesting effect can occur in an atomic gas with only one bound electron, for example hydrogen or singly

ionized helium. The electron collisional energy loss term will exhibit a maximum with increasing T_e . This can be seen by the following argument: the electron energy balance equation is

$$\sigma_o E_y^2 = 2(m_e/m_a) n_e (3k/2) (T_e - T_g) v .$$

For $\sigma_o = (n_e e^2)/(m_e v)$, and $v \propto n_e/T_e^{3/2}$ (Coulomb collisions), the energy input term, $\sigma_o E_y^2$, then increases as $T_e^{3/2}$ while the energy loss term is proportional to $n_e^2 (T_e - T_g)/T_e^{3/2}$.

Thus, when the degree of ionization approaches unity, and n_e saturates, the energy loss term reaches a maximum as T_e increases while the Joule heating term continues to increase. Note that the collision frequency then decreases as $T_e^{-3/2}$ and thus the Hall parameter increases as $T_e^{3/2}$.

The effect is to introduce a singularity in the steady state solution, that is, above a certain value of T_e , no steady state solution exists. If the variation of T_e with Joule heating rate is considered, then above a certain value of Joule heating rate (or electric field) or, if the Joule heating is provided by relative motion of the gas and magnetic field, above a certain value of B , the electron temperature will increase without bound or until some other energy loss process such as radiation or thermal transport

begins to limit T_e .

The exact physical meaning of this runaway condition is not clear, that is, whether it will tend to produce more non-uniformities in the current distribution or whether it will tend to smooth out and stabilize the spatial distribution. It is interesting to consider the behavior of the growth rate for small perturbations (equation 3.39) in this region. Both the terms $\omega\tau_0$ and $(d \ln T_e)/(d \ln n_e)$ will increase although at different rates, depending on the state of the gas, such as pressure and magnetic field. Calculations made in the same way as described in Section 3.2.1 except considering only one ionization level of the argon atom (equation 3.24 replaced by equation 3.14) indicate that the growth rate increases very sharply in the region of the n_e saturation. This may indicate that, contrary to proposals made in the literature⁴⁹, the instability may not be suppressed as complete ionization is approached. Experimental results^{7,101,102,117} made in electron-atom collision dominated plasmas indicate that stability may be increased as the degree of ionization of the additive approaches unity. However, this may not be the case for a Coulomb collision dominated plasma.

In conclusion, the ionization instability dealt with in this work is a basic instability of a partially ionized plasma in crossed electric and magnetic fields and can manifest itself in MHD generators, electric arcs, lasers utilizing a gas flow and a magnetic field for arc balancing, MHD lasers, and magnetoplasmadynamic accelerators, for example. Thus, continuing investigations into the properties of this instability are certainly justified.

LIST OF REFERENCES

- (1) A.R. Akhmedov, A.A. Zaitsev, "Instability of a plasma in a magnetic field upon transition from low to high pressures", Sov.Phys.-JETP, 18, 4, p. 977, (April, 1964).
- (2) C.W. Allen, Astrophysical Quantities, (Athlone Press, University of London, 1963).
- (3) T.K. Allen, G.A. Paulikas, R.V. Pyle, "Instability of a positive column in a magnetic field", Phys. Rev. Lett., 5, 9, p. 409, (1960).
- (4) R.A. Alpher, D.R. White, "Visible continuum emission from shocked noble gases", Phys. Fluids, 7, 8, p. 1239, (Aug., 1964).
- (5) J.P. Azalbert, R. Scaricabarozzi, C. Vavasseur, P. Zettwoog, "Present state of work conducted by the French Atomic Energy Commission pertaining to magnetohydrodynamic conversion", High Temperature, 7, 6, p. 1178, (November-December, 1969).

- (6) M.N. Bahadori, S.L. Soo, "Non-equilibrium transport phenomena of partially ionized argon", Int. J. Heat Mass Transfer, 9, p. 17, (1966).
- (7) V.N. Belousov, V.V. Eliseev, I.Y. Shipuk, "Ionization instability and turbulent conductivity of non-equilibrium plasma", Electricity from MHD, Proc. of a Symp., Salzburg, 1966, vol. 2, p. 323, (International Atomic Energy Agency, Vienna, 1966).
- (8) L.E. Belousova, "Hollow positive column in a longitudinal magnetic field", Sov. Phys.-Tech. Phys., 11, 5, p. 658, (Nov., 1966).
- (9) D.J. Ben Daniel, S. Tamor, "Theory of non-thermal ionization in cesium discharges", Phys. Fluids, 5, p. 500, (1962).
- (10) D.M. Benenson, A.J. Baker, "Stability and shape of magnetically balanced cross-flow arcs", AIAA J., 7, 12, p. 2335, (Dec., 1969).

- (11) A.R. Bishop, L.D. Nichols, "Conductivity of an impure, nonequilibrium plasma with electrothermal instabilities", AIAA J., 8, 4, p. 829, (April, 1970).
- (12) C.E. Bond, "Magnetic confinement of an electric arc in transverse supersonic flow", AIAA J., 3, 4, p. 142, (January, 1965).
- (13) C.E. Bond, "Slanting of a magnetically stabilized electric arc in transverse supersonic flow", Phys. Fluids, 9, 4, p.705, (April, 1966).
- (14) C.E. Bond, R.W. Potillo, "Stability and slanting of the electric arc in a thermionic rail accelerator", AIAA J., 6, 8, p.1565, (Aug., 1968).
- (15) C.E. Bond, D.N. Wickersheim, "Convective electric arcs at Mach numbers up to 6.5", AIAA J., 8, 10, p.1748, (Oct., 1970).
- (16) S. Chapman, T.G. Cowling, The Mathematical Theory of Non-Uniform Gases, chap.8, (Cambridge University Press, 1958).

- (17) R.M. Chmielewski, J.H. Ferziger, "Transport properties of a nonequilibrium partially ionized gas", Phys. Fluids, 10, 2, p.364, (Feb., 1967). For a treatment including the effects of a magnetic field, see Phys. Fluids, 10, 12, p.2520, (Dec., 1967). See also S.I. Braginskii, Sov. Phys.-JETP, 6, p.358, (1958); and I.P. Stachanov, and R.S. Stepanov, Sov. Phys.-Tech. Phys., 9, p.315, (1964)
- (18) M.D. Cowley, "A boundary layer model for balanced arcs", Pub. No. 67-6, Fluid Mechanics Laboratory, Dept. of Mech. Eng., M.I.T., (July, 1967).
- (19) R. Decher, M.A. Hoffman, J.L. Kerrebrock, "Behavior of a large nonequilibrium MHD generator", AIAA J., 9, 3, p.357, (March, 1971).
- (20) R.S. Devoto, "Transport coefficients of partially ionized argon", Phys. Fluids, 10, 2, p.354, (Feb., 1967). See also: R.S. Devoto, C.P. Li, "Transport coefficients of partially ionized helium", J. Plasma Physics, 2, 1, p.17, (Feb., 1968); and R.S. Devoto, "Transport coefficients of partially ionized hydrogen", J. Plasma Physics, 2, 4, p.617, (Dec., 1968).

- (21) A.M. Dykhne, "Ionization instability in a bounded region", Electricity from MHD, Proc. of a Symp., Warsaw, 1968, Vol. 1, p.605, (International Atomic Energy Agency, Vienna, 1968).
- (22) A.M. Dykhne, "Anomalous plasma resistance in a strong magnetic field", Sov.Phys.-JETP, 32, 2, p.348, (Feb., 1971).
- (23) A. von Engel, Ionized Gases, (Oxford University Press, 1965), 2nd edition, p.238-241.
- (24) E. Fischer, J. Uhlenbusch, "DC arcs in transverse force fields", Seventh International Conf. on Phenomena in Ionized Gases, vol. 1, p.725, (Belgrade, 1965).
- (25) G.A. Garosi, G. Bekefi, "Response of a weakly ionized plasma to turbulent gas flow", Phys. Fluids, 13, 11, p.2795, (Nov., 1970).
- (26) G.W. Garrison, H.A. Hassan, "Screw instability in a linear Hall accelerator", Phys. Fluids, 10, 4, p.711, (April, 1967).

- (27) R.R. Gilpin, E.E. Zukoski, "Experimental and theoretical studies of electrothermal waves", AIAA J., 7, 8, p.1439, (Aug., 1969).
- (28) R.R. Gilpin, "Simplified derivation of the condition for electrothermal instability", Phys. Fluids, 13, 6, p.1642, (June, 1970).
- (29) I.S. Glushkov, V.T. Karpukhin, A.V. Nedospasov, "Current distribution in an E×H discharge with sectionalized electrodes for nonequilibrium conductivity of the plasma", High Temperature, 7, 2, p.208, (March-April, 1969).
- (30) M.E. Goldstein, J.A. Fay, "The shape of a magnetically balanced arc", AIAA J., 5, 8, p.1510, (Aug., 1967).
- (31) V.S. Golubev, M.M. Malikov, A.V. Nedospasov, "A model of the Faraday-type MHD generator with hot electrons", Energy Conversion, 10, p.123, (1970).
- (32) F.E. Gowen, E.W. Perkins, "Drag of circular cylinders for a wide range of Reynolds numbers and Mach numbers", TN2960, June, 1953, NACA.

- (33) H.A. Hassan, C.C. Thompson, "Onset of Instabilities in coaxial Hall current accelerators", AIAA J., 7, 12, p.2300, (Dec., 1969).
- (34) T. Hiramoto, "Critical condition for the electro-thermal instability in a partially ionized plasma", Phys. Fluids, 13, 6, p.1492, (June, 1970)
- (35) S.F. Hoerner, Fluid Dynamic Drag, (published by the author, 1965), p.3-9.
- (36) F.C. Hoh, B. Lehnert, "Screw instability of a plasma column", Phys.Rev.Lett., 7, 3, p.75, (1961).
- (37) F.C. Hoh, "Low-temperature plasma diffusion in a magnetic field", Rev.Mod.Phys., 34, 2, p.267, (April, 1962).
- (38) K.P. Horn, H. Wong, D. Bershader, "Radiative behavior of a shock heated argon plasma flow", J.Plasma Physics, 1, 2, p.157, (May, 1967).
- (39) H. Hurwitz Jr., G.W. Sutton, S. Tamor, "Electron heating in magnetohydrodynamic power generators", ARS J., 32, 8, p.1237, (Aug., 1962).

- (40) F.P. Incropera, J.R. Viegas, "Nonequilibrium in an arc constrictor", AIAA J., 8, 9, p.1722, (Sept., 1970).
- (41) J.D. Jackson, Classical Electrodynamics, (John Wiley, 1962), p.141.
- (42) W.D. Jackson, M. Petrick, J.E. Klepeis, "A critique of MHD power generation", Journal of Engineering for Power, Trans. ASME, 92, Ser.A, #3, p.217, (July, 1970).
- (43) R.R. Johnson, D.A. Jerde, "Instability of a plasma column in a longitudinal magnetic field", Phys. Fluids, 5, 8, p.988, (Aug., 1962).
- (44) B.B. Kadomtsev, A.V. Nedospasov, "Instability of the positive column in a magnetic field and the 'anomalous' diffusion effect", Plasma Physics (J. Nucl. Energy, Part C), 1, p.230, (1960).
- (45) Yu. A. Kareev, V.T. Karpukhin, A.V. Nedospasov, "Mercury seeded with cesium as a working substance for studying the properties of MHD generators operating on the Rankine cycle", Electricity from MHD, Proc. of a Symp., Warsaw, 1968, Vol. 1, p.547, (International Atomic Energy Agency, Vienna, 1968).

- (46) B. Karlowitz, D. Halasz, U.S. Patent 2,210,918, (August 13, 1940).
- (47) B. Karlowitz, D. Halasz, "History of the K and H generator and conclusions drawn from the experimental results", Third Symp. on the Engineering Aspects of MHD, Univ. of Rochester, (March, 1962).
- (48) W. Kaufmann, Fluid Mechanics, (McGraw-Hill, 1963), p.287-290.
- (49) J.L. Kerrebrock, "Nonequilibrium ionization due to electron heating: I. Theory", AIAA J., 2, 6, p.1072, (June, 1964).
- (50) J.L. Kerrebrock, M.A. Hoffman, "Nonequilibrium ionization due to electron heating: II. Experiments", AIAA J., 2, 6, p.1080, (June, 1964).
- (51) J.L. Kerrebrock, "Magnetohydrodynamic generators with nonequilibrium ionization", AIAA J., 3, 4, p.591, (April, 1965).

- (52) J.L. Kerrebrock, R. Dethlefsen, "Experimental investigation of fluctuations in a nonequilibrium MHD plasma", AIAA J., 6, 11, p.2115, (Nov., 1968).
- (53) J. Klepeis, R.J. Rosa, "Experimental studies of strong Hall effects and $U \times B$ induced ionization", AIAA J., 3, 9, p.1659, (Sept., 1965).
- (54) V.A. Kirillin, M.A. Styrikovich, "Technical progress in the power industry", High Temperature, 8, 2, p.235, (March-April, 1970).
- (55) H. Klingenbergs, "Arc phenomena and gasdynamic effects due to interaction of shock waves with magnetic fields", Z. Naturforsch, 23a, p.1929, (1968).
- (56) C.H. Kruger, J.R. Viegas, "Influence of the Ramsauer effect on nonequilibrium electron temperatures", Phys. Fluids, 7, p.1789. (1964).
- (57) C.H. Kruger, "Nonequilibrium in confined arc plasmas", Phys. Fluids, 13, 7, p.1737, (July, 1970).

- (58) T.H. Lee, "Plasma physics and the interruption of an electric circuit", Proc. IEEE, 57, 3, p.307, (March, 1969).
- (59) J.H. de Leeuw, "The Interaction of a Plane Strong Shock Wave with a Steady Magnetic Field", Institute for Aerospace Studies, University of Toronto, UTIA Report No. 49, (March, 1958).
- (60) S.C. Lin, E.L. Resler, A. Kantrowitz, "Electrical conductivity of highly ionized argon produced by shock waves", J.Appl.Phys., 26, 1, p.95, (Jan., 1955).
- (61) W.T. Lord, "An electric arc in a transverse magnetic field: a theory for low power gradient", J.Fluid Mech., 35, 4, p.689, (March, 1969).
- (62) M. McChesney, Z. Al-Attar, "Continuum radiation losses in shock heated argon", J. Quant. Spectrosc. Radiat. Transfer, 5, p.553, (1965).
- (63) H. Maecker, T. Peters, "Das Elektronenkontinuum in der Säule des Hochstromkohlebogens und in anderen Bögen", Zeitschrift für Physik, 139, p.448, (1954).

- (64) W.A. Mair, J.A. Beavan, in Modern Developments in Fluid Dynamics, High Speed Flow, ed. L. Howarth, (Oxford University Press, 1953), p.682-686.
- (65) M.M. Malikov, "Rotation of the gas in an electric arc in a longitudinal magnetic field", High Temperature, 7, 3, p.572, (May-June, 1969).
- (66) M.M. Malikov, "Experimental study of non-equilibrium plasma", High Temperature, 8, 2, p.247, (March-April, 1970).
- (67) M.D. Millionshchikov, A.M. Lyul'ka, A.V. Nedospasov, A.E. Sheindlin, "The possibilities of using gas-turbine units and magnetohydrodynamic generators in atomic power plants with high-temperature gas-cooled reactors", High Temperature, 8, 2, p.379, (March-April, 1970).
- (68) J.C. Morris, R.P. Rudis, J.M. Yos, "Measurements of electrical and thermal conductivity of hydrogen, nitrogen, and argon at high temperatures", Phys. Fluids, 13, 3, p.608, (March, 1970).

- (69) T.W. Myers, "Experimental investigation of the balancing mechanism and electrical properties of an argon arc in crossed convective and magnetic fields", Seventh Symp. on the Engineering Aspects of MHD, 1966, p.20.
- (70) T.W. Myers, "Experimental investigation of a magnetically balanced arc in a transverse argon flow", Journal of Engineering for Power, Trans. ASME, Ser.A, 88, p.27, (Jan., 1966).
- (71) A.V. Nedospasov, I. Ya. Shipuk, High Temperature, 3, p.166, (1965).
- (72) A.V. Nedospasov, "Velocity of ionization waves in a low-temperature plasma", Electricity from MHD, Proc. of a Symp., Salzburg, 1966, Vol. 2, p.345, (International Atomic Energy Agency, Vienna, 1966).
- (73) A.V. Nedospasov, "Striations", Sov.Phys.-Uspekhi, 11, 2, p.174, (Sept.-Oct., 1968).
- (74) A.H. Nelson, M.G. Haines, "Analysis of the nature and growth of electrothermal waves", Plasma Physics, 11, p.811, (1969).

- (75) A.H. Nelson, "Development of the ionization (electro-thermal) instability with boundary effects", Proc. of Ninth Int'l Conf. on Phenomena in Ionized Gases, (1969), paper 4.3.3.17, p.467.
- (76) A.H. Nelson, "Development of the MHD electrothermal instability with boundary effects", AIAA J., 8, 10, p.1753, (October, 1970).
- (77) L.M. Nicolai, A.M. Kuethe, "Properties of magnetically balanced arcs", Phys. Fluids, 12, 10, p.2072, (Oct., 1969).
- (78) W.L. Nighan, R.T. Brown, R.J. Hall, "Laser excitation using a nonequilibrium MHD generator", AIAA Bulletin, 8, 1, p.19, (January, 1971).
- (79) G.J. Pert, "Flow modes in shock tubes with electromagnetic driving sections", J. Phys. D: Appl. Phys., 3, p.203, (1970).
- (80) H.E. Petschek, P.H. Rose, H.S. Glick, A. Kane, A. Kantrowitz, "Spectroscopic studies of highly ionized argon produced by shock waves", J. Appl. Phys., 26, 1, p.83, (January, 1955).

- (81) M.G.R. Phillips, The Production of Hypersonic Shock Waves in an Electrothermal Diaphragm Shock Tube, Ph.D. thesis, University of British Columbia, (Physics Department), 1969.
- (82) Yu.P. Raizer, "A simple method of calculating the degree of ionization and thermodynamic functions of a multiply-ionized ideal gas", Sov. Phys. JETP, 9, p.1124, (1959); see also ref. 125, chap. 3, sect. 7.
- (83) W. Reider, "Circuit breakers, physical and engineering problems", IEEE Spectrum, July, 1970, p.35; Aug., 1970, p.90; Sept., 1970, p.80.
- (84) J.R. Reitz, F.J. Milford, Foundations of Electromagnetic Theory, (Addison-Wesley, 1960), chap.9.
- (85) ibid., p.136.
- (86) ibid., p.322.
- (87) W. Riedmüller, "Experimental investigation of instabilities in a potassium-seeded argon plasma in crossed electric and magnetic fields", Electricity from MHD, Proc. of a Symp., Warsaw, 1968, vol.1, p.519,

- (88) F. Robben, "Nonequilibrium ionization in MHD generators", Phys. Fluids, 5, p.1308, (1962).
- (89) W.C. Roman, T.W. Myers, "Experimental investigation of an electric arc in transverse aerodynamic and magnetic fields", AIAA J., 5, 11, p.2011, (Nov., 1967).
- (90) D.J. Rose, M. Clark Jr., Plasmas and Controlled Fusion, (MIT Press, 1961), chap. 8.
- (91) R.J. Rosa, "Nonequilibrium ionization in MHD generators", Proc. IEEE, 51, p.774, (May, 1963).
- (92) R.J. Rosa, Magnetohydrodynamic Energy Conversion, chap. 5, (McGraw-Hill, 1968).
- (93) ibid., p.110-111.
- (94) ibid., p.29.
- (95) J. Rosciszewski, "Electric arc moving at hypersonic speed", AIAA J., 8, 3, p.590, (March, 1970).

- (96) R.W. Rutowski, D. Bershader, "Shock tube studies of radiative transport in an argon plasma", Phys. Fluids, 7, 4, p.568, (April, 1964).
- (97) G. Schmidt, Physics of High Temperature Plasmas, (Academic Press, 1966), p.118.
- (98) W. Schottky, Physik. Z., 25, p.342, (1924).
- (99) F.H. Shair, "A compatibility equation for nonequilibrium ionization", AIAA J., 2, 11, p.2026, (Nov., 1964).
- (100) A. Sheindlin et al, Proceedings of 8th Symp. on Engineering Aspects of MHD, Stanford U., Stanford, Calif., 1967.
- (101) I.Ya. Shipuk, S.V. Pashkin, "Plasma ionization instability in crossed fields", Sov. Phys.-Doklady, 12, 10, p.959, (April, 1968).
- (102) I.Ya. Shipuk, S.V. Pashkin, "Characteristics of an unstable quasi-equilibrium plasma in crossed electric and magnetic fields", Electricity from MHD, Proc. of a Symp., Warsaw, 1968, vol. 1, p.569, (International Atomic Energy Agency, Vienna, 1968).

- (103) A. Solbes, "Quasi-linear plane wave study of electro-thermal instabilities", Electricity from MHD, Proc. of a Symp., Warsaw, 1968, vol. 1, p.499, (International Atomic Energy Agency, Vienna, 1968).
- (104) L. Spitzer, Physics of Fully Ionized Gases, (Interscience, 1962), 2nd edition, p.26-28.
- (105) ibid., p.30.
- (106) ibid., p.137.
- (107) P. Thiene, "Convective flexure of a plasma conductor", Phys. Fluids, 6, 9, p.1319, (Sept., 1963).
- (108) A.V. Timofeev, "The instability of the positive column in short discharge tubes in longitudinal magnetic fields", Sov. Phys.-Tech. Phys., 6, 12, p.1039, (June, 1962).
- (109) A. Unsöld, "Über das kontinuierliche Spektrum der Hg-Hochdrucklampe, des Unterwasserfunkens und ähnlicher Gasentladungen", Ann. Physik, 33, p.607, (1938).

- (110) H.B. Valentini, "Ionization instability and the effective electrical conductivity of a plasma in a strong transverse magnetic field in three dimensional treatment", Proc. of Ninth Int'l Conf. on Phenomena in Ionized Gases, (1969), paper 4.2.3.5, p.412.
- (111) R.V. Vasil'eva, K.V. Donskoi, N.M. Lobasheva, V.A. Shingarkina, "Nonequilibrium ionization for injection of plasma streams into a magnetic field", Sov. Phys.-Tech. Phys., 15, 6, p.901, (Dec., 1970).
- (112) R.V. Vasil'eva, K.V. Donskoi, N.M. Lobasheva, V.A. Shingarkina, "Kinetics of ionization of an ionized gas flow in a magnetic field", Proc. of Ninth Int'l Conf. on Phenomena in Ionized Gases, (1969), paper 1.3.2.9, p.75.
- (113) E.P. Velikhov, A.M. Dykhne, "Plasma turbulence due to the ionization instability in a strong magnetic field", Proc. of 6th Int'l. Conf. on Phenomena in Ionized Gases, Paris, 1964, vol.4, p.511.

- (114) E.P. Velikhov, A.M. Dykhne, I.Y. Shipuk, Proc. Seventh Int'l. Conf. on Phenomena in Ionized Gases, (Belgrade, Yugoslavia), 1966, vol.2, p.675.
- (115) E.P. Velikhov, L.M. Degtyarev, A.A. Samarskii, A.P. Favorskii, "Calculating the ionization instability in low-temperature magnetized plasma", Sov. Phys.-Doklady, 14, 1, p.68, (July, 1969).
- (116) J.R. Viegas, C.H. Kruger, "Electron distribution function for a nonequipartition plasma in a strong electric field", Phys. Fluids, 12, 10, p.2050, (Oct., 1969).
- (117) A.F. Vitshas, V.S. Golubev, M.M. Malikov, "Investigation of ionization instability in a disc Hall generator", Electricity from MHD, Proc. of a Symp., Warsaw, 1968, vol. 1, p.529, (International Atomic Energy Agency, Vienna, 1968).
- (118) Y.Y. Winograd, J.F. Klein, "Electric arc stabilization in crossed convective and magnetic fields", AIAA J., 7, 9, p.1699, (Sept., 1969).

- (119) V. Zampaglione, "Effective conductivity of an MHD plasma in a turbulent state", Electricity from MHD, Proc. of a Symp., Warsaw, 1968, vol.1, p.593, (International Atomic Energy Agency, Vienna, 1968).
- (120) B. Zauderer, "Experimental study of the relaxation process and the magnitude of non-thermal ionization in an MHD generator", Electricity from MHD, Proc. of a Symp., Salzburg, 1966, vol.1, p.248, (International Atomic Energy Agency, Vienna, 1966).
- (121) B. Zauderer, "Electrical characteristics and loss mechanisms of a non-equilibrium linear MHD generator", Electricity from MHD, Proc. of a Symp., Salzburg, 1966, vol.2, p.597, (International Atomic Energy Agency, Vienna, 1966).
- (122) B. Zauderer, "Electrical characteristics of linear Hall and Faraday generators at small Hall parameters", AIAA J., 5, 3, p.575, (March, 1967).
- (123) B. Zauderer, "Experimental study of nonequilibrium ionization in a linear MHD generator", AIAA J., 6, 4, p.701, (April, 1968).

- (124) B. Zauderer, "Discharge structure and stability of a nonequilibrium plasma in a magnetohydrodynamic channel", Phys. Fluids, 11, 12, p.2577, (Dec., 1968).
- (125) Ya.B. Zel'dovich, Yu.P. Raizer, Physics of Shock Waves and High Temperature Hydrodynamic Phenomena, vol. 1, chap. 3, sect. 5, (Academic Press, 1966).
- (126) E.E. Zukoski, R.R. Gilpin, "Large amplitude electro-thermal waves in a non-equilibrium plasma", Phys. Fluids, 10, 9, p.1974, (Sept., 1967).

APPENDIX 1 EQUILIBRIUM PROPERTIES OF SHOCK
HEATED ARGON

Figures A.1.1 to A.1.3 show density ratio, flow velocity, temperature, and degree of ionization of shock heated argon in thermal equilibrium. The curves were derived from the tables of de Leeuw⁵⁹. The initial (unshocked) gas was assumed at a temperature of 300 degrees Kelvin and a pressure of 0.5 mm. Hg. M_1 is the ratio of the shock speed to the speed of sound, a_1 , in the unshocked gas ($a_1 = 3.3 \times 10^2$ m/sec). ρ_2/ρ_1 is the ratio of the shocked gas density to the unshocked gas density. $u_2/(a_1 M_1)$ is the ratio of the shocked gas flow velocity to the shock wave velocity, both velocities measured in the laboratory frame. T_2 and α_2 are the temperature and degree of ionization respectively of the shock heated gas.

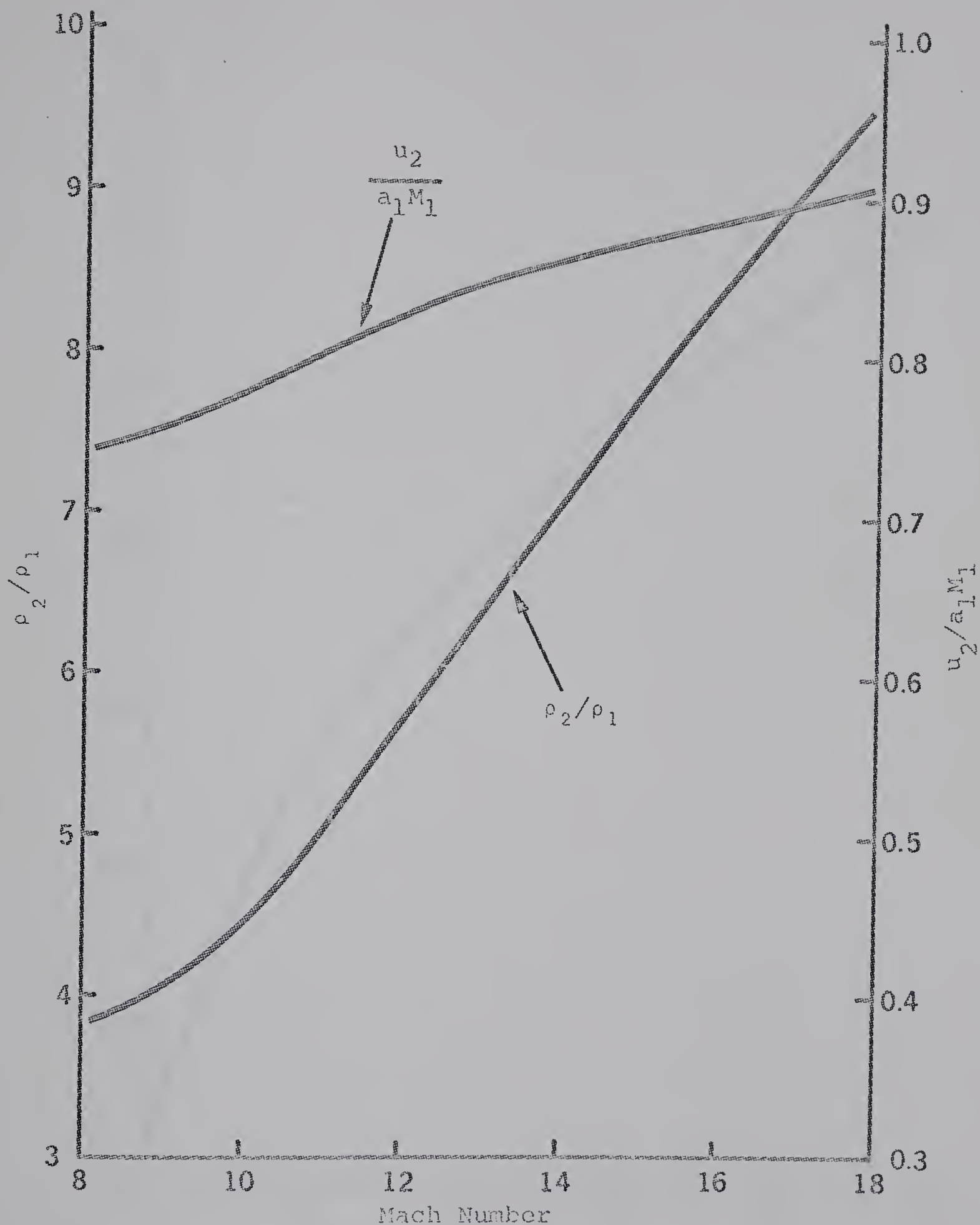


Figure A.1.1

Density Ratio and Flow Velocity vs. Mach No.

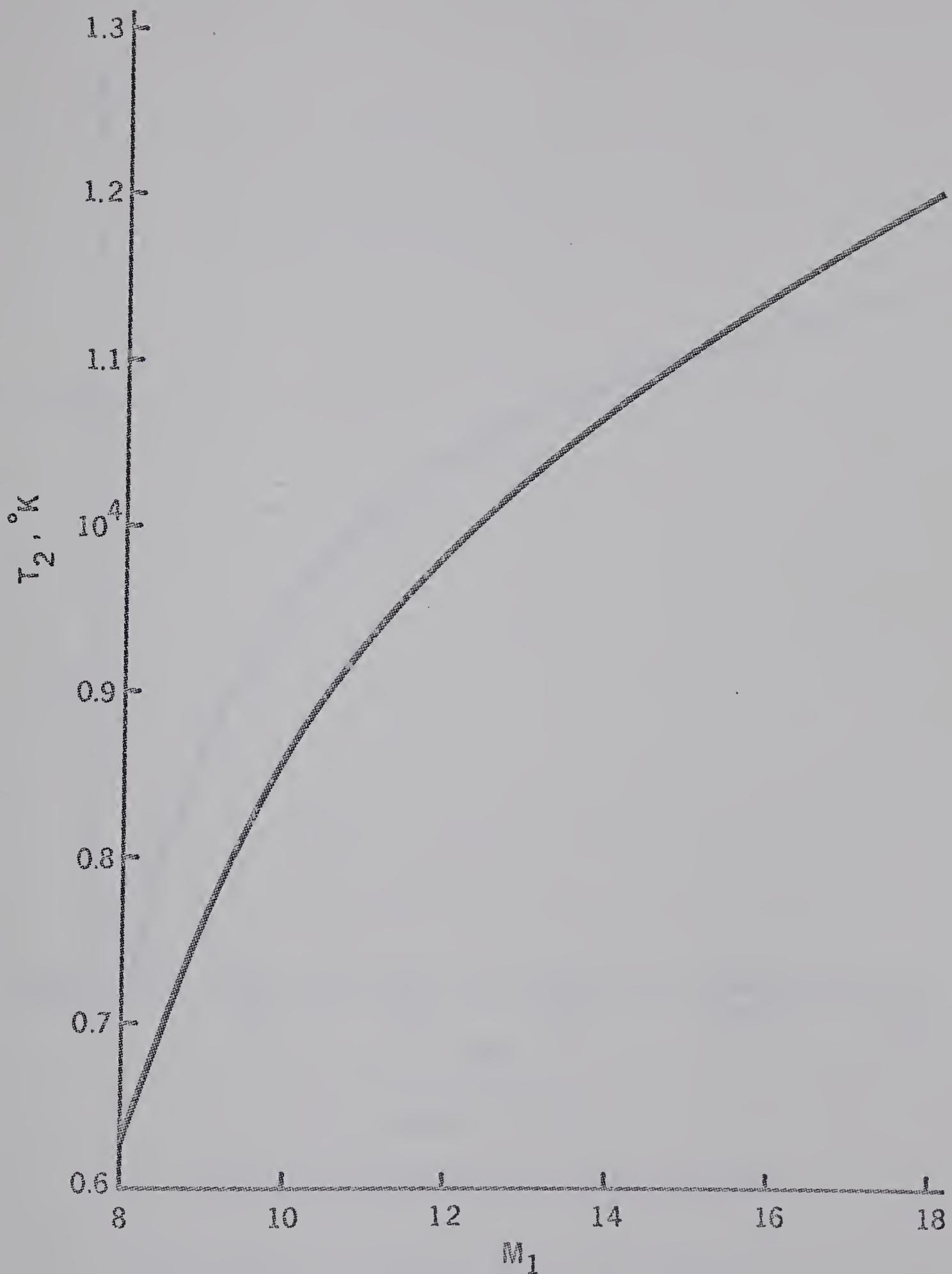


Figure A.1.2

Equilibrium Temperature of Shocked Gas

vs. Mach Number

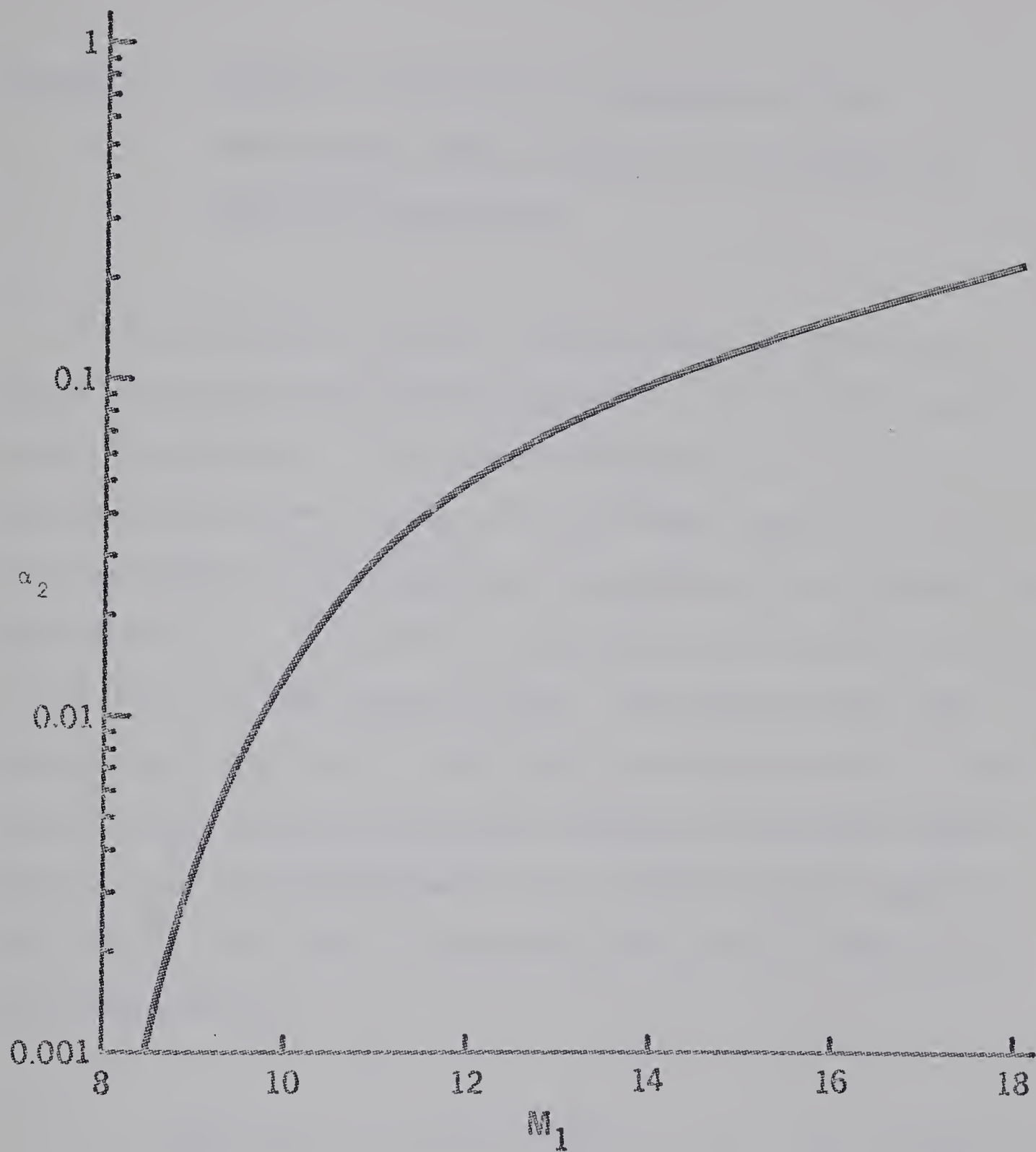


Figure A.1.3
Degree of Ionization vs. Mach Number

APPENDIX 2 RAIZER'S METHOD FOR CALCULATION OF AN APPROXIMATE IONIC CHARGE IN THE REGION OF MULTIPLE IONIZATION.

An approximate method of calculation of the ionic charge has been developed by Raizer⁸². The method rests on two assumptions. The first assumption is that the ion number density n_m and the ionization potentials I_{m+1} are considered to be continuous functions of the ionic charge multiplicity m , obtained by connecting the discrete values of n_m and I_{m+1} by continuous curves. We denote these two continuous functions by $n(m)$ and $I(m)$ respectively. The system of recurrence relations defined by the Saha equation can then be transformed into a differential equation for the function $n(m)$ by replacing the finite differences by differentials:

$$n(m + 1) = n(m) + dn/dm \dots (A.2.1)$$

Then, from Saha's equation,

$$\frac{n_{m+1} n_e}{n_m} = 2 \frac{u_{m+1}}{u_m} A T_e^{3/2} \exp\left(-\frac{I_{m+1}}{kT_e}\right) \dots (A.2.2)$$

where

$$A = \frac{2\pi m_e k}{h^2}^{3/2}$$

and using, from equation (A.2.1),

$$\frac{n(m+1)}{n(m)} = 1 + \frac{d \ln n(m)}{dm},$$

$$\left[1 + \frac{d \ln n(m)}{dm} \right] n_e = A T_e^{3/2} \exp \left[- \frac{I(m+1)}{k T_e} \right] \dots (A.2.3)$$

We assume the ratio of the partition functions is approximately equal to unity. For argon, $(u_{m+1})/u_m$ is 6 for $m=0$, 1.5 for $m=1$, 0.44 for $m=2$, and 2.25 for $m=3$ (see Table A.2.1). However, the variation in this term is small compared to the variation in the exponential term.

The conservation of the number of ions $\sum n_m = n_g$ becomes

$$\int n(m) dm = n_g, \dots (A.2.4)$$

where n_g is the total number density of ions and electrons.

The conservation of charge $\sum m n_m = n_e$ becomes

$$\int_m n(m) dm = n_e , \quad \dots (A.2.5)$$

where n_e is the total number density of electrons.

So the average number of free electrons per original atom or the average heavy particle charge multiplicity is

$$\bar{m} = \frac{\int_m n(m) dm}{\int n(m) dm} = \frac{n_e}{n_g} \quad \dots (A.2.6)$$

The second approximation is that the average value of the ionic charge multiplicity, \bar{m} , is equal to that value of m for which the distribution function $n(m)$ has a maximum. Obviously, this assumption is more justified the sharper and narrower is the peak of the distribution $n(m)$.

(Raizer⁸² shows that the peak is in fact narrow and sharp).

Thus, from equations (A.2.3) and (A.2.6), we have the following simple transcendental equation in \bar{m} , noting that $(dn)/(dm) = 0$ at the peak or maximum:

$$n_e = \bar{m} n_g = A T_e^{3/2} \exp\left[-\frac{\bar{I}}{kT_e}\right] \quad \dots (A.2.7)$$

where \bar{I} is the ionization potential of ions with an average charge multiplicity \bar{m} .

A certain degree of arbitrariness in defining \bar{I} occurs which is connected purely with the formalism (in the exact theory) of assigning subscripts to ionization potentials. If we denote the ionization potentials of an m -ion by I_{m+1} (the ionization potential of a neutral atom is I_1), then formally we should have set $\bar{I}=I(\bar{m}+1)$. Sometimes, however, the ionization potential of an m -ion is denoted by I_m (the ionization potential of a neutral atom is then I_0). In this case, in the Saha equation, I_{m+1} should be replaced by I_m and \bar{I} should be formally set equal to $I(\bar{m})$.

Of course, if we consider heavy elements at high temperatures, where the degree of ionization is very high, the arbitrariness does not result in any substantial change in the value of \bar{m} (since in this case, $I_{m+1} - I_m \ll I_m$). Where the average charge of the ions is not large, however, the arbitrariness has a marked effect on both values of \bar{m} and values of the thermodynamic functions. This results from the approximation of replacing discrete values by continuous functions.

Comparison of the results of approximate and exact calculations shows that best agreement is obtained when we denote the ionization potential of an m -ion by I_{m+1} ,

setting $I_0 = I(0) = 0$, but referring the "average" value of the potential, \bar{I} , to the point $\bar{m} + \frac{1}{2}$, i.e., assuming $\bar{I} = I(\bar{m} + \frac{1}{2})$. This procedure appears to be quite natural, when we note that the sequence of discrete values of m is separated by finite intervals $\Delta m = 1$.

Now, for argon, the function $I(m)$ can be approximated very closely (see Table A.2.1) for the first four or five stages of ionization by the expression

$$I(m) = 15 m \text{ electron-volts} \quad \dots \text{(A.2.8)}$$

Taking the logarithm of equation (A.2.7), we have

$$I(\bar{m} + \frac{1}{2}) = k T_e \ln \left[\frac{AT_e^{3/2}}{\bar{m} n_g} \right] \quad \dots \text{(A.2.9)}$$

which can be easily solved numerically to obtain \bar{m} and thus n_e for a given T_e and n_g .

Table A.2.1
Table of Ionization Potentials
and Partition Functions (to first order)
for Argon (from ref. 2)

	Ionization potential (eV)	Partition Function (u_m)
AI (atom)	15.755	1
AII (singly- ionized)	27.62	6
AIII	40.90	9
AIV	59.79	4
AV	75.0	9
AVI	91.3	6
AVII	124.0	1
AVIII	143.46	2
AIX	422.6	1
AX	479.4	6
AXI	538.9	9

APPENDIX 3 DETAILED CALCULATION OF THE GROWTH RATE
EXPRESSION FOR IONIZATION INSTABILITY

The following derivation is an extension of the work of Velikhov and Dykhne¹¹³, Kerrebrock⁴⁹, and Nedospasov^{72,73}. Their work is extended to the multiply-ionized, Coulomb collision dominated regime.

The procedure is to consider small perturbation solutions to the three equations:

i) Generalized Ohm's Law (eq. 3.21)

$$\sigma_0 \left(\vec{E} + \frac{k}{e} \left(\nabla T_e + T_e \frac{\nabla n_e}{n_e} \right) \right) = \vec{j} + \vec{j} \times \frac{\omega}{v} \vec{B} \quad \dots (A.3.1)$$

ii) Electron energy balance equation (eq. 3.23)

$$\begin{aligned} \frac{3}{2} k \frac{d}{dt} (n_e T_e) + n_e \frac{d\bar{I}}{d\bar{m}} \frac{dn_e}{dt} + \bar{I} \frac{dn_e}{dt} \\ = \vec{j} \cdot \vec{E} - 2(m_e/m_a) n_e v (3k/2) (T_e - T_g) \quad \dots (A.3.2) \end{aligned}$$

iii) Ionization equilibrium expression (eq. 3.25)

$$\left[1 + \frac{n_e}{kT_e} \frac{d\bar{I}}{n_g d\bar{m}} \right] \frac{dn_e}{n_e} = \left[\frac{3}{2} + \frac{\bar{I}}{kT_e} \right] \frac{dT_e}{T_e} \quad \dots (A.3.3)$$

We assume small initial perturbations to the equilibrium values of n_e , T_e , \vec{E} , and \vec{j} as in equation (3.26). We take the mean free time for electron-ion collisions (eq.3.7) as

$$\tau = \frac{32\sqrt{2\pi} \epsilon_0^2 m_e^{1/2} (kT_e)^{3/2}}{e^4 Z n_e \ln\Lambda} \quad \dots (A.3.4)$$

Thus, using $\tau \propto T_e^{3/2}/n_e$ (neglecting the $\ln\Lambda$ variation), and inserting the perturbed expressions for n_e and T_e , we have

$$\tau = \tau_0 \left[1 + \frac{3T_{e1}}{2T_{e0}} - \frac{n_{e1}}{n_{e0}} \right] \quad \dots (A.3.5)$$

Similarly,

$$\nu = 1/\tau = \left[1/\tau_0 \right] \left[1 + \frac{n_{e1}}{n_{e0}} - \frac{3T_{e1}}{2T_{e0}} \right] \quad \dots (A.3.6)$$

Using $\sigma = (n_e e^2)/(m_e \nu)$ or $\sigma \propto T_e^{3/2}$, we have

$$\sigma = \sigma_0 \left[1 + \frac{3T_{e1}}{2T_{e0}} \right] \quad \dots (A.3.7)$$

Inserting the perturbed expressions for n_e , T_e , \vec{E} , and \vec{j} , Ohm's Law becomes, to zero'th order,

$$\sigma_0 \vec{E}_0 = \vec{j}_0 + \omega \tau_0 \vec{j}_0 \times (\vec{B}/B) \quad \dots (A.3.8)$$

We neglect the diffusion terms in Ohm's Law.

To first order, Ohm's Law is:

$$\begin{aligned} \sigma_0 \vec{E}_1 + \sigma_0 \vec{E}_0 \frac{3T_{el}}{2T_{e0}} &= \vec{j}_1 + \omega \tau_0 \vec{j}_1 \times (\vec{B}/B) \\ + \omega \tau_0 \left[\frac{3T_{el}}{2T_{e0}} - \frac{n_{el}}{n_{e0}} \right] \vec{j}_0 \times (\vec{B}/B) & \quad \dots (A.3.9) \end{aligned}$$

The energy balance equation becomes, to zero'th order,

$$\vec{j}_0 \cdot \vec{E}_0 = (2m_e/m_a) (3k/2) (n_{e0}/\tau_0) (T_{e0} - T_g) \quad \dots (A.3.10)$$

To first order, the energy balance equation is

$$\begin{aligned} \tau \tilde{\omega} \left[(3/2)n_{el}kT_{e0} + (3/2)n_{e0}kT_{el} + \frac{d\bar{I}}{n_g d\bar{m}} n_{e0} n_{el} \right. \\ \left. + \bar{I} n_{el} \right] &= \vec{j}_1 \cdot \vec{E}_0 + \vec{j}_0 \cdot \vec{E}_1 - \left[(2m_e/m_a) (3k/2) \right] \cdot \\ \cdot \left[\frac{n_{e0}}{\tau_0} \left(\frac{n_{el}}{n_{e0}} - \frac{3T_{el}}{2T_{e0}} \right) (T_{e0} - T_g) + \frac{n_{e0}}{\tau_0} T_{el} + \frac{n_{el}}{\tau_0} (T_{e0} - T_g) \right] \\ \dots (A.3.11) \end{aligned}$$

Note that including the diffusion terms in Ohm's Law would add imaginary terms to Ohm's Law (equation A.3.9) and thus on the right side of the dispersion relation (A.3.11), through the Joule heating terms $\vec{j}_1 \cdot \vec{E}_0$ and $\vec{j}_0 \cdot \vec{E}_1$. These terms would not affect the growth rate but would introduce a finite phase velocity (see refs. 34 and 72).

The ionization equilibrium expression (A.3.3) becomes, by inspection,

$$\left[1 + \frac{n_{e0}}{kT_{e0}} \frac{d\bar{I}}{n_g d\bar{m}} \right] \frac{n_{e1}}{n_{e0}} = \left[\frac{3}{2} + \frac{\bar{I}}{kT_{e0}} \right]_{T_{e0}}^{T_{e1}} \dots \text{(A.3.12)}$$

We note that, from equation (A.3.3),

$$\begin{aligned} \frac{d \ln T_e}{d \ln n_e} &= \left[1 + \frac{n_{e0}}{kT_{e0}} \frac{d\bar{I}}{n_g d\bar{m}} \right] \left[\frac{3}{2} + \frac{\bar{I}}{kT_{e0}} \right]^{-1} \\ &= \frac{T_{e1}/T_{e0}}{n_{e1}/n_{e0}} \end{aligned}$$

We need two more conditions in order to eliminate the first order quantities from the dispersion relation (A.3.11). We shall exclude electromagnetic wave propagation from consideration and assume that the electric field has a potential ϕ so that $\vec{E} = -\text{grad}\phi$ and thus

$$\text{curl } \vec{E} = 0 \dots \text{(A.3.13)}$$

We also make the plasma approximation that the net charge

density is zero and thus

$$\operatorname{div} \vec{j} = 0 \quad \dots \text{(A.3.14)}$$

From $\operatorname{div} \vec{j} = 0$ and the form of \vec{j} , $\vec{j}_1 \cdot \vec{K} = 0$. Thus,
 $|\vec{j}_1 \times \vec{K}| = j_1 K$.

From $\operatorname{curl} \vec{E} = 0$ and the assumed form of \vec{E} , $\vec{E}_1 \times \vec{K} = 0$,
and thus $\vec{E}_1 \cdot \vec{K} = E_1 K$.

Thus, since $\vec{j}_1 \perp \vec{K}$ and $\vec{E}_1 \parallel \vec{K}$, \vec{j}_1 must be \perp to \vec{E}_1 or
 $\vec{j}_1 \cdot \vec{E}_1 = 0$.

So, we have

$$\begin{aligned} \vec{j}_1 \cdot \vec{K} &= 0 & \vec{E}_1 \times \vec{K} &= 0 \\ |\vec{j}_1 \times \vec{K}| &= j_1 K & \vec{E}_1 \cdot \vec{K} &= E_1 K \\ \vec{j}_1 \cdot \vec{E}_1 &= 0 \end{aligned} \quad \left. \right\} \dots \text{(A.3.15)}$$

We see that there are two possible orientations of the \vec{j}_1 and K vectors:

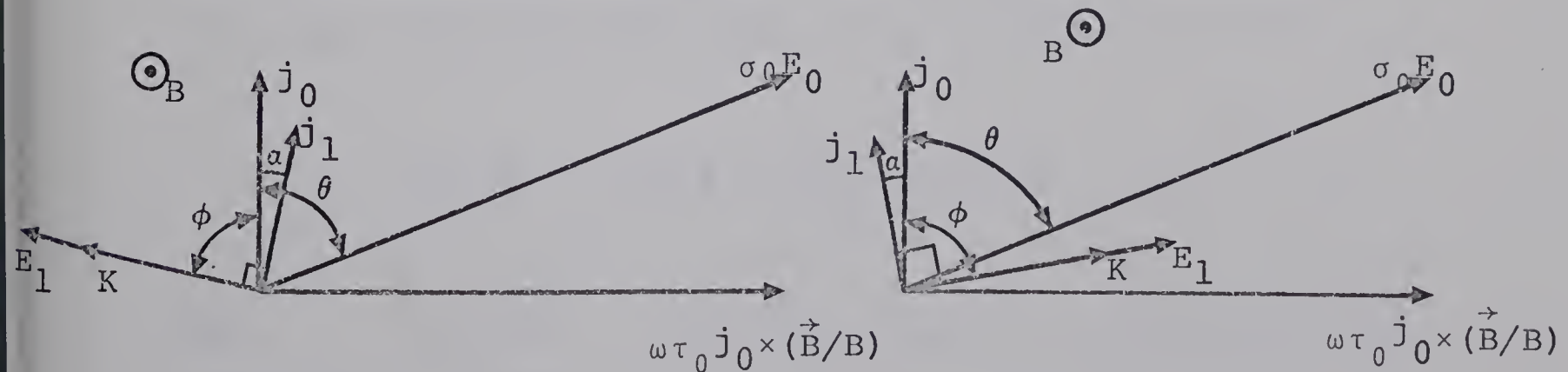


Figure A.3.1

$$(\pi/4) < \phi < (\pi/2)$$

Figure A.3.2

Figure A.3.1 corresponds to the perturbed current vector \vec{j}_1 on the electric field side of the unperturbed current \vec{j}_0 . Figure A.3.2 corresponds to \vec{j}_1 on the side of \vec{j}_0 opposite to \vec{E}_0 . ϕ is the angle between \vec{j}_0 and \vec{k} . θ is the angle between j_0 and E_0 .

We will seek to express all products of vectors in terms of $\vec{j}_0 \cdot \vec{k}$ or $\vec{j}_0 \times \vec{k}$. In the following expressions, when a double sign is written (\pm or $\begin{smallmatrix} + \\ - \end{smallmatrix}$), the upper sign refers to Figure A.3.1 and the lower to Figure A.3.2.

Next, we evaluate the terms $\vec{j}_0 \cdot \vec{E}_1$ and $\vec{j}_1 \cdot \vec{E}_0$ in equation (A.3.11). From equation (A.3.15) and Figures A.3.1 and A.3.2,

$$\vec{j}_0 \cdot \vec{E}_1 = (\vec{j}_0 \cdot \vec{k}) \frac{E_1}{K} = j_0 E_1 \cos \phi \quad \dots \text{(A.3.16)}$$

$$\vec{j}_1 \cdot \vec{E}_0 = + |\vec{k} \times \vec{E}_0| \frac{j_1}{K} \quad \text{for Figure A.3.1}$$

Now, for Figure A.3.2, $\vec{k} \times \vec{E}_0$ changes sign as $\omega\tau$ increases.

$\vec{j}_1 \cdot \vec{E}_0$ goes from positive to negative as $\omega\tau$ increases.

Now, from the zero-order Ohm's Law, equation (A.3.8),

$$\sigma_0 \vec{E}_0 \times \vec{k} = \vec{j}_0 \times \vec{k} + \frac{\omega\tau_0}{B} (\vec{j}_0 \times \vec{B}) \times \vec{k}$$

and $(\vec{j}_0 \times \vec{B}) \times \vec{k} = (\vec{j}_0 \cdot \vec{k}) \vec{B}$ since all quantities are perpendicular to \vec{B} .

So,

$$\vec{E}_0 \times \vec{K} = \frac{1}{\sigma_0} \vec{j}_0 \times \vec{K} + \frac{\omega \tau_0}{\sigma_0} (\vec{j}_0 \cdot \vec{K}) (\vec{B}/B)$$

From Figure A.3.1,

$$|\vec{E}_0 \times \vec{K}| = \frac{1}{\sigma_0} j_0 K \sin \phi + \frac{\omega \tau_0}{\sigma_0} j_0 K \cos \phi$$

From Figure A.3.2,

... (A.3.17)

$$|\vec{E}_0 \times \vec{K}| = \frac{1}{\sigma_0} j_0 K \sin \phi - \frac{\omega \tau_0}{\sigma_0} j_0 K \cos \phi$$

Thus, $\vec{j}_1 \cdot \vec{E}_0$ is given by

$$\vec{j}_1 \cdot \vec{E}_0 = \frac{j_1 j_0}{\sigma_0} (\sin \phi \pm \omega \tau_0 \cos \phi) \quad \dots (A.3.18)$$

We will need $\vec{E}_0 \cdot \vec{K}$ in terms of \vec{K} and \vec{j}_0 . We again use the zero order Ohm's Law:

$$\sigma_0 (\vec{E}_0 \cdot \vec{K}) = \vec{j}_0 \cdot \vec{K} + \frac{\omega \tau_0}{B} (\vec{j}_0 \times \vec{B}) \cdot \vec{K}$$

Now, $\vec{K} \cdot (\vec{j}_0 \times \vec{B}) = \vec{B} \cdot (\vec{K} \times \vec{j}_0)$. In Figure A.3.1, $\vec{K} \times \vec{j}_0$ is antiparallel to \vec{B} . In Figure A.3.2, $\vec{K} \times \vec{j}_0$ is parallel to \vec{B} .

So,

$$\vec{E}_0 \cdot \vec{K} = \frac{1}{\sigma_0} \vec{j}_0 \cdot \vec{K} + \frac{\omega \tau_0}{\sigma_0} |\vec{K} \times \vec{j}_0|$$

or,

$$\vec{E}_0 \cdot \vec{K} = \frac{1}{\sigma_0} j_0^K \cos \phi + \frac{\omega \tau_0}{\sigma_0} j_0^K \sin \phi \quad \dots (A.3.19)$$

Next, we seek to express \vec{j}_1 and \vec{E}_1 in the above expressions in terms of n_{el} , T_{el} , ϕ , and the zero-order quantities.

To find \vec{j}_1 , we take the outer product of \vec{K} with the first-order Ohm's Law, equation (A.3.9):

Term 1 vanishes from equation (A.3.15).

Term 2 is, from Figures A.3.1, A.3.2, and equation (A.3.17),

$$\sigma_0 \frac{\frac{3}{2} \frac{T_{el}}{T_{e0}} E_0}{K} = \frac{\frac{3}{2} \frac{T_{el}}{T_{e0}}}{K} (j_0^K \sin \phi + \omega \tau_0 j_0^K \cos \phi)$$

Term 3 is, from equation (A.3.15),

$$\vec{j}_1 \times \vec{K} = j_1^K (\vec{B}/B)$$

Term 4 vanishes since $(\vec{j}_1 \times \vec{B}) \times \vec{K} = (\vec{j}_1 \cdot \vec{K}) \vec{B} - (\vec{B} \cdot \vec{K}) \vec{j}_1$, and $\vec{j}_1 \cdot \vec{K} = 0$ from equation (A.3.15) and $\vec{B} \cdot \vec{K} = 0$ since \vec{B} is perpendicular to all other quantities.

Term 5 is

$$(\vec{j}_0 \times \vec{B}) \times \vec{K} = (\vec{j}_0 \cdot \vec{K}) \vec{B} - (\vec{B} \cdot \vec{K}) \vec{j}_0,$$

and $\vec{B} \cdot \vec{K} = 0$ by the same reasoning as in term 4. So term 5 is

$$\omega \tau_o \left(\frac{3T_{el}}{2T_{e0}} - \frac{n_{el}}{n_{e0}} \right) j_0 K (\cos \phi) (\vec{B}/B), \text{ and the first-}$$

order Ohm's Law becomes

$$\begin{aligned} & \frac{3T_{el}}{2T_{e0}} \left[+j_0 K \sin \phi + \omega \tau_o j_0 K \cos \phi \right] \\ &= +j_1 K + \omega \tau_o \left[\frac{3T_{el}}{2T_{e0}} - \frac{n_{el}}{n_{e0}} \right] \left[j_0 K \cos \phi \right] \end{aligned}$$

or,

$$j_1 = \left[\frac{3T_{el}}{2T_{e0}} j_0 \sin \phi \right] + \left[\frac{n_{el}}{n_{e0}} \omega \tau_o j_0 \cos \phi \right] \dots (A.3.20)$$

To find \vec{E}_1 , we take the inner product of the first-order Ohm's Law, equation (A.3.9), with \vec{K} :

$$\begin{aligned} \sigma_o E_1 K + \sigma_o \frac{3T_{el}}{2T_{e0}} \vec{E}_0 \cdot \vec{K} &= \frac{\omega \tau_o}{B} (\vec{j}_1 \times \vec{B}) \cdot \vec{K} \\ &+ \frac{\omega \tau_o}{B} \left[\frac{3T_{el}}{2T_{e0}} - \frac{n_{el}}{n_{e0}} \right] \left[(\vec{j}_0 \times \vec{B}) \cdot \vec{K} \right] \end{aligned}$$

Now, from Figures A.3.1 and A.3.2 and equation (A.3.15),

$$\vec{K} \cdot (\vec{j}_1 \times \vec{B}) = \vec{B} \cdot (\vec{K} \times \vec{j}_1) < 0, \text{ and}$$

$$|\vec{K} \cdot (\vec{j}_1 \times \vec{B})| = BK j_1$$

$$\vec{K} \cdot (\vec{j}_0 \times \vec{B}) = \vec{B} \cdot (\vec{K} \times \vec{j}_0) < 0$$

$$|\vec{K} \cdot (\vec{j}_0 \times \vec{B})| = |\vec{B}| |\vec{K} \times \vec{j}_0|$$

So, the first order Ohm's Law becomes, using equation (A.3.19),

$$\begin{aligned} \sigma_o E_1 + \frac{3T_{el}}{2T_{e0}} j_0 \left(\cos \phi + \omega \tau_o \sin \phi \right) \\ = + \omega \tau_o j_1 + \omega \tau_o \left(\frac{3T_{el}}{2T_{e0}} - \frac{n_{el}}{n_{e0}} \right) j_0 \sin \phi \end{aligned}$$

or,

$$\sigma_o E_1 + \frac{3T_{el}}{2T_{e0}} j_0 \cos \phi + \omega \tau_o \frac{n_{el}}{n_{e0}} j_0 \sin \phi$$

$$+ \omega \tau_o j_1 = 0$$

Using equation (A.3.20) for \vec{j}_1 ,

$$\begin{aligned} \sigma_o E_1 + \frac{3T_{el}}{2T_{e0}} j_0 \cos \phi + \frac{3T_{el}}{2T_{e0}} \omega \tau_o j_0 \sin \phi \\ + \frac{n_{el}}{n_{e0}} (\omega \tau_o)^2 j_0 \cos \phi + \omega \tau_o \frac{n_{el}}{n_{e0}} j_0 \sin \phi = 0 \end{aligned}$$

Simplifying,

$$\begin{aligned} E_1 &= \frac{j_0}{\sigma_o} \frac{3T_{el}}{2T_{e0}} \left(-\cos \phi + \omega \tau_o \sin \phi \right) \\ &+ \frac{j_0}{\sigma_o} \omega \tau_o \frac{n_{el}}{n_{e0}} \left(-\omega \tau_o \cos \phi + \sin \phi \right) \end{aligned} \dots \text{(A.3.21)}$$

Combining equations (A.3.18) and (A.3.20),

$$\begin{aligned} \vec{J}_1 \cdot \vec{E}_0 &= \frac{j_0^2}{\sigma_0} \left[\frac{3T_{el}}{2T_{e0}} \sin^2 \phi + \frac{n_{el}}{n_{e0}} (\omega \tau_o)^2 \cos^2 \phi \right. \\ &\quad \left. + \left(\frac{3T_{el}}{2T_{e0}} + \frac{n_{el}}{n_{e0}} \right) \omega \tau_o \sin \phi \cos \phi \right] \end{aligned} \dots (A.3.22)$$

Combining equations (A.3.16) and (A.3.21),

$$\begin{aligned} \vec{J}_0 \cdot \vec{E}_1 &= \frac{j_0^2}{\sigma_0} \left[-\frac{3T_{el}}{2T_{e0}} \cos^2 \phi - \frac{n_{el}}{n_{e0}} (\omega \tau_o)^2 \cos^2 \phi \right. \\ &\quad \left. + \left(\frac{3T_{el}}{2T_{e0}} - \frac{n_{el}}{n_{e0}} \right) \omega \tau_o \cos \phi \sin \phi \right] \end{aligned} \dots (A.3.23)$$

Adding equations (A.3.22) and (A.3.23),

$$\begin{aligned} \vec{J}_0 \cdot \vec{E}_1 + \vec{J}_1 \cdot \vec{E}_0 &= \frac{j_0^2}{\sigma_0} \left[\frac{3T_{el}}{2T_{e0}} (\sin^2 \phi - \cos^2 \phi) \right. \\ &\quad \left. + 2 \frac{n_{el}}{n_{e0}} \omega \tau_o \sin \phi \cos \phi \right] \end{aligned}$$

Thus, the dispersion relation, equation (A.3.11), becomes,

$$\begin{aligned} i \omega n_{e0} k T_{e0} &\left[\frac{3n_{el}}{2n_{e0}} + \frac{3T_{el}}{2T_{e0}} + \frac{d\bar{I}}{n_g \bar{d}m} \frac{n_{el}}{k T_{e0}} + \bar{I} \frac{n_{el}}{n_{e0} k T_{e0}} \right] \\ &= \frac{j_0^2}{\sigma_0} \left[\frac{3T_{el}}{2T_{e0}} (\sin^2 \phi - \cos^2 \phi) + 2 \frac{n_{el}}{n_{e0}} \omega \tau_o \cos \phi \sin \phi \right] \\ &\quad - 3 \frac{m_e n_{e0} k T_{e0}}{m_a \tau_o} \left[\left(\frac{n_{el}}{n_{e0}} - \frac{3T_{el}}{2T_{e0}} \right) \left(1 - \frac{T_q}{T_{e0}} \right) + \frac{T_{el}}{T_{e0}} + \frac{n_{el}}{n_{e0}} \left(1 - \frac{T_q}{T_{e0}} \right) \right] \end{aligned}$$

Now, from equation (A.3.10),

$$3 \frac{m_e}{m_a} \frac{kT_{e0}}{\tau_o} = \frac{\vec{j}_0 \cdot \vec{E}_0}{n_{e0}} \left(1 - \frac{T_g}{T_{e0}} \right)^{-1}$$

From equation (A.3.8), $j_0 E_0 = j_0^2 / \sigma_o$. Thus,

$$3 \frac{m_e}{m_a} \frac{kT_{e0}}{\tau_o} = \frac{j_0^2}{\sigma_o n_{e0}} \left(1 - \frac{T_g}{T_{e0}} \right)^{-1}$$

Also, from equation (A.3.12),

$$\frac{T_{el}}{T_{e0}} = \frac{\left(\frac{d \ln T_e}{d \ln n_e} \right) n_{el}}{\left(\frac{d \ln n_e}{d \ln n_e} \right) n_{e0}}$$

The dispersion relation becomes:

$$\begin{aligned} i\tilde{\omega} = & \frac{j_0^2}{\sigma_o n_{e0} \bar{I}} \left\{ \frac{3}{2} \frac{d \ln T_e}{d \ln n_e} \left(\sin^2 \phi - \cos^2 \phi \right) \pm 2\omega \tau_o \sin \phi \cos \phi \right. \\ & \left. - 2 + \frac{3}{2} \frac{d \ln T_e}{d \ln n_e} - \left(\frac{T_{e0}}{T_{e0} - T_g} \right) \frac{d \ln T_e}{d \ln n_e} \right\} \cdot \\ & \cdot \left\{ \frac{3}{2} \frac{kT_{e0}}{\bar{I}} \left(1 + \frac{d \ln T_e}{d \ln n_e} \right) + \frac{n_{e0}}{n_g} \frac{1}{\bar{I}} \frac{d \bar{I}}{d \bar{m}} + 1 \right\}^{-1} \quad \dots (A.3.24) \end{aligned}$$

We see that the amplitude of the growth rate depends on ϕ , the angle between \vec{j}_0 and \vec{k} . This means that there is a preferred directional dependence of the instability.

To find the maximum value of the growth rate, $\tilde{\omega}$, and the angle, ϕ , for which the growth rate is a maximum, we maximize the function

$$F = \frac{3 \frac{d \ln T_e}{d \ln n_e}}{2} \left(\sin^2 \phi - \cos^2 \phi \right) + 2\omega\tau_O \sin \phi \cos \phi$$

with respect to ϕ . That is, we solve for ϕ_{\max} and F_{\max} under the conditions $(dF)/(d\phi) = 0$; $(d^2F)/(d\phi^2) < 0$.

Now,

$$F = - \frac{3 \frac{d \ln T_e}{d \ln n_e}}{2} \cos 2\phi + \omega\tau_O \sin 2\phi \quad \dots (A.3.25)$$

$$\frac{dF}{d\phi} = 3 \frac{d \ln T_e}{d \ln n_e} \sin 2\phi + 2\omega\tau_O \cos 2\phi \quad \dots (A.3.26)$$

$$\frac{d^2F}{d\phi^2} = 6 \frac{d \ln T_e}{d \ln n_e} \cos 2\phi + 4\omega\tau_O \sin 2\phi \quad \dots (A.3.27)$$

The condition $(dF)/(d\phi) = 0$ leads to, from equation (A.3.26),

$$\tan 2\phi = \pm \left[\frac{\omega\tau_O}{\frac{3 \frac{d \ln T_e}{d \ln n_e}}{2}} \right] \quad \dots (A.3.28)$$

The condition $(d^2F)/(d\phi^2) < 0$ leads to, for Figure A.3.1, $\sin 2\phi > 0$; $\cos 2\phi < 0$. Thus, $(\pi/2) \leq 2\phi \leq \pi$.

Thus,

$$\cos 2\phi_{\max} = -\frac{\frac{3}{2} \frac{d \ln T_e}{d \ln n_e}}{\sqrt{(\omega \tau_0)^2 + \left(\frac{3}{2} \frac{d \ln T_e}{d \ln n_e}\right)^2}}$$

... (A.3.29)

and,

$$\sin 2\phi_{\max} = +\frac{\omega \tau_0}{\sqrt{(\omega \tau_0)^2 + \left(\frac{3}{2} \frac{d \ln T_e}{d \ln n_e}\right)^2}}$$

... (A.3.30)

and F_{\max} is given by, from equations (A.3.25), (A.3.29), and (A.3.30),

$$F_{\max} = \sqrt{(\omega \tau_0)^2 + \left(\frac{3}{2} \frac{d \ln T_e}{d \ln n_e}\right)^2} \quad \dots (A.3.31)$$

Similarly, for Figure (A.3.2), the condition $(d^2 F)/(d\phi^2) < 0$ leads to, from equation (A.3.27), $\cos 2\phi < 0$; $\sin 2\phi < 0$.

Thus, $\pi \leq 2\phi \leq (3\pi/2)$, and

$$\cos 2\phi_{\max} = -\frac{\frac{3}{2} \frac{d \ln T_e}{d \ln n_e}}{\sqrt{(\omega \tau_0)^2 + \left(\frac{3}{2} \frac{d \ln T_e}{d \ln n_e}\right)^2}}$$

... (A.3.32)

$$\sin 2\phi_{\max} = - \frac{\omega \tau_o}{\sqrt{(\omega \tau_o)^2 + \left(\frac{3}{2} \frac{d \ln T_e}{d \ln n_e} \right)^2}} \dots (A.3.33)$$

and F_{\max} is given by, from equations (A.3.25), (A.3.32), and (A.3.33),

$$F_{\max} = \sqrt{(\omega \tau_o)^2 + \left(\frac{3}{2} \frac{d \ln T_e}{d \ln n_e} \right)^2} \dots (A.3.34)$$

Thus, we see that F_{\max} is the same for both orientations of \vec{j}_1 with respect to \vec{j}_0 , given by Figures A.3.1 (equation A.3.31) and Figure A.3.2 (equation A.3.34).

This means that the growth rate is a maximum for both orientations of \vec{j}_1 with respect to \vec{j}_0 and implies²⁸ that a streamer will break up into two parts, each at the characteristic angle to the original.

The maximum value of the growth rate is:

$$\begin{aligned} |\tilde{\omega}|_{\max} &= \frac{j_0^2}{\sigma_0 n_{e0} \bar{I}} \left\{ \sqrt{(\omega \tau_o)^2 + \left(\frac{3}{2} \frac{d \ln T_e}{d \ln n_e} \right)^2} \right. \\ &\quad \left. - 2 + \frac{3}{2} \frac{d \ln T_e}{d \ln n_e} - \left(\frac{T_{e0}}{T_{e0} - T_g} \right) \frac{d \ln T_e}{d \ln n_e} \right\} \cdot \\ &\quad \cdot \left\{ \frac{3}{2} \frac{kT_{e0}}{\bar{I}} \left(1 + \frac{d \ln T_e}{d \ln n_e} \right) + \frac{n_{e0}}{n_g} \frac{1}{\bar{I}} \frac{d\bar{I}}{dm} + 1 \right\}^{-1} \dots (A.3.35) \end{aligned}$$

For both orientations of j_1 ,

$$2\phi = \pi - \tan^{-1} \left[\frac{\omega \tau_o}{\frac{3 d \ln T_e}{2 d \ln n_e}} \right]$$

where the value of \tan^{-1} is taken between 0 and $\pi/2$.

Thus, the angle between \vec{j}_0 , the average or unperturbed current, and \vec{j}_1 , the perturbation current, is (see Figures A.3.1 and A.3.2):

$$\alpha \equiv \left(\frac{\pi}{2} - \phi \right) = \frac{1}{2} \tan^{-1} \left[\frac{\omega \tau_o}{\frac{3 d \ln T_e}{2 d \ln n_e}} \right] \dots (A.3.36)$$

where, again, \tan^{-1} is taken between 0 and $\pi/2$.

B30004